Alma Mater Studiorum – Università di Bologna

DOTTORATO DI RICERCA IN

Meccanica e Scienze Avanzate dell'Ingegneria: Progetto n°4 Meccanica dei Materiali e Processi Tecnologici

_____

Ciclo XXIV°

Settore Concorsuale di afferenza: 09/B1

Settore Scientifico disciplinare: ING-IND 16

EXPERIMENTAL ANALYSIS AND FE MODELING OF ALUMINUM ALLOYS MICROSTRUCTURAL EVOLUTION IN EXTRUSION

ANALISI SPERIMENTALE E MODELLAZIONE EF DELL'EVOLUZIONE MICROSTRUTTURALE DI LEGHE DI ALLUMINIO NEL PROCESSO DI ESTRUSIONE

Presentata da: Dott. Ing. Antonio Segatori

Coordinatore Dottorato **Relatore**

Chiar.mo. Prof. Ing. Vincenzo Parenti Castelli **Chiar.mo. Prof. Ing. Luca Tomesani**

Esame finale anno 2012

Index

Introduction

Hot plastic deformation processes are technologies that involve from simple to very complex deformation of a material by means of dies. Among those, forging and extrusion are marked by highest deformations and more complex strain gradients. In particular, Extrusion is used to form long products of constant cross section from simple billets; typical products being bars, solid and hollow profiles of high variety of shapes, wire and tubes.

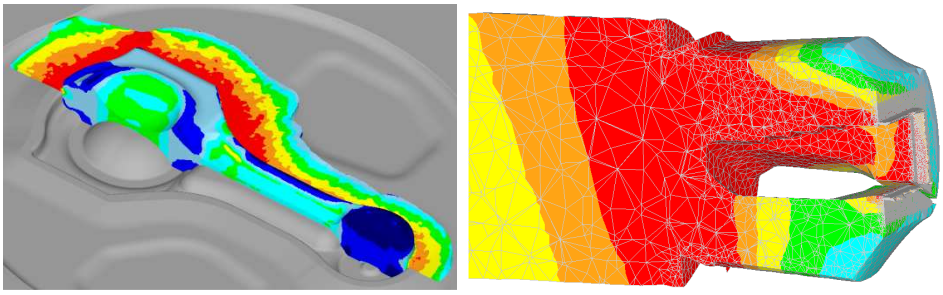

Figure 1. Examples of strain gradients in forging (left) and extrusion (right) operations.1

Aluminum alloys are the materials most processed in the extrusion industry due to their deformability and the wide field of applications that range from buildings to aerospace and from design to automotive industries. The diverse applications imply therefore different requirements that can be fulfilled by the wide range of alloys and treatments, that is from critical structural application to high quality surface and aesthetical aspect. Whether one of the other is the critical aspect of the product, they both depend directly from microstructure.

As it is well known in literature, microstructure and mechanical properties are strongly bound. The Hall-Petch relationship itself is the direct correlation between the yield stress of a pure material and the grain diameter (eq 1) where the yield stress is dependent, beside a constant, on the inverse of the square root of grain size [1]:

$$\sigma = \sigma_c + \frac{k}{\sqrt{d}} \qquad (1)$$

with σ_c and k constants of the material.

Regarding aesthetical defects, two major categories can be identified in relation to the inner cause: on one side are geometrical-mechanical defects, that arise due to removal or deposition of material and impurities caused by errors in tooling or processing parameters; on the other side are appearance defects that arise from non-uniform microstructure. The latter ones are bound to two main

factors: impurities that can contaminate certain areas of the product and particular condition or gradients of metal flow (i.e. strain, strain rate and temperatures).

Stated the above, it is widely recognized the importance of microstructure for high quality products and for improvements of the process performance towards a minimization of defects. In the last decades there has been an increasing interest in the aluminum extrusion technology aside with its development, which brought investigation on mainly billet metallurgy, process control and tool design in order to enhance process efficiency and product quality. Nevertheless, stated the basic knowledge of aluminum alloys microstructure phenomena, only partial attempts have been done to evaluate and fully control the evolution of microstructure in the field of extrusion especially linking all the production steps together.

Recent years have seen the great evolution of Finite Element codes for technological processes, which have now reached a maturity that allow them to be a useful tool in the extrusion industry, both for tool and process designing (2,3,4,5,6). Thus, a useful tool is available for both support the understanding of the microstructure evolution as well as offer the means to predict and control it.

In the extrusion process, the material undergoes a variety of different thermo-mechanical steps, up to five major ones. As shown in Figure 2 the material undergoes a DC casting, homogenization treatment, extrusion and quenching, solution treatment (only in particular production) and ageing. Examples of the diverse type of microstructure that can be present in an extruded profile due to the complex metal flow are shown in Figure 3. A deeper description of the microstructure behavior in each step is given in PAPER VI.

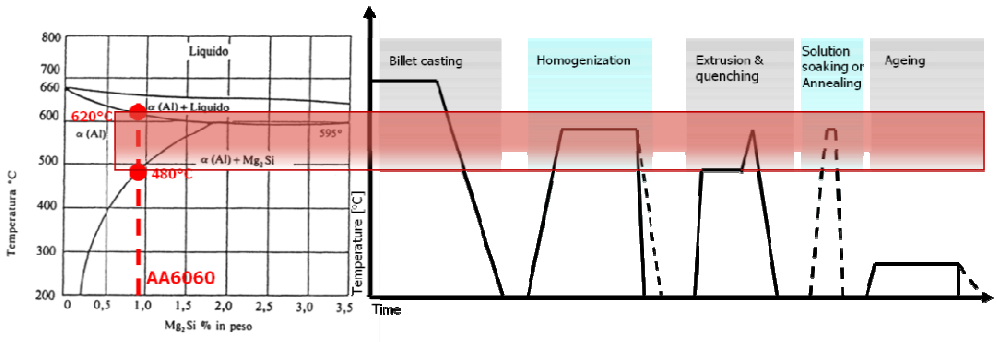

Figure 2. Thermal history of material undergoing a classical extrusion process.

This thesis will analyze the evolution within the last three steps thus dealing with the microstructural evolutions throughout the entire process so as to provide a tool usable by the extrusion industry that is now days attempting a further step in the Fitness For Service. The following thesis will deal with 6XXX series aluminum alloys, mainly AA6060 and AA6082, which are highly widespread in the extrusion industry and can cover a broad variety of requirements and applications.

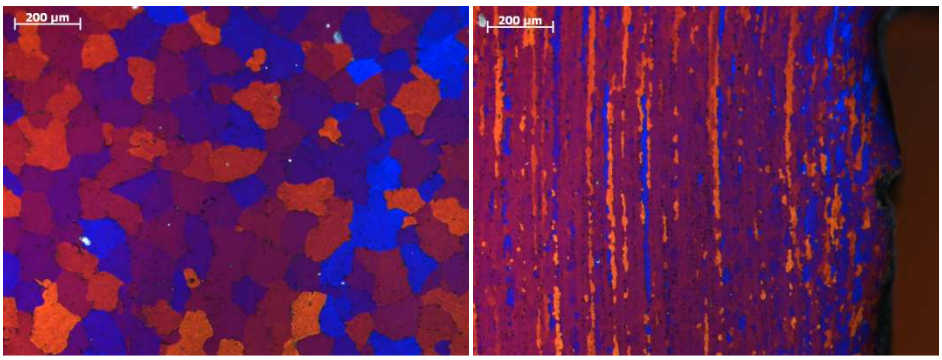

Figure 3. Examples of microstructure present in extruded profile: left, equiaxed structure, right highly elongated and recrystallized (gDRX) grains.

Thesis Outline

This thesis deals with the development of a tool to be used in industrial practice for the prediction of microstructure in extrusion processes for 6XXX aluminum alloys, thus requiring validation and calibration of the code and the experimental characterization of the microstructure evolution of 6XXX alloys.

Indeed the conception of an evolution model and its implementation in commercial FE langrangian code for industrial scope requires a deep understanding of the extrusion process itself, so to build, together with the evolution model a set of competences and boundary condition required to make the model versatile enough for industry. In the recent years the FEM simulation is gaining more and more space as a tool in support of die design for a 'one step design'. In fact, still today most extrusion die design is based on the knowhow and experience of the die maker thus requiring on the request of a new profile a series of prototypes, corrections and trials. This inhibits as well the possibility to fully verify the actual optimization of the design due to high cost of die production and testing.

Furthermore the boost of the market to the development of new frontier products requires a joint design of the tooling and the process involving both the die maker and the extruder. In this situation, not only the simulation is perfect tool for communication, but it is the only one for integrated analysis of die and process design, which is required in the solution of problem that involve both process efficiency and quality of the product.

Part I - Calibration of simulation model

The calibration of FE code starts with the choice of the code itself depending on the simulation results that are more important for the user(4,6). Moreover codes for massive deformation simulation differ in the approach to the problem; for the present study DEFORM, a Lagrangian approach code, has been used due to the fact that its approach allows to follow the entire evolution of the material flow (fundamental for the evaluation of microstructure. Furthermore a validation of the code as to be done on actual experimental data, which is often not available or limited. In this direction several monitoring activities have been carried out during the doctorate to build together knowledge of the process and adjustments on the code. In PAPER I PAPER II a complete activity of process and tool monitoring is reported.

A good FEM requires a good calibration of all process boundary conditions, among them friction is the most critical one (7,8,9). Within a process, friction is responsible for the evaluation of loads, heat generation and metal flow. As many software well represent the strong influence of friction, its modeling is crucial; nevertheless it cannot be retrieved by any type of monitoring of industrial

extrusions, but a dedicated couple experimental-simulation campaign has to be carried out.

An investigation on the value of friction in different condition as well as its influence was carried out by means of the visioplasticity technique and comparison with different codes modeling as discussed in PAPER III. For this activity, a small scale extrusion has been designed in order to perform experiments in the same condition as the industrial cases of final interest. In fact in literature friction is often analyzed with standard tests (e.g. pin on disc) which cannot resembled the real industrial condition (as the high pressure in extrusion containers) and do not give results of direct implementation on codes. The experimental activity allowed moreover to investigate the effect of different coatings and wear.

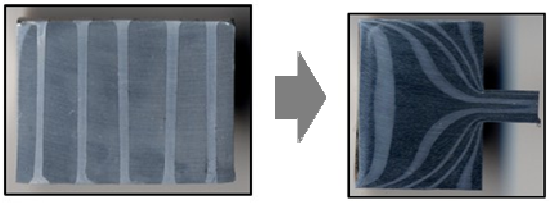

Figure 4. Section of visioplasticity specimens, prior (left) and after (right) extrusion.

Along with the calibration of the code and the implementation of microstructure evolution routine, a problem arose in the computation of strain. The effective strain did not match the deformative gradient shown by the metal flow; moreover, comparison with Von Mises strain shown an underestimation of the effective strain. A preprocessor subroutine was therefore written in the code to compute the strain from the single deformative components. The results of this activity, described in APPENDIX A, shows an improvement in the matching of strain with metal flow with evident reduction in the dispersion of coupled experimental-numerical data.

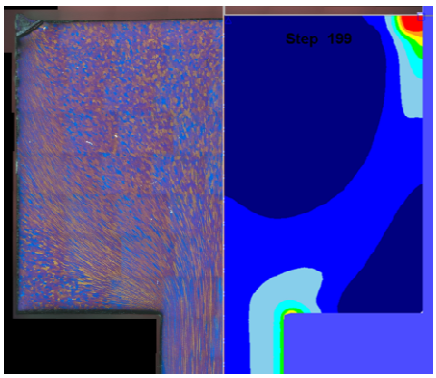

Figure 5. Example of comparison between microstructure and computer strain distribution for a small scale direct extrusion specimen.

Part II - Microstructure model

It is to be noticed that the present study mainly focused on the grain shape, leaving aside the analysis of precipitates and intermetallics behavior mainly to a phenomenological investigation and no modeling has yet been developed for that. In order to analyze the evolution of grain size and shape during the extrusion process, a research has been done on the proposed theories available in literature.

It is widely recognized that three main stages of microstructure evolution are present for aluminum alloys:

- Recrystallization during deformation (i.e. under mechanical and thermal solicitation): DRX;
- Static Recrystallization (i.e. under sole thermal solicitation): SRX;
- Grain growth (i.e. under sole thermal solicitation) producing defects as Abnormal Grain Growth and Peripheral Coarse Grain: PCG.

Due to the occurance of the two recrystallization mechanisms subsequently one to the other at a separate time, the two phenomena can and were investigated individually although an analysis was done to evaluate the full sequence within the same process.

Despite the pure aluminum were a Discontinus Dynamic Recrystallization (i.e. nucleation and growth) can occur, two different theories are discussed in literature for the dynamic recrystallization (DRX). One, Continuous Dynamic Recrystallization (cDRX) (10, 11), proposes the creation of new grains as a consequence of the transformation of subgrain boundaries into grain boundaries within the existing grains; this occurs as dislocations accumulate on subgrain boundaries. In detail, when the misorientation angle exceeds the critical value of 15° a new high angle boundary is formed. The other, Geometrical Dynamic Recrystallization (gDRX) (11, 12) proposes a geometrical approach: original grains flatten under compression or elongate under tension or torsion; with the increasing of deformation, due to subgrain formation, grain boundaries become increasingly serrated, till a point where different point of the grain boundary come into contact thus pinching off the grain in two or more separate ones ().

Figure 6. Representation of the pinch-off phenomena in the geometric dynamic recrystallization.

More accordance is present in literature around the static recrystallization (SRX), which occurs after the deformation process with a sufficient stored energy. The computation can be performed by mean of the Kolmogorov–Johnson–Mehl–Avrami (JMAK) model (13, 14) thus computing evolution of

subgrain size and density of recrystallization in order to evaluate the size of the recrystallized grains.

The majority of works reported in literature deal with analysis performed by means of laboratory tests, mainly hot torsion tests, which are far from the typical extrusion conditions (15). Therefore, for the evaluation of the dynamic recrystallization a dedicated experiment was designed: a small scale extrusion of solid round profile performed on a tensile-compression press. The type of experiment had the multiple benefits of recreating the industrial condition of metal flow and allowing easy handling thus permitting a rapid freeze of microstructure after deformation. The process parameters were chosen in order to investigate the characteristic industrial ones. The grain size data retrieved from the experimental condition was coupled with that of a simulation campaign, allowing to identify the evolution of the grain shape, the onset of gDRX and consequentially build a model. The detailed description of the experiment and results is shown in PAPER IV.

The creation of a static recrystallization model was performed based on the available models in literature, thus using a second experimental analysis to validate both dynamic and static models, PAPER V, within the same environment; a coupling that is not shown in any scientific contribution. The second experimental set up consisted in a small scale inverse extrusion. The specimens produced were immediately quenched for dynamic evolution analysis, and later annealed for static recrystallization analysis.

To date, no complete implementation of microstructure evolution has been performed on commercial FE codes for aluminum alloys. In general, developed models (15, 14), of which few were implemented in FE codes, did not compute both the dynamic and static recrystallization but only the latter one, thus not applicable in presence of deformation gradients for common industrial manufacturing processes. PAPER IV and V present the building of an integrated model in a commercial software validated in the range of industrial processes.

Part III - Microstructure related defects

Aside with the above studies, an inverse approach has been taken during the doctorate aimed to investigate the conditions, of process parameters as well of microstructure, that lead to defectiveness on extruded profiles hence building a knowledge for an effective interpretation of microstructure evolution simulation.

As part of this defects investigation, two main problems typical of the extrusion industry have been examined. First, the streak formation on profile surface. This is a dreadful problem for extruder, which can do nothing but witness the appearance of such aesthetical defect at the end of the process, that is after anodizing, thus scrapping the profile. The causes of such problem can be multiple but as shown in PAPER VI are due to differences in microstructure. The understanding of such microstructure and the possibility to predict those conditions are the only tools to solve or even prevent the occurrence of streaks.

If streaks are merely aesthetical, a deceitful problem lays on the charge weld, that occurs at the joining of two subsequent billets in the common billet to billet extrusion. Due to the complex gradient of metal flow in the die, the flat mating surface of the two billets is stretched through long section of the profile, invisible to most non-destructive inspections. Due to impurities and process conditions, the welding of the two billet surface is highly likely to be poor and has therefore to be scrapped anytime the profile has structural applications. The location of such weld is critical and involves empirical scouting of profile section with a waist of the material. The position and evolution of the weld is however strictly determined from the metal flow in the tool. A knowledge of such dependence can lead to not only an immediate identification of the length and position to be scrapped, but furthermore to an optimization of the die and process efficiency through a correct designed aided by the simulation as shown in PAPER VII.

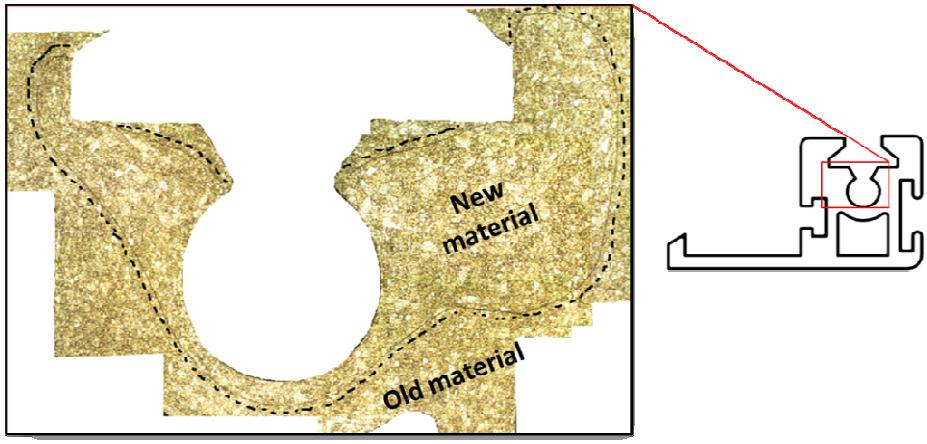

Figure 7. Example of charge weld appearance in a section of extruded profile.

References

[1] G. Saada, "Hall–Petch revisited." Materials Science and Engineering A 400–401 (2005) pg. 146–149

[2] B. Reggiani, L. Donati, L. Tomesani, "Evaluation of different FE simulation codes in the stress analysis of extrusion dies". Internationa Journal of Material Forming, 2010, Vol. 3 Suppl 1:395– 398, pp. 395 - 398

[3] L. Donati, N. Ben Khalifa, L. Tomesani, A. E. Tekkaya, "FEM Codes Benchmark for Aluminum Extrusion Process Analysis", Proceedings of the 12th International Conference on Aluminium Alloys, TOKYO, The Japan Institute of Light Metals, 2010, pp. 583 - 588

[4] L. Donati, L. Tomesani, N. Ben Khalifa, D. Pietzka, "Extrusion Benchmark 2007", Proceedings of The international congress on simulation technology for the engineering analysis community, GLASGOW, Nafems ltd, (2009)

[5] T. Kloppenborg, M. Schikorra, M. Schoemacker, A.E. Tekkaya, "Numerical Optimization of Bearing Length in Composite Extrusion Processes". Key Engineering Materials 367 (2008)

[6] L. Donati, L. Tomesani, N. Ben Khalifa, A. E. Tekkaya, *Extrusion Benchmark 2009 – A step ahead in virtual process optimization*, «LIGHT METAL AGE», 2009, 67, n. 2, pp. 54 - 55 [articolo]

[7] P.K.Saha, "Use of tribology to improve perormance and quality in aluminum extrusion". Proceedings of 8th Extrusion Technology Seminar (2004) vol. 2, pag. 277-287

[8] N.C. Parson, J.D. Hankin, A. J. Bryant, "The Metallurgical Background to Problems Occurring During the Extrusion of 6XXX Alloys" Proceedings of 5th Extrusion Technology Seminar, Chicago, USA (1992) vol. 2, pp. 13-23

[9] M. Schikorra, L. Donati, L. Tomesani, A. E. Tekkaya "Microstructure Analysis Of Aluminum Extrusion: Prediction Of Microstructure On AA 6060 Alloy" Journal of Materials Processing Technology 201 (2008) 156–162

[10] S. Gourdet, F. Montheillet, "An experimental study of the recrystallization mechanism during hot deformation of aluminium" Materials Science and Engineering: A, Volume 283, Issues 1–2, 15 May 2000, Pages 274-288

[11] R. D. Doherty, D. A. Hughes, F. J. Humphreys, J. J. Jonas, D. Juul Jensen, M. E. Kassner, King, H. J. McQueen, A. D. Rollett, "Current issues in recrystallization: a review" 1997, Materials Science and Engineering A, Volume 238, Issue 2, Pages 219-274

[12] H. J. McQueen, S. Spigarelli, M.E. Kassner, E. Evangelista, "Hot Deformation and Processing of Aluminum Alloys", 2011, CRC Press.

[13] T. Sheppard, X. Duan, "Modelling of static recrystallisation by combining FEM with empirical models" Journal of Materials Processing Technology, Volumes 130–131, 20 December 2002, Pages 250-253

[14] Z. Peng, T. Sheppard, "Prediction of Static Recrystalization during Shaped Extrusion" 2004, Proceedings of Extrusion Technology.

[15] H.E. Vatne, T. Furu, R. Ørsund, E. Nes, "Modelling recrystallization after hot deformation of aluminium" Acta Materialia, Volume 44, Issue 11, November 1996, Pages 4463-4473

Extrusion Benchmark 2011: Evaluation of different design strategies on process conditions, die deflection and seam weld quality in hollow profiles

Alessandro Selvaggio[1,a], Antonio Segatori[2,b], Ahmet Guzel[1,c], Lorenzo Donati[2,d], Luca Tomesani[2,e] and A. Erman Tekkaya[1,f]

[1]Institute of Forming Technology and Lightweight Construction, TU Dortmund University, Baroperstr. 301, 44227 Dortmund, Germany

[2]Department of Mechanical Construction Engineering (D.I.E.M.) University of Bologna, V.le Risorgimento 2, 40136 Bologna, Italy

[a]alessandro.selvaggio@iul.tu-dortmund.de, [b]antonio.segatori2@unibo.it
[c]ahmet.Guezel@iul.tu-dortmund.de, [d]l.donati@unibo.it
[e]luca.tomesani@unibo.it, [f]erman.tekkaya@iul.tu-dortmund.de

Keywords: Extrusion, Benchmark, Die Deformation, Deflection measurements

Abstract. In the paper experimental investigations aimed at allowing a detailed and accurate comparison of different FEM codes were presented and discussed. Two hollow profiles within the same die were characterized by different thicknesses within the profile, two welding chambers and critical tongues (one fully supported and one partially supported). The material flow balance was performed by means of feeder size and position on a profile and by means of bearings on the other one. Accurate monitoring of process parameters was carried out by using a self-calibrating pyrometer for profile temperature, six thermocouples for die thermal monitoring, a laser velocitymeter for profile speed and two laser sensors for die deflection on critical tongues. AA6082 alloy was used as deforming material, while H-11 hot-work tool steel was selected for the die material. The experiments were repeated at least three times under the same conditions in order to provide a nearly steady state statistical distribution of the acquired data. These are used as a reference for the 2011 edition of the extrusion benchmark.

Introduction

Still today, the design of extrusion dies is mainly based on the experience and skill of the die makers. When a new profile has to be manufactured, some trials and prototypes are often necessary in order to achieve the optimal compromise between die productivity and die life. This procedure is very costly and also time consuming. Furthermore, the transfer of knowledge between different generations of die designers or, within the same company, between employees is not always given. It is then clear that software tools supporting die design are essential for an effective and reliable ´one step die design´. In this direction, in the past years, many papers demonstrated that FEM simulations are the only feasible way to predict the material flow and the die stress and to allow, as a consequence, die optimization [1, 2].

The increasing demand for reliable simulations of the extrusion process has led to the organization of the biannual international conference "Extrusion Conference and Benchmark", specifically focused on the optimization of FEM codes for extrusion analysis. In particular, the Extrusion Benchmark is a conference where the capabilities of different commercial codes capabilities are analyzed in deep by comparing the results with the data of an extrusion experiment. The procedure is divided in three main steps: in the first step an experiment is designed and performed under strictly monitored conditions and repeated several times in order to provide a statistical significance of the monitored results. The second step is the process simulation: the organizers provide the information for carrying out the simulations; then every interested participant (software houses, scientific and industrial users) performs the simulation before the conference. The third step is the comparison of the results: during the conference, the hidden results of the experiment are disclosed

and the different FEM codes predictions are compared to the experimental data, thus providing an interesting evaluation of codes capabilities. It is important to note that, due to the complexity of the matter, it would be useless to consider the benchmark simply as a contest: it is, instead, an opportunity to fix some points about the everyday simulation practice, each participant with own particular interest. In this respect, for example, the software houses can promote their codes capabilities on the basis of scientific and well monitored experimental data, the industrial users can verify their ability to properly perform a simulation with their own code or even select a code among those participating to the contest. In the 2007 edition of the extrusion benchmark, it was shown that the FE simulation of the extrusion process can predict all main process parameters (press load, profile speed and temperature development) when different pocket shapes are used [3]. There, it was found that the simulation of the material flow, in particular by flat dies, can be very accurate if proper thermal conditions are given.
On the other hand, the increasing complexity of the profile geometries, often of big size and small thickness, and the use of porthole dies with very slender mandrels (often multiple) and supporting legs leads to the ever increasing importance of die deflection in determining the material flow. It is well known that a die can behave in a very different way from what is expected because of its deformation under process loads. In the scientific literature, investigations on the die deformation cannot be found explicitly. Only some approaches for measuring the pressure on the die face can be found [4, 5]. In particular, investigations on the influence of the die deflection on the profile distortion, profile speed and temperature development at the die exit are completely missing. All these aspects, together with the problem of die life assessment, were pointed out as cause of concern among extruders and die makers at the 2007 benchmark edition [6]. For this reason, in the 2009 edition, it was chosen to make clear if, and how much, a simulation code can properly manage this problem [7,8].
For 2011 benchmark, as suggested by 2009 ICEB participants, a hollow profile with two seam welds, critical tongues and material flow balancing by means of feeders was developed. The press load, the thermal evolution in the die (six different locations), the temperature of the profile, the profile speed and the die deflection were selected as critical parameters for experimental monitoring. Moreover, the quality and the position of the seam welds were analyzed trough tensile tests and microstructure analyses.

Die design

As suggested by 2009 ICEB participants, a hollow profile with seam weld generation, different material flows and the computation of die stresses was the starting reference for die design: the organizers decided to select the profile shape shown in figure 1 with, in addition, different profile thicknesses, in order to induce a more complex material flow for the FEM computation. When a profile shape with very big differences in thicknesses has to be produced through porthole dies, different material flow balancing strategies can be used. In particular, some die makers prefer to balance the material through porthole sizes and position, where others operate by means of variable bearing lengths or pockets. In the designed die (figure 2), both approaches were used for the two openings: for the fully supported profile, variable bearings and a profile pocket were used, while for the partially supported one, a 4mm constant bearing was used and the material flow balanced through the size and position of the two portholes. A first indication that this type of design would provide is which strategy requires less deforming energy, thus allowing faster material flows. A second information is related to the seam weld quality and position: in figure 2 right, it can be seen how each profile is composed by two seam welds generated by big (2b and 1b) and small (2s and 1s) welding chambers. The profile was design in order to be able to extract specimens to be tensile tested across the weld. Then, six holes for thermal monitoring were introduced into the die: two in the legs (T3 and T6) where the material is divided and material seams are generated, two in the tongues next to the bearings (T1 and T4), where the die deflection may alter the friction conditions, and two more very close to the bearings (T2 and T5). Finally, in order to consistently monitor die deflection, two different tongues were introduced: one fully supported and one partially supported

(25 mm less supported, for a total of 33mm depth), the latter condition being critical for the die, as experimentally verified during trials (the tongue broke).

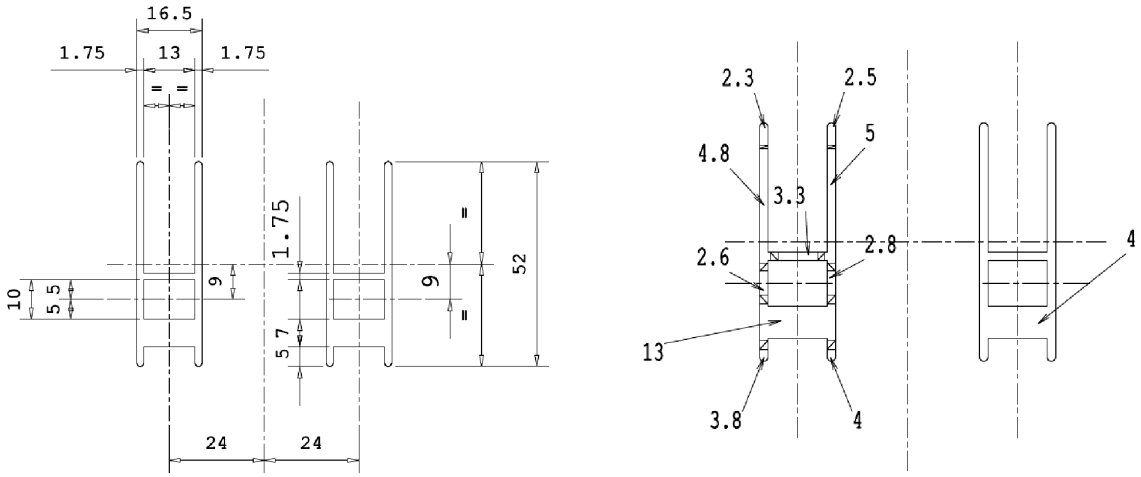

Fig. 1: Profiles dimensions (left) and bearing lengths (right)

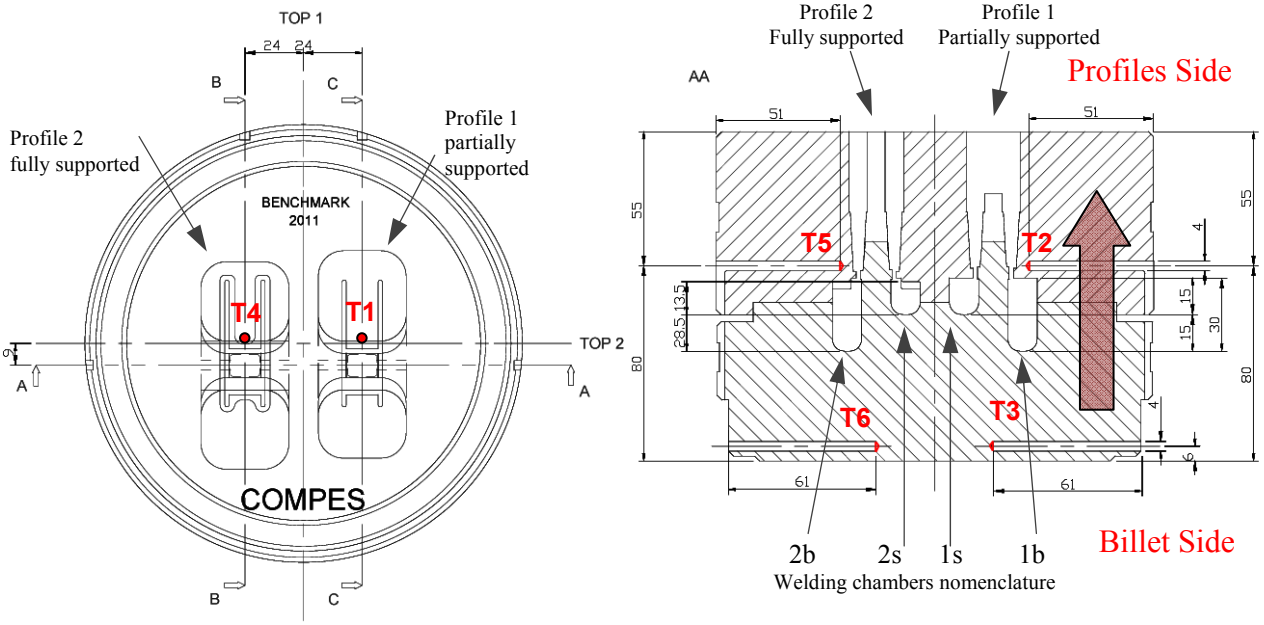

Fig. 2: Feeder shape and thermocouples position

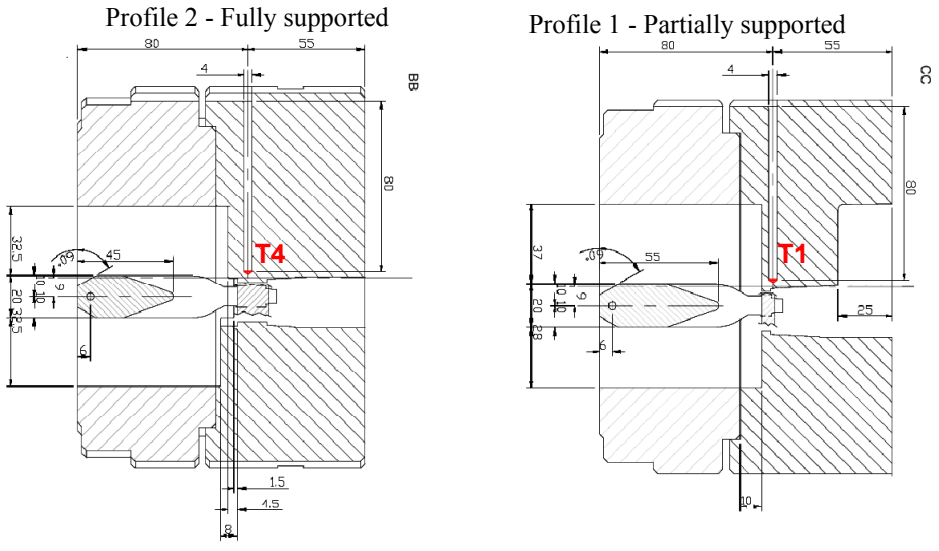

Fig. 3: Die sections and thermocouples position

Indeed, one of the most critical features of extrusion dies are the tongues that are necessarily adopted in the manufacturing of some types of dies; in particular, in the selected die design, the tongues are also weakened by the holes for thermocouples insertion. With this configuration, a higher deflection of the partially supported tongue of profile 1 is expected. The die, built by the die maker COMPES, was made of hot-working tool steel AISI H-11 tempered between 45 HRC and 47 HRC hardness.

Experimental setup and conditions

AA6082 aluminum billets of 140 mm diameter and 300 mm length were used for the experiments. For the whole campaign around 25 billets were used. The experiments were carried out on a 10 MN extrusion press at the laboratory of the Institute of Forming Technology and Lightweight Construction (IUL) of TU Dortmund University. The diameter of the container is 146 mm, so that an upsetting of the billets took place at the beginning of the extrusion process.
The die was initially heated to a target temperature of 420 °C inside the machine. The six thermocouples allowed to measure the die temperature during extrusion, as described. Two thermocouples were additionally required to control the die heating system. The billets were heated up to 550 °C in a furnace. Because of the billet loading procedure, that took about 1 minute, the billet temperature decreased to 520°C before extrusion could start. The temperature of the container was considered as constant and equal to 435 °C due to its high thermal inertia, while the ram temperature, measured with a contact thermometer, was 410°C. The profile temperature was continuously measured through a *Williamson 120* self calibrating pyrometer only on the profile 1 (the partially supported one). This pyrometer works with two different wavelengths so as to calculate the workpiece temperature independently from the material surface emissivity. The detection point was located 140 mm ahead from the die surface, as reported in fig. 4. Detailed information on temperature evolutions are reported in table 1.

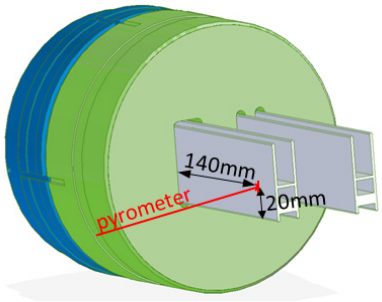

Fig. 4: Pyrometer detection point

A laser velocitymeter was used in order to continuously monitor the profile speed of profile 1 (partially supported). The velocitymeter worked contactless with a laser beam based on the Doppler principle.
The die deflection was continuously measured with two laser beam distance sensors Keyence LK-G402. The sensors operated with the triangulation method and had an accuracy of ±0.05 mm. The working range was between 300 and 500 mm. The application of the laser sensor showed great advantages in comparison to the use of strain gauges or tactile deflection sensors: the laser beam worked without any direct contact with the hot die, it did not require any holes or joining procedure, although providing a continuous measure of the tool deformation. The sensors were mounted on a frame in front of the press without contact to the press to prevent measuring errors which result from the deformation of the press during extrusion (a problem which arose in 2009 edition). In order to consider the deformation of the press, the difference between the deflections of the two tongues is used in the benchmark. Both sensors were arranged at a small angle to the profile direction in the inner area of the profile shape (figure 5). It was necessary to evaluate the exact angle between tool and sensors, to compensate for the diagonal path of the laser sensor. The

positions of the lasers were measured after heating up the extrusion press and the die, in order to eliminate thermal effects. In Fig. 5 on the right, the position where the sensors hit the die tongue is shown by the red reflection points on the die surface.

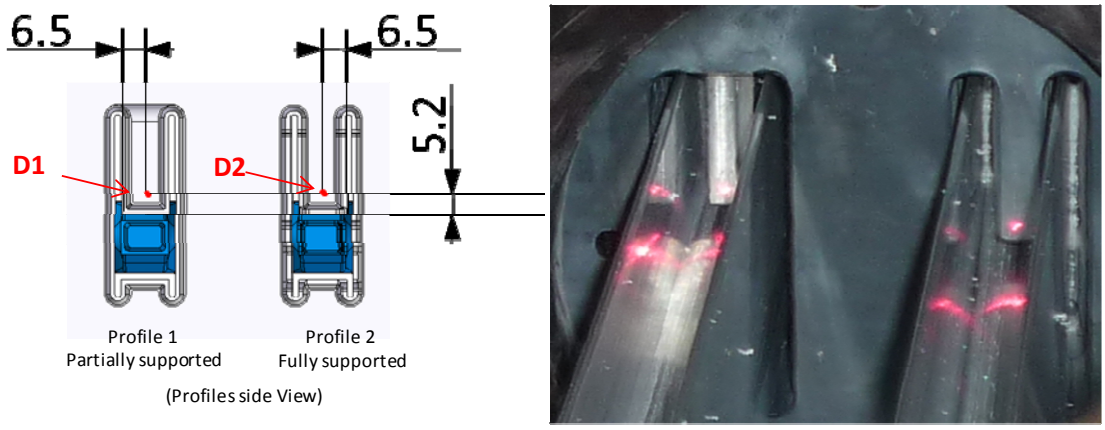

Fig. 5: Position of the sensors on the die

The function principle of the laser sensor is based on the triangulation method (Fig. 6). The distance d1 between laser and die is automatically calculated by the controller of the laser displacement sensor. The angle α was manually determined to be 17.17°. The deformation of the die along the press axis distance d2 can be evaluated by:

$$d2 = d1 * \cos \alpha \quad (1)$$

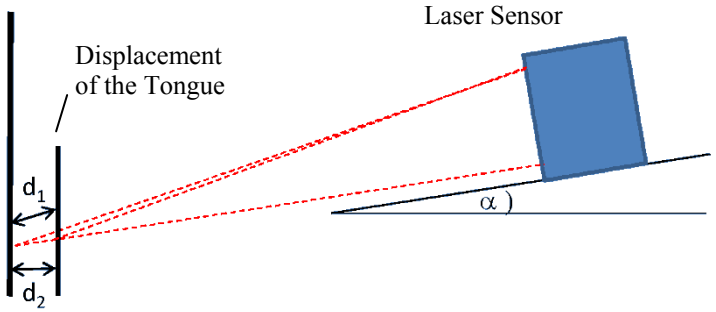

Fig. 6: Determination of the sensors position in relation to the die

The deformation along the press axis will be compared to the simulation results of the FEM codes that will take part to the extrusion benchmark.
In order to achieve steady state conditions, 4 billets were initially extruded. The 300 mm long billets were extruded 290 mm to a final 10 mm butt height with a ram speed of 2mm/sec. It was found that, when a steady state die temperature was reached, a temperature of 460°C for thermocouple T1 (Fig. 2) was found. All experiments were repeated in these conditions: three billets of the same casting batch were extruded under constant processing conditions. Three repetitions were performed to show the possible scattering range of the measured parameters and to evaluate the accuracy of the results.

Results and discussion

In figure 7 the process load and profile temperature over the ram stroke are illustrated: as reference data, the trial n.3 was used, but the values of the repetitions (trials 2 and 4) were also reported as an indication of the scattering. The extrusion force showed the typical trend of direct extrusion, with approximately 8.7 MN maximum load. The initial slope of the curve was very steep in relation to

the condition of the die already filled with aluminum. The temperature of profile 1 is shown in Fig. 7b: it reached a maximum of nearly 530 °C, increasing during the first third of the process. Here, the evolution of the temperature shows that the extrusion is an almost steady process for strokes between 100 mm and 250 mm.

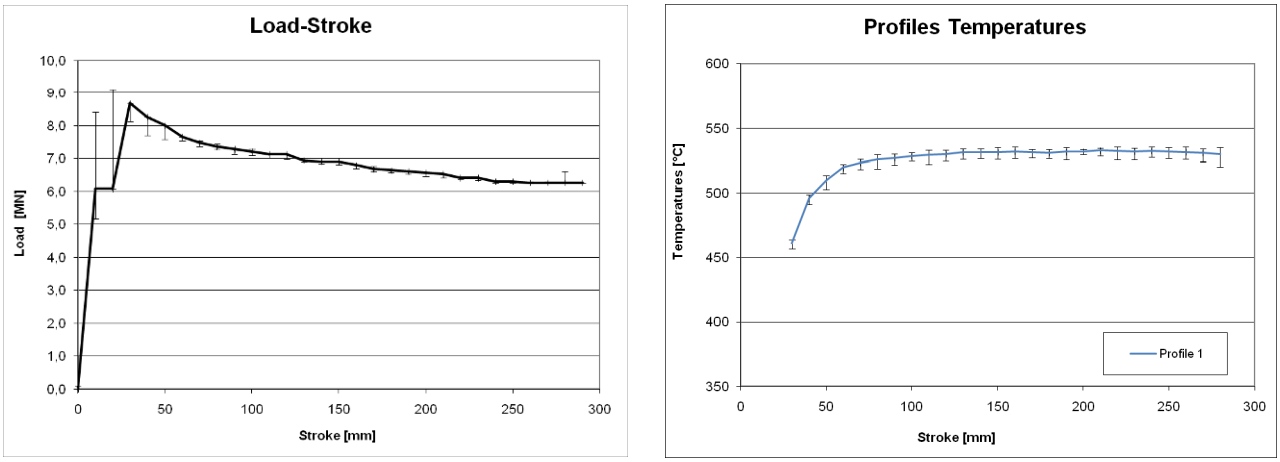

a) Ram force b) Temperature of profile 1

Fig. 7: Ram force and profile temperature

The speed of both profiles is shown in Fig. 7 (left). Profile 1 (the partially supported one) always ran faster because of the much shorter bearing length and correction strategy. In contrast to what is usually considered, the speeds of the profiles were not always constant during the stroke: in all the trials, profile 2 initially ran more slowly compared to profile 1, but after the initial heating up (related to the deformation work) profile 2 started to increase its speed, even though it always remained below the speed of profile 1. The difference in profile speeds can be visualized also in terms of the final profiles lengths: profile 1 was 2575 mm longer than profile 2 (8980 mm compared to 6405 mm) (Fig. 8, (right)).

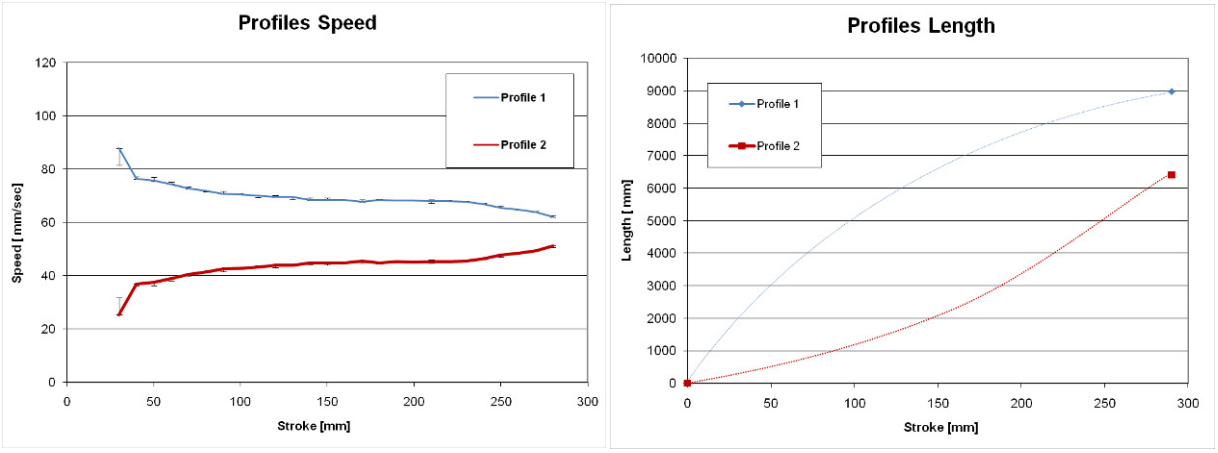

Fig. 8: Profile speeds (left) and profile lengths (right)

In figure 9 (left) the evolution of the die temperatures in the six locations (locations T1 to T6 as illustrated in figures 2 and 3) is shown for the benchmark trials; data distribution can be obtained by the analysis of table 1. During loading, the billet, that is at an initial temperature of 520°C, is kept for 25 seconds in contact with the die face (460°C) without any ram stroke in order to shift the container to its operative position. For this reason, the thermocouples 3 and 6, at 0mm ram stroke, started from a higher value (514°C) compared to T1, T2, T4 and T5 (460°C) located in the bearings. All the thermocouples located in the partially supported profile (1, 2 and 3) recorded higher values, especially at the beginning of the process: the behaviour, in relation to the faster material flow, is

generated by the die design of this profile. Near the end of the stroke, the temperature differences between fully supported and partially supported are lower as a consequence of the decreasing difference in speed (also evidenced in figure 8 left). Thermocouples 3 and 6 (in the bridges) showed a maximum when billet upsetting is ended and the deformation energy produces an increment of the bridge temperature to 532°C for T3 and to 523°C for T6. After this condition, the material, being cooled by the container, (435°C) evidenced decreasing values. In the bearings a similar trend is achieved: only after the upsetting phase the temperature rised (more in the partially supported tongue than in the fully supported one) up to a steady state condition characterized by a higher temperature in the toungues locations in relation to a reduced capacity of heat dissipation.
Figure 9 (right) shows the measured displacement of the tongues: in red for the fully supported (D2), in blu for the partially supported (D1). The absolute displacement of the tongues was approximately 2 mm, including the elastic deformation of the whole press during extrusion. The displacement of the tongue of profile 1 is slightly higher (see scale on the left) than the displacement of the other tongue, caused by the reduced support (25 mm less supported). The difference of these displacements is illustrated in figure 9 (right) by the green dashed line, with the scale on the right side of the diagram. As a mean value for such difference, a deflection of about 0.1 mm was determined.

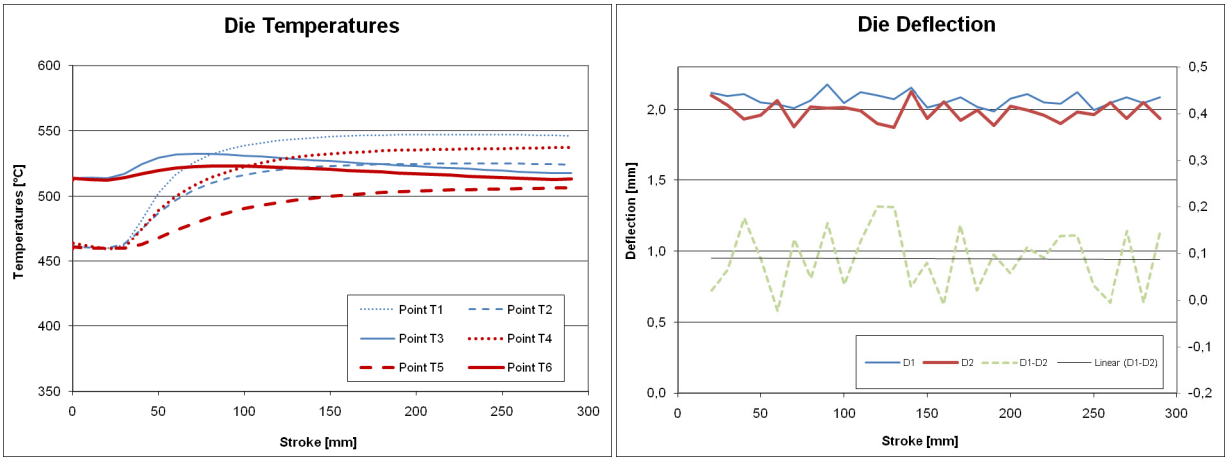

Fig. 9: Die temperatures (left) and elastic deformation of the tongues (right)

An overview of all recorded data is shown in table 1, where the data for the repetition of the billets 2 to 4 are evidenced.

Table 1: Temperature data and results for the extrusion benchmark

Billet No.	**Ram Speed [mm/s]**	**Die Temp. [°C]**		**Max. Profile Temp. [C°]**	**Max. ram Force [MN]**	**Profile Length [mm]**	**Max. Deformation [mm]** ±0.06
2	2	Start T1 461 T2 461 T3 514 T4 459 T5 459 T6 512	End T1 547 T2 526 T3 518 T4 539 T5 506 T6 514	530	9.09	Profile 1: 900 Profile 2: 640	Profile 1: 2.599 Profile 2: 2.432
3	2	Start T1 460 T2 460 T3 514 T4 459	End T1 546 T2 524 T3 518 T4 537	528	8.79	Profile 1: 898 Profile 2: 640.5	Profile 1: 2.316 Profile 2: 2.217

		T5 459 T6 512	T5 506 T6 513				
4	2	Start T1 459 T2 459 T3 511 T4 458 T5 459 T6 509	End T1 545 T2 524 T3 516 T4 536 T5 505 T6 512	532	9.13	Profile 1: 897 Profile 2: 632	Profile 1: 2.434 Profile 2: 2.258

Profiles were then analyzed in terms of localization of the seam welds and of welds resistance. Figure 10 shows the nose of the two profiles (front and back), while figure 11 illustrates the section of the profiles from billet 3 grinded and etched. In figure 11, it is possible to notice that the welds of profile 2 are slightly below the bridge location while the ones of profile 1 are very shifted towards the bottom part of the profile, this being in relation with different material speed in the feeders. Similar considerations can be done by analyzing the nose of the profile, although the position resulted even different in relation to the lack of steadiness of the process.

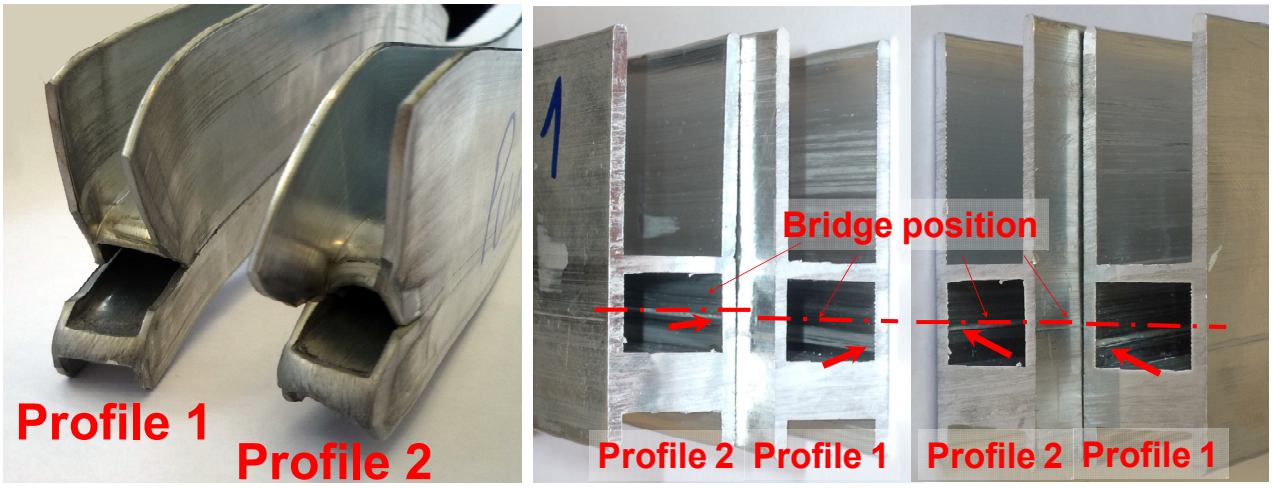

Fig. 10: Pictures of the nose (front and back) with evidenced the seam welds respect to bridge localization

Tensile tests were then performed on specimens extracted from profile 1 (partially supported) and profile 2 (fully supported), from both sides (small and big welding chambers), respectively. Four conditions were thus analyzed (1s, 1b, 2s and 2b) with 5 repetitions for each condition as shown in figure 11. Elongation at fracture was selected for the comparison, because it provides a more clear classification of the welds quality [9]. Figure 12 summarizes the results of elongation at fracture of the welds in the four conditions: a good quality was generally found, this being evidenced by a mean elongation at fracture of 14%, in line with that required by the standards for AA6082 alloy (13%). As a classification of the welding quality, it is possible to notice that profile 1 (feeder corrected) realizes slightly better weld quality with respect to the bearing corrected one. On the other hand, in term of welding chamber size, differences are even lower and only in profile 1 bigger welding chamber produces a weld with a higher elongation.

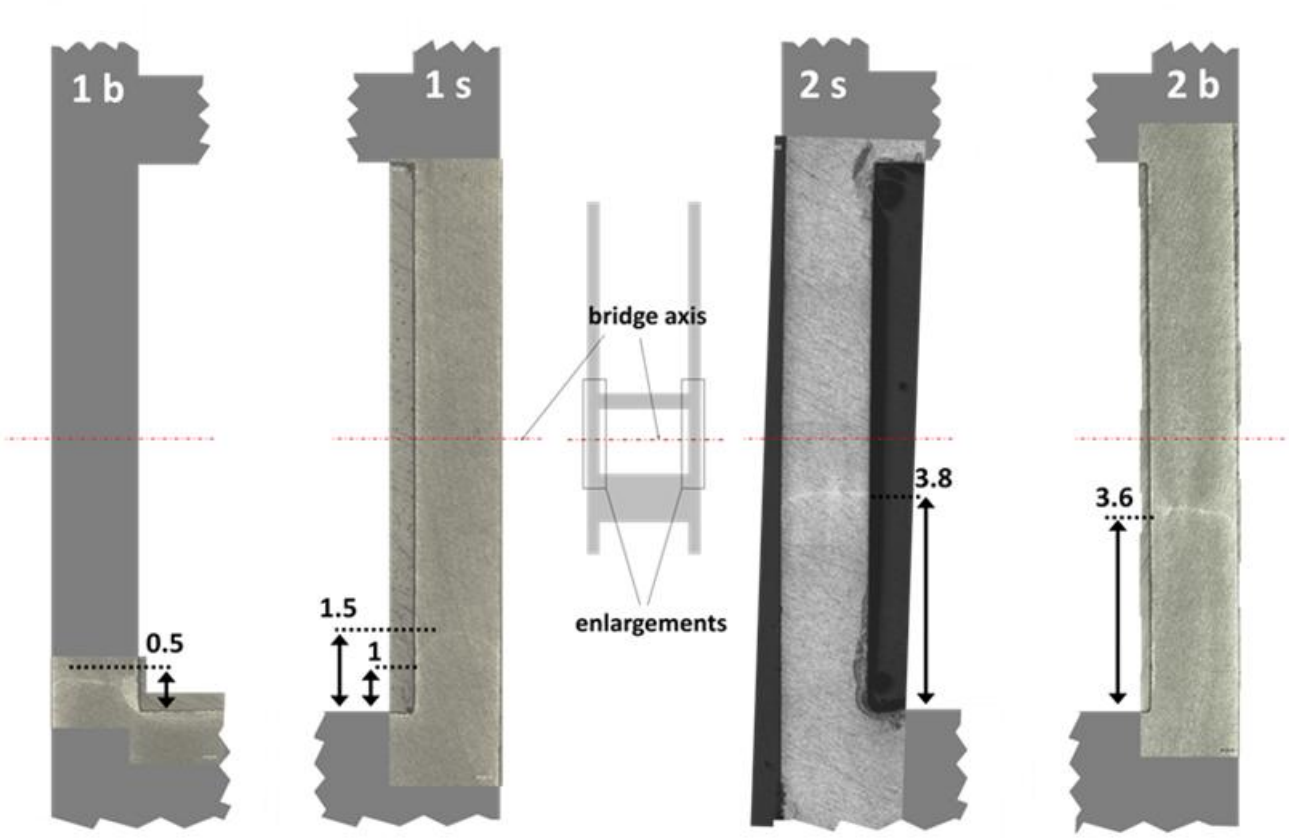

Fig. 11: Section of the profiles from billet 3 showing the position of seam welds [mm]

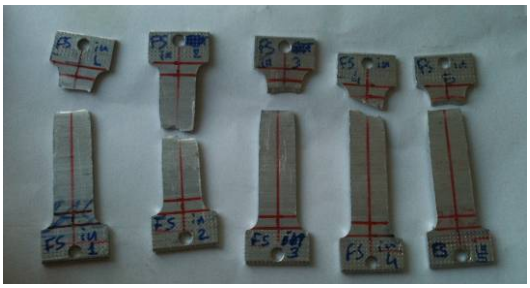

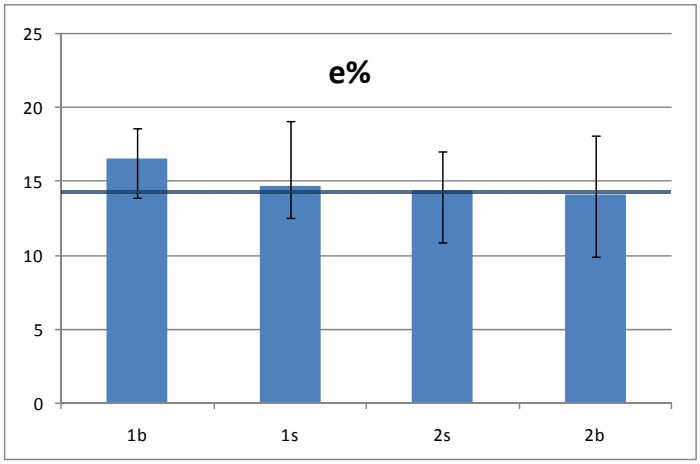

Fig. 12: Elongation at fracture of the specimens (5 repetitions for each condition).

Conclusions

An experiment for evaluating FEM codes accuracy in predicting extrusion load, profile temperature, die thermal fields, material flow, die deflection and seam weld quality was designed and performed under strictly monitored conditions. Two hollow profiles were simultaneously extruded through a die with two openings with different design strategies each. The input conditions as well as the acquired data were presented and discussed. The profile, that was balanced by porthole size and position, produced the highest speeds and temperatures. Profile speeds were continuously recorded, evidencing variable speeds along the process stroke. The monitoring of die deflection showed a greater displacement of around 0.1mm for the profile 1 tongue in relation to the less supported conditions. Finally, concerning the seam weld quality, the elongation at fracture of the four welds

was evaluated and a general good quality was found; the big welding chamber of profile 1 produced higher elongations, while the others showed almost the same deformability.

Acknowledgements

This paper is based on investigations of the subproject A1 - "Multi-Axis Curved Profile Extrusion" of the Transregional Collaborative Research Center/Transregio 10, which is kindly supported by the German Research Foundation (DFG). The authors would like to thank COMPES, Italy for die manufacturing and Trimet, Germany for billet supplying.

References

[1] T. Kloppenborg, M. Schikorra, M. Schomäcker, A. E. Tekkaya: *Numerical Optimization of Bearing Length in Composite Extrusion Processes*, In: Proceedings of International Workshop and Extrusion Benchmark, Bologna (Italy), Key Engineering Materials Vol. 367, 2008, pp.47-54.

[2] M. Schikorra, L. Donati, L. Tomesani, M. Kleiner: *The role of friction in the extrusion of AA6060 aluminum alloy, process analysis and monitoring***,** In: Journal of Materials Processing Technology, Volume 191, Issues 1-3, 1 August 2007, pp. 288-292

[3] L. Donati, L. Tomesani, M. Schikorra, A. E. Tekkaya, "*Extrusion Benchmark 2007 – Benchmark Experiments: Study on Material Flow Extrusion of a Flat Die"*, Proceedings of the Extrusion Workshop and Benchmark, Key Engineering Materials Vol. 367 (2008) pp. 1-8

[4] T. Mori, N. Takatsuji, K.Matsuki, T.Aida, K.Murotani, K.Uetoko: *Measurement of pressure distribution on die surface and deformation of extrusion die in hot extrusion of 1050 aluminum rod,* Journal of Materials Processing Technology (2002), p421-425.

[5] W. Assaad, H.J.M. Geijselaers, J.Huétink: *3-D numerical simulation of direct aluminum extrusion and die deformation* (Extrusion Technology, Orlando 2008).

[6] N. Ben Khalifa, A. E. Tekkaya , L. Donati, L. Tomesani,: *Extrusion Benchmark 2009 – A Step Ahead in Virtual Process Optimization*, in Light Metal Age, April 2009, pp. 54-55.

[7] D. Pietzka, N. Ben Khalifa, L. Donati, L. Tomesani, A. E. Tekkaya. (2010). "*Extrusion Benchmark 2009 - Experimental analysis of deflection in extrusion dies*". Key Engineering Materials. vol. 424, pp. 19 - 26.

[8] L. Donati, L. Tomesani, N. Ben Khalifa, A. E. Tekkaya "*ICEB 2009, Dortmund: International Conference on Extrusion and 3rd Extrusion Benchmark*" in Light Metal Age, September 2009, pp. 20-23.

[9] L. Donati, L. Tomesani, "Seam Welds in Hollow Profile Extrusion: Process Mechanics and Product Properties", Materials Science Forum Vols. 604-605 (2009) pp 121-131;

Effect of liquid nitrogen die cooling on extrusion process conditions

Lorenzo Donati[1,a], Antonio Segatori[1,b], Barbara Reggiani[1,c], Luca Tomesani[1,d], Pietro Alfredo Bevilacqua Fazzini[2,e]

[1]University of Bologna, DIEM Department, Viale Risorgimento 2 – 40136 Bologna (Italy),

[2]Compes S.p.A., Via Castegnato, 6/C - 25050 Rodengo Saiano Brescia (Italy),

[a]l.donati@unibo.it; [b]antonio.segatori2@unibo.it; [c]barbara.reggiani4@unibo.it; [d]luca.tomesani@unibo.it, [e] pietroalfredo.bevilacqua@compes.com

Keywords: extrusion, dies, nitrogen cooling, process monitoring.

Abstract. In the paper, a die for the production of a complex hollow profile made by AA6060 alloy on an industrial 2500 ton press has been manufactured and tested under strict monitored conditions. In particular 5 thermocouples were placed in proximity of interesting positions inside the die: 3 next to the bearings and two near the welding chambers. A self-calibrated pyrometer was used for the temperature monitoring of profile. Press loads, ram speeds and container temperatures were continuously recorded directly from the press system. Six billets were initially extruded in order to reach a steady state condition being the last three used as industrial benchmark for the 2011 edition of the ICEB conference. Then the nitrogen was completely and partially opened and the evolution of the temperature in the die and in the profile recorded together with the process load. The effect on bearing temperature was extreme, in particular in proximity of nitrogen inlet, while almost no change in welding chamber thermocouples and in the process load was revealed.

Introduction

Temperature control during aluminum extrusion is today a mandatory activity in order to produce defect-free profiles and for optimizing process productivity. Indeed, defects related to too low or too high profile exit temperatures are well known thus requiring an optimization activity for any new dies [1,2]. With the aim of reaching maximum production rates with sound production, narrow processing windows have to be identified [3]. While in the past years, temperature monitoring was mainly limited to billet pre-heating temperature (or temperatures in case of taper heating), die pre-heating and container temperatures, in the recent years many extrusion companies installed on their presses pyrometers for the contactless monitoring of profile temperature along the whole profiles production. By analyzing the data acquired trough pyrometers, many companies realized how many defects are related to excessively high exit temperature thus limiting production rates and consequently productivity. One option for lowering exit temperature is to reduce billet pre-heating temperature. However on the one hand this action produces higher press loads and consequently higher stresses of the dies (with a related risk of die failure); while on the other hand it produces only limited speed increasing in relation to a strong dependency of the profile temperature with production rates [4]. Another option is the isothermal extrusion [5], where exit profile temperature is controlled by a retroacted variation of ram speed: the speed of the ram is increased or decreased as a function of the temperature monitored by the pyrometer on the profile. A further option is to limit the temperature of the profiles in the hottest point of the process, the die bearing: here the profiles expires the highest temperatures, strain and friction conditions before exchanging heat with the air or the quenching media, thus producing the most critical conditions for defects occurrence. In the last decades, systems for bearing cooling through gas or liquid nitrogen have been presented and installed on some extrusion plants but mainly without a reliable profile temperature monitoring system, without nitrogen flow control systems or without methodical investigations on die channel design thus producing unclear effects and limited advantages. In recent years the reduction of costs for profile temperature monitoring and of the nitrogen control, combined with the market imposition of increasing production rates, have led many companies to revaluate the die cooling

systems, in particular with the use of liquid nitrogen [6,7,8]. The applications of the liquid nitrogen cooling add consequently other important key-parameters for the die design optimization: the position and shape of the nitrogen channels and the selection of the positioning of inlet and outlet channels. Aim of the activity described in the paper is to monitor the evolution of thermal and process parameters of a critical case study on an industrial press. The temperatures of the profile and of the die in five locations (three points in the bearings, two in the welding channels) together with press load and ram speed were continuously acquired. Ten billets were extruded with and without the use of nitrogen cooling thus providing detailed information on cooling efficiency, on effect of cooling on profile temperature and press loads. Moreover information for die cooling channel design and inlet position are presented and discussed.

Experimental investigation

A single complex multi-hollow profile with 65,97 extrusion ratio has been selected for the experimental trials (figure 1); the profile was chosen in relation to the requirements of aesthetical quality on the external flat surfaces thus being very critical for this type of die. The temperature evolution over the profile surface is indeed very important in order to select the proper production rate. The porthole die is composed of three parts as reported in figure 2: the mandrel, the die and the backer with the nitrogen cooling channel. From cooling channel, transferring holes (figures 2b, 3b and 5) convey the nitrogen on the profile surface thus allowing a gaseous cooling of the profile surface and some protection towards high temperature oxidation.
The mandrel is composed by 5 portholes thus generating 5 seam welds under the bridges and 3 more seam welds in the inner square features of the profile. Two thermocouples were placed in the mandrel (thermocouples 2 and 4 in figure 3 and 5) at 20mm far from welding chamber wall.
The die is manufactured in a single piece and the material flow is correct through pockets and variable bearing lengths. Holes of 5mm diameter were drilled in the die for transferring nitrogen from cooling channels to profile surface. Three thermocouples (1, 3 and 5 in figure 3 and 5) were used in order to monitor temperatures of the die; thermocouples 1 and 3 were placed at 13mm far from the bearings while thermocouple 5 at 16mm. A nitrogen channel of 6,1 mm wide and 2mm deep was placed in the backer as reported in figure 2c) and 5 and connected to the profiles throughout holes in the die as described before; in figure 2c) is possible to check also the position of the inlet of nitrogen cooling on the right side of the die when observed from the profile point of view (left side if billet view is considered). The cooling channel is also located at 37mm far from the bearing in extrusion direction (figure 3b) but it follows the profile shape with a lower definition of profile details (figure 5) thus generating different radial distance respect to bearings; in this way the several parts of the profiles are located at different distance from cooling channels thus generating dissimilar cooling in profile parts. K-type thermocouples of 1500mm length and 1 mm diameter were used for the thermal monitoring and the data were continuously acquired by means of an Agilent acquisition system connected to a laptop (figure 4). A Williamson PRO 120 self-calibrating pyrometer placed out of the press, continuously recorded profile temperature at a distance of 1660mm out from die face as reported in figure 1b) and 4a). Ten AA6060 billets were deformed at 2,71mm/sec of ram speed during the trials: three billets were initially extruded for homogenizing the temperature of the system without the use of the nitrogen, then three more billets were processed in the same conditions in order to evaluate the repeatability of the acquired data and finally four billets were extruded with the use of nitrogen die cooling. A conical taper was applied during billet heating along billet axis thus producing an output temperature gradient of 499-445°C (front-back) in the billet; a temperature of 427°C and 413°C was recorded for container and ram respectively while a die pre-heating of 490°C was set thus producing an average die temperature of 480°C after loading in the press. The 3D geometries and the detailed process parameters are available for download at ICEB conference website [9] under the benchmark page, industrial benchmark experiment.

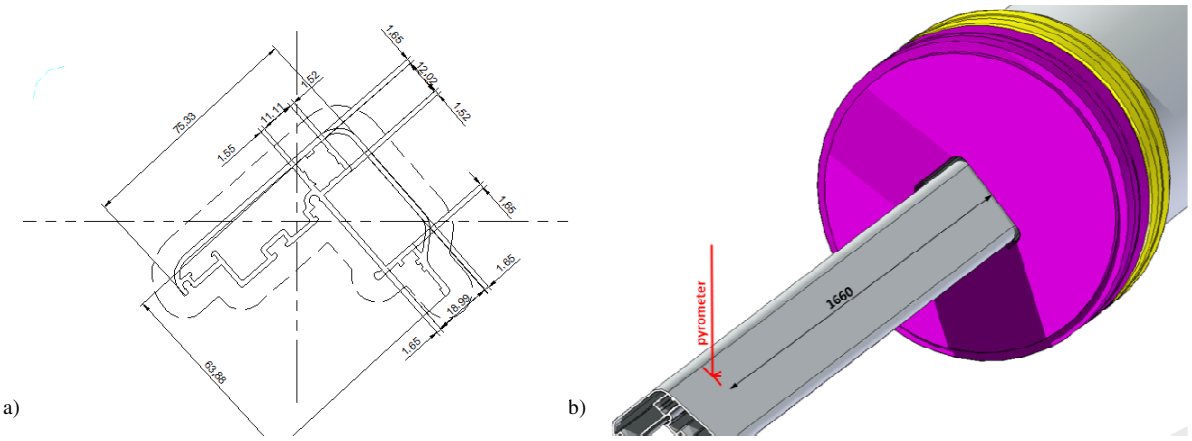

a) b)

Figure 1: a) Profile shape billet view and b) run out position at the press.

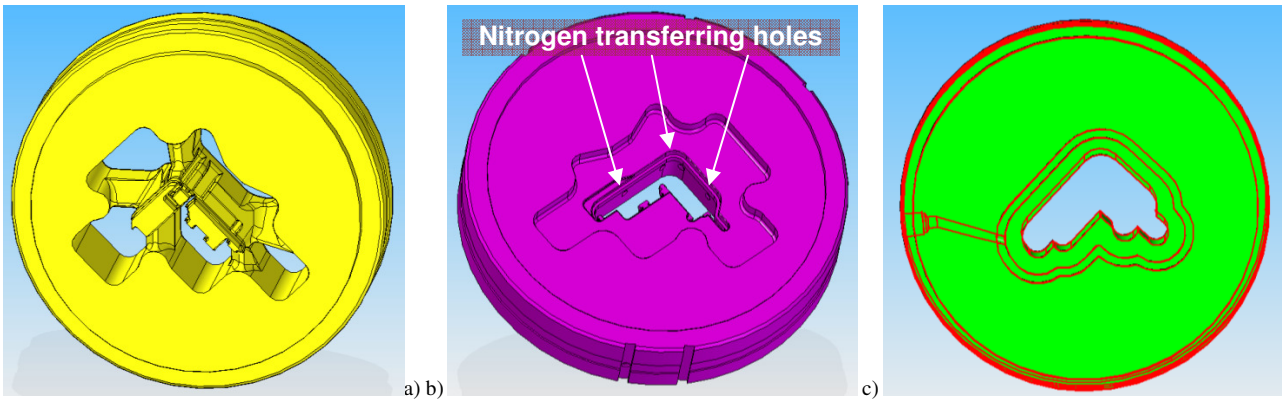

a) b) c)

Figure 2: Porthole die: a) Mandrel, b) Die, c) Backer and nitrogen channel

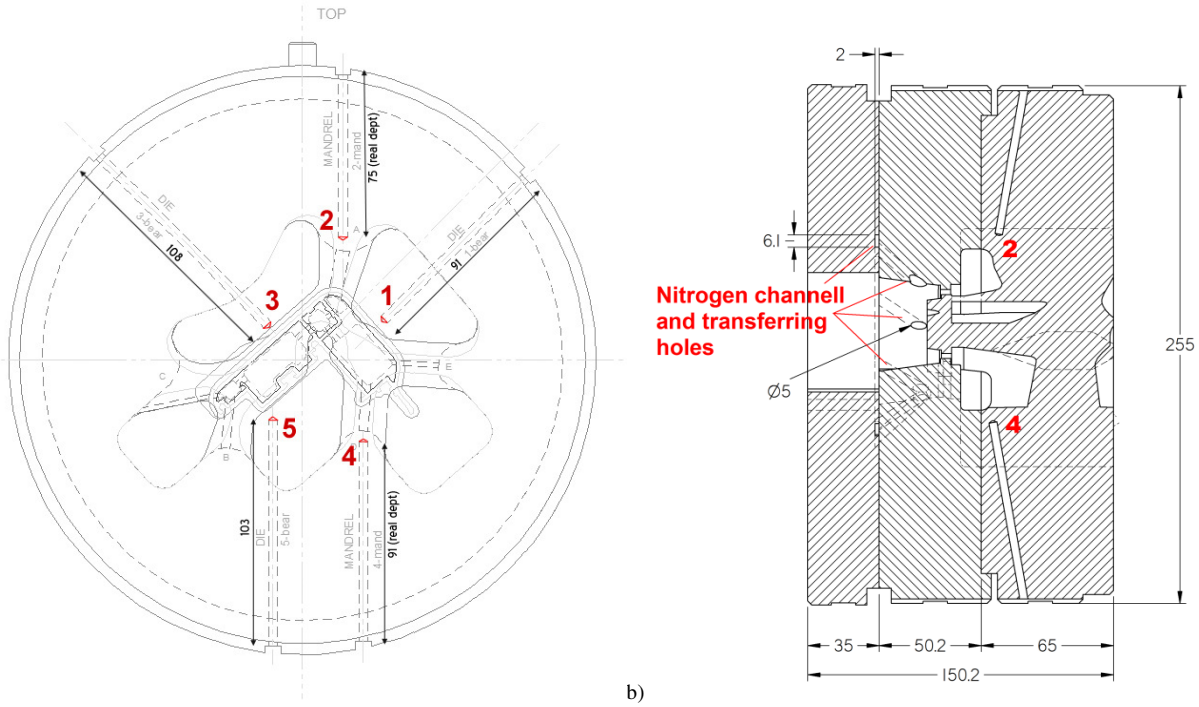

a) b)

Figure 3: Thermocouples and nitrogen device in the mandrel, die and backer: a) billet view, b) section view.

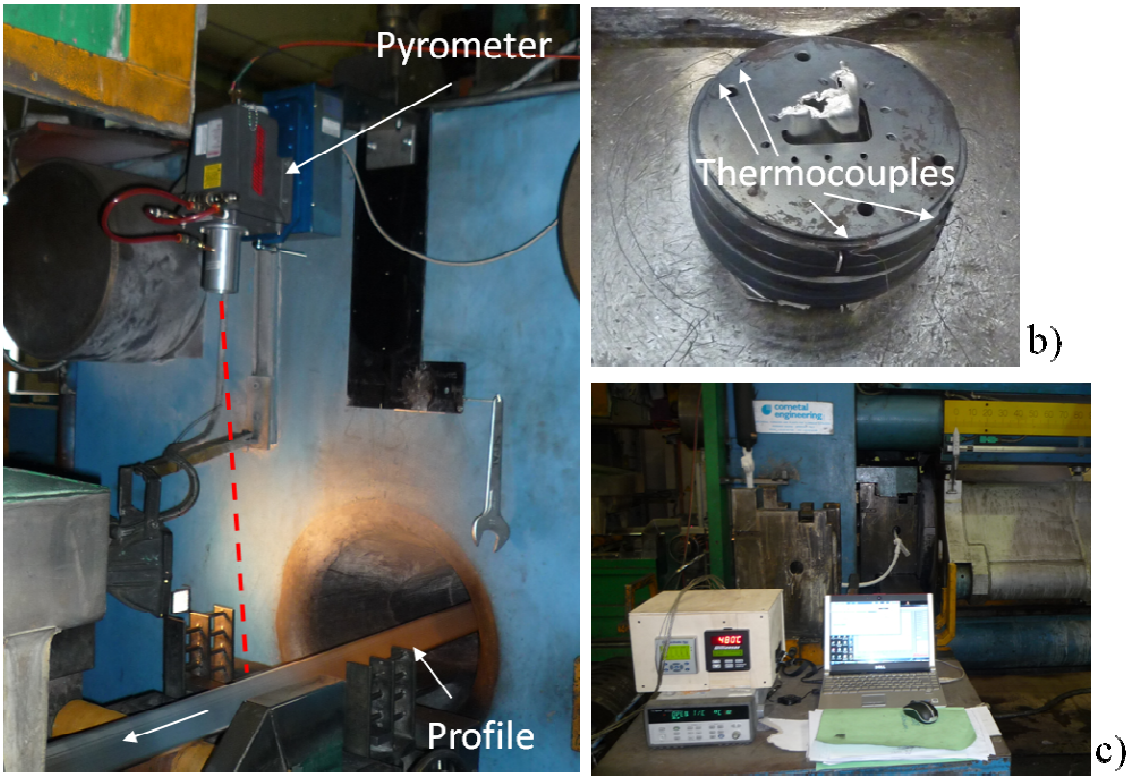

Figure 4: Temperature monitoring devices: a) profile pyrometer, b) die thermocouples, c) acquisition devices.

Results and Discussion

Figure 6 reports the thermal evolution of the die (thermocouples 1 to 5) and of the profile (pyrometer) during the trials while figure 7 reports the recorded press load. During the initial 800 seconds the thermocouples were plugged to the system, the die loaded into the press and the first billet extruded. As usually happen in industrial plants, the first billet stroke (time 500 to 800 sec) is divided in two parts: initially the profile was extruded at a reduced speed up to the puller position, then the ram was stopped (time=600sec), the profile engaged into the puller then the extrusion started again with the selected process parameters (2,71mm/sec ram speed). During the stop, temperatures decreased both in the die and in the profile as result of the heat transfer with the tools and the air. The stop is also clearly visible in the load-stroke diagram of figure 7; by analyzing the press peak load it is also evident that the initial speed was lower than the target one. Then the second and the third billets were processed in the time 800-1100 sec and 1100-1400sec respectively: the load reached its maximum level of 2.000 tons in the second billet in relation to the lower temperatures of the process not yet at the steady state condition. Indeed, from billet 1 to 4 it is possible to notice a constant increase of the temperatures both for the die (510 to 515°C for the thermocouple 1) and for the profile (550 to 560°C). From billet 4 the process can be considered stationary so billet 4, 5 and 6 were used as benchmark conditions (industrial benchmark [9]). When steady state condition was reached, it is possible to notice that the maximum temperature, as expected, was located in the profile with values higher of 40°C respect to the die temperatures. During each steady state stroke, profile temperature initially increased then decreased at the end of the stroke: within a stroke the difference between maximum and minimum profile temperature is extraordinarily low with values lower than 15°C within each stroke, thus meaning that the taper heating of the billet is properly applied and the set temperature of the container (427°C) contributes to cool down the profile on this particular die shape. A similar behavior is found also for the die temperatures: initially temperature rose to a peak then colder material arrived reducing the measured values. In particular it was found that thermocouple 4 located in the mandrel always expired the highest temperature, then thermocouples 3, 2 and 1 reported comparable values while thermocouple 5 (the most distant from the bearings) always reported minimum temperature.

Anyhow, it is possible to notice that differences of temperatures up to 20°C (505-525°C) can be found within the same die and, in our experience on different dies, it is possible to detect even much bigger gradients. In term of process loads almost no differences can be found between billets 3 to 6.

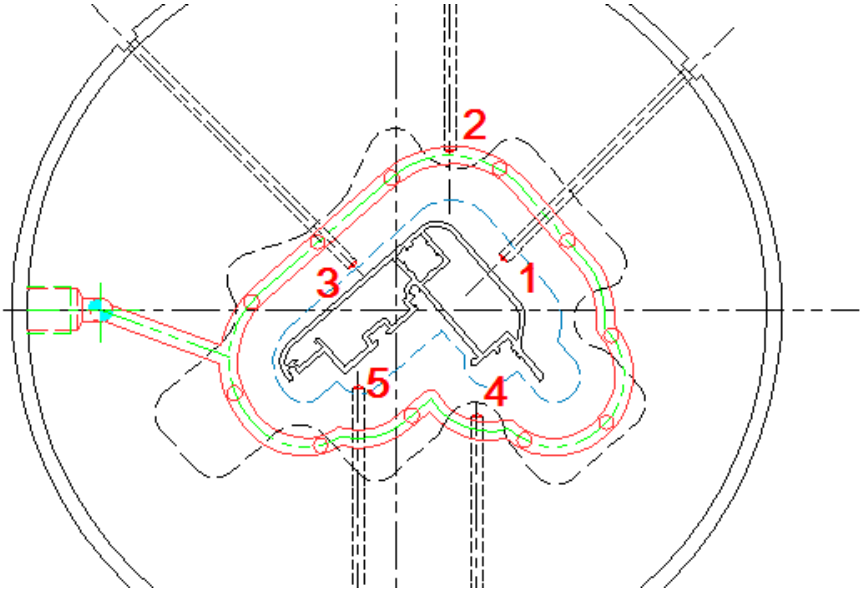

Figure 5: In plane view of profile, thermocouples location and nitrogen cooling channel (billet view).

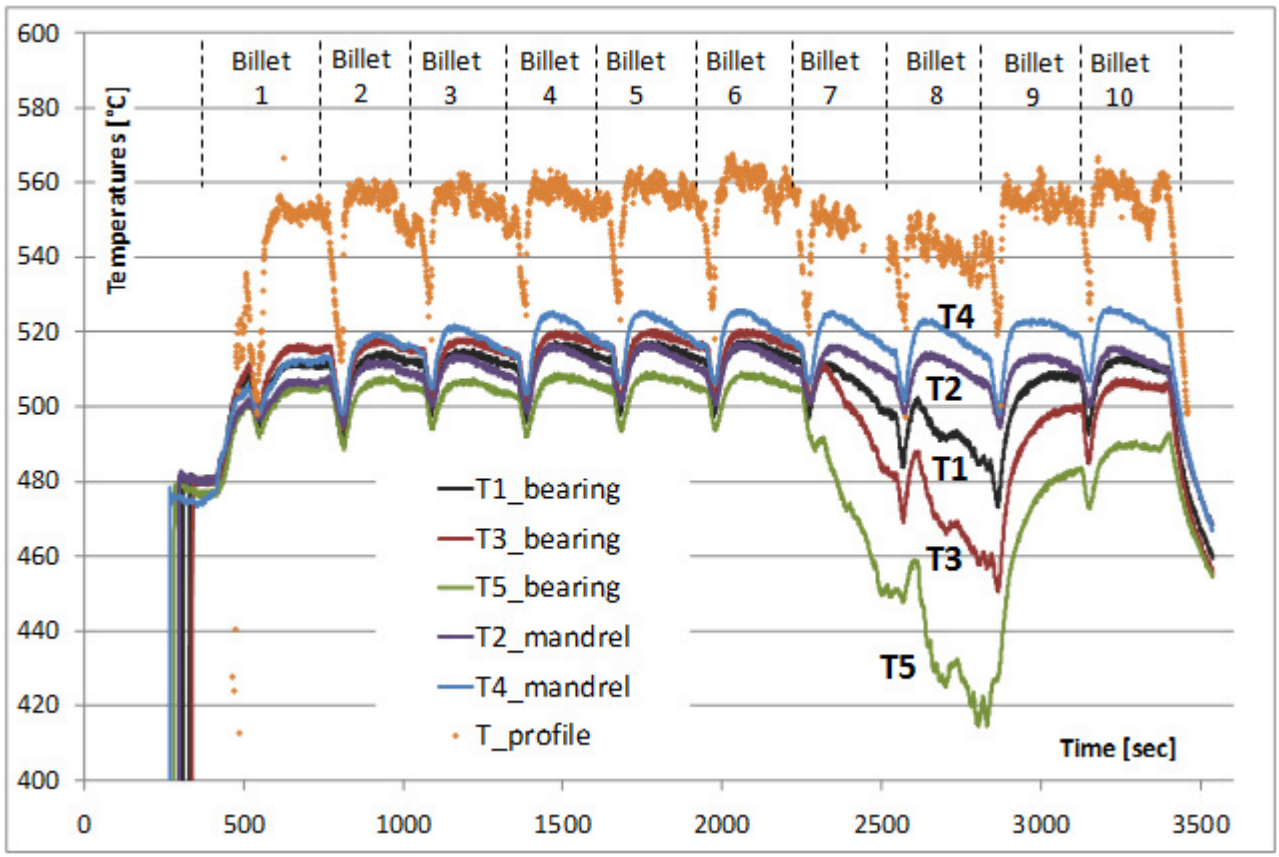

Figure 6: Temperature history of the thermocouples in the mandrel and in the die over the experimental testing time.

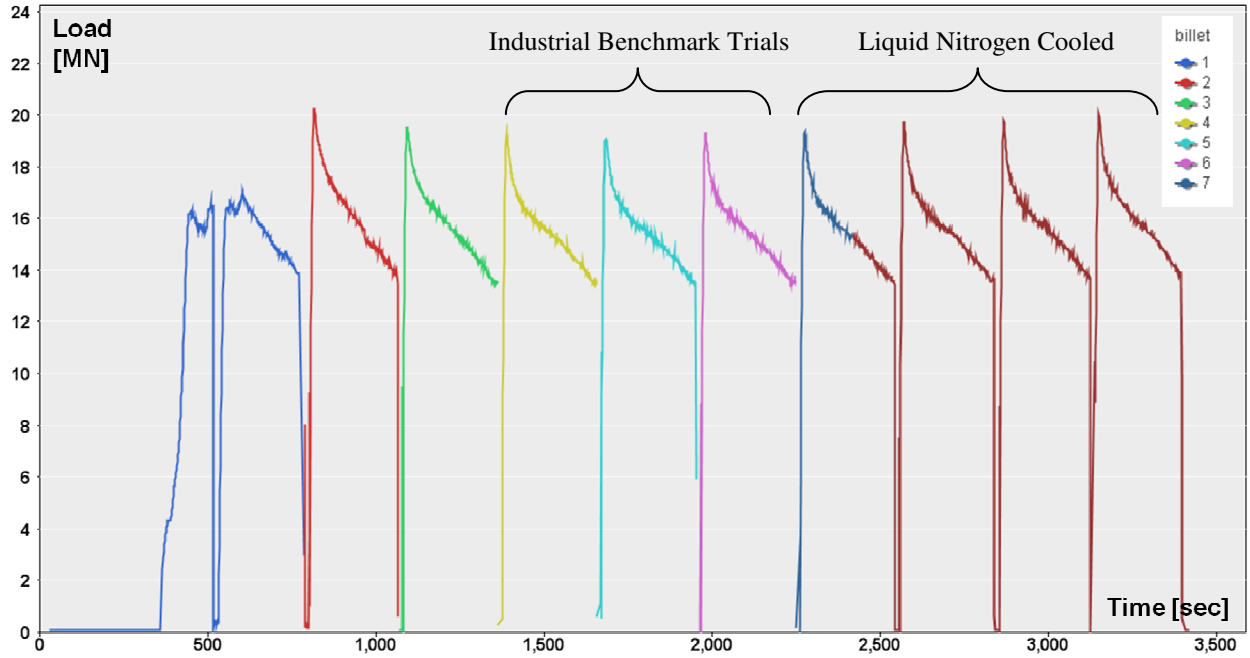

Figure 7: Press loads over the experimental testing time

Before extruding billet 7, the liquid nitrogen was completely opened: it is immediately visible a very marked reduction of die temperature (figure 6) strongly related to thermocouples locations (figure 5) while those located into the mandrel expired no difference respect to trials without liquid nitrogen. Moreover it is interesting to notice that the cooling channel is located at 37mm far from the bearings in the extrusion direction (figure 3b), being located in the interface between die and backer. The strongest reduction happened in proximity of die inlet (sensor 5): this is probably also in relation with the shape of inlet channels that promotes a higher nitrogen flux in the bottom part of the die; the second most sensitive location is thermocouples 3 that expires a reduction lower than thermocouples 5 but still significant. The less sensitive location is the thermocouple 1 as consequence of the combined action of the greater distance from inlet and of the dissipation of liquid nitrogen flux trough profile transferring holes. Moreover it is not clear if the nitrogen remains in the liquid phase along the whole cooling channel or if the location 1 is cooled only by a less efficient gas phase. During the extrusion of billet 7, the reduction of temperature is remarkable: at the end of the stroke a temperature of 450°C respect to 505°C of the previous trial was found for thermocouple 5; cooling effects were found also for thermocouples 3 and 1 (both on bearings) although with a reduced extent (30° and 20°C degrees respectively) in relation to the localization in the cooling channel. As a matter of fact, the shape of the liquid nitrogen channel and the localization of inlet and outlet strongly influenced the entity of the cooling in the different parts of a die. Billet 8 was extruded with the same condition of trial 7 and, despite of a slight initial rise of temperatures at the beginning of the stroke, temperatures still fell down to 420°, 460° and 480°C for location 5,3 and 1 respectively.

As consequence of die temperature decreasing, also profile temperature decreased even if of a lower extent: a reduction of 15°C in the measurement location was found for billet 7 and of 20°C for billet 8. Such decreasing was recorded by the pyrometer in the monitored locations that corresponds to a die location between thermocouples 1 and 3. It is worth noting that such reduction of temperatures generated no changes of extrusion load thus without influencing what happen to the material in the die filling and most likely also in welding.

Before starting the extrusion of billet 9, nitrogen flow was reduced to 30%: temperatures immediately rose again to higher values even though a temperature steady state condition was not reached in the die during billet 9. Also profile temperature rose again to temperatures of 10°C lower respect to un-cooled condition. A nitrogen flow of 20% was used for billet number 10: thermocouple 1 expired a temperature comparable to un-cooled condition while thermocouples 3

and 5 lower values. On the profile, such reduction generated conditions comparable with billet 6 ones. Also for billet 9 and 10 no changes in extrusion load was found.

The effect of liquid nitrogen on die cooling is extremely relevant: very high decreases of temperatures (up to 100°C) are obtained within the die thus generating in the monitored trials reduction up to 20°C on the profile. It is very important to notice that such cooling affects only backer and bearings while no change in temperatures are obtained in the welding chambers as well as in process load. In particular, die thickness and channel design result very critical for an efficient cooling system design. Thick dies reduce the effect of cooling (cooling position is shifted far from bearings) as well as the shape of cooling channel respect to the real detailed profile shape. Moreover, the positioning of nitrogen inlet in the channel and channel dimensions and shape strongly influence the cooling efficiency in the several part of the profile. An oriented die design is thus required in order to optimize die efficiency and also finite element simulations may support die design procedure in order to avoid thermal shocks or to optimize distances between cooling channel and bearings.

Conclusions

In the present work, a strict monitoring of an industrial die was performed in order to verify the influence of liquid nitrogen cooling on process conditions. It was found that, with un-cooled die, steady state condition is generally reached after only 4 billets and that profile temperature was higher respect to die temperature of 40°C. Trials 4 to 6 were used for the industrial benchmark at the 2011 edition of the ICEB conference. When liquid nitrogen cooling was used, a big decrease of die temperature in proximity of die channels was found. In particular three aspects resulted very critical for liquid nitrogen cooling:

- Channel shape and position: the thickness of the die (i.e. distance from bearings to cooling channel), the shape of the channel in relation to the profile shape, the dimension of the channel and of the transferring holes as well as their position strongly influence the cooling effect on the profile surface and consequently the process efficiency;
- Positioning on inlet: if a single inlet is used the nitrogen produces unbalanced cooling rates between inlet and the other extremity; moreover the nitrogen may change its phase during the path thus producing a less remarkable cooling effect at location far from inlet;
- Liquid nitrogen flow rate: the changes of flow rates deeply influence die cooling efficiency and consequently final profile temperature.

A reduction of profile temperature up to 20°C was reached in the monitored profile location when die temperature was reduced in a comparable location of 60°C. No rupture occurred in the die although thermal stresses have to be carefully considered in die design with nitrogen cooling channels. A great effort is needed in order to design nitrogen cooled dies because all the presented and discussed parameters have to be evaluated and optimized.

Acknowledgments

Authors would thanks Sepal management for the opportunity to perform the experiments on their plant and all the employees for the great support and patience during the trials. In particular authors would thank eng. Angoscini for the effort provided during the trials planning and execution.

References

[1] Parson, N.C., “Surface Defects on 6xxx Alloy Extrusions,” Proceedings of the 6th International Extrusion Technology Seminar, 1996, Vol.1, 57-67.

[2] Matienzo, L.J.; Holub, K.J.; Vandatta, W. Investigation on surface defects produced during the extrusion of some aluminum alloys. Source: Applications of surface science, n 15, p 307-320, Apr 1982

[3] Donati, L., Tomesani, L."The effect of die design on the production and seam weld quality of extruded aluminum profiles" Journal of Materials Processing Technology (2005) 164-165, pp. 1025-1031

[3] R. Twigg, R. Oesterreich "Extrud-Al^{TM} – An alternative approach to nitrogen die cooling" Proceedings of the 8th International Extrusion Technology Seminar, 2004, Vol.2, 373-376.

[4] J. Zasadziński, W. Libura, J. Richert "Fundamentals of Advanced Aluminum Extrusion Processes" Proceedings of the 8th International Extrusion Technology Seminar, 2004, Vol.2, 391-397.

[6] Stratton, P. Raising productivity of aluminium extrusion with nitrogen, International Heat Treatment and Surface Engineering, v 2, n 3-4, p 105-108, 2008;

[7] Ward, Thomas J.; Kelly, Richard M.; Jones, Gary A.; Heffron, James F.Effects of nitrogen - liquid and gaseous - on aluminum extrusion, Journal of Metals, v 36, n 12, p 29-33, Dec 1984;

[8] Ruppin, Dietrich; Mueller, Klaus, Influence of Mandrel Cooling in the Direct Extrusion of Aluminum Tubing using Stationary or Moving Mandrels. (Einfluss der dornkuehlung beim direkten strangpressen von aluminiumrohren ueber stehenden und mitlaufenden dorn.), Aluminium Dusseldorf, v 58, n 7, p 402-406, Jul 1982

[9] www.ice-b.net

EFFECT OF TOOL COATINGS ON FRICTION BEHAVIOR AND MATERIAL FLOW DURING HOT ALUMINUM EXTRUSION

A. SEGATORI[1], N. BEN KHALIFA[2] ,A. JÄGER[2]
L. DONATI[1], L. TOMESANI[1] ,A. E. TEKKAYA[2]

[1] Dept. DIEM, ALMA MATER STUDIORUM, UNIVERSITY OF BOLOGNA - V.le Risorgimento 2 -40136 Bologna - Italy
l.donati@unibo.it; antonio.segatori2@unibo.it; luca.tomesani@unibo.it
[2] INSTITUTE OF FORMING TECHNOLOGY AND LIGHTWEIGHT CONSTRUCTION (IUL), TU Dortmund University - Baroper Str. 301 - 44227 Dortmund - Germany
andreas.jaeger@iul.tu-dortmund.de, nooman.ben_khalifa@iul.tu-dortmund.de; erman.tekkaya@iul.tu-dortmund.de

Abstract

Two different coatings for extrusion dies (TiC-TiN-Al_2O_3-CVD and TiN-PVD) are compared to the classical uncoated tools in a laboratory scale experiment in order to check the coating influence on process load, material flow and friction. The material flow, and consequently the friction, is investigated by means of visioplasticity techniques, by the insertion of marker rods in the deforming billet. AA6082 billets are deformed at typical extrusion conditions (520°C billet preheating, 5mm/sec ram speed) at three different extrusion ratios The deformed rods pattern of the butt is measured in order to analyze the friction effect. Finally, the test is repeated several times in order to monitor the rate of wear of the coated layers by means of optical microscopy measurements.

Keywords**:** friction, hot extrusion, aluminum, CVD and PVD coatings, tribology.

1 INTRODUCTION

The direct hot extrusion of aluminum alloys is a forming process characterized by high hydrostatic pressures and consequently high friction conditions act at the tool-material interface. To some extent, the high friction can be considered useful in order to limit some problems related to inhomogeneous microstructure distribution inside the billet, but at the same time product defects (like profile cracking or Peripheral Grain Coarsening [1],[2]) that usually appear in relation to the high shear accumulated on the profile surface as a consequence of such high friction. Moreover, the use of lubricants is generally avoided in industrial practice because lubricant may remain embedded as a contaminant in the final extrudate, leading to defects such as blisters, poor seam weld quality.

In latest years, die coating has become a fast growing trend in the die design [3,4,5]: die makers claim that lower exit profile temperatures are obtained in relation to the lower friction, thus leading to higher production rates and die life, but no experimental data have been published on the matter yet . Several papers have been published describing the different coating types and technologies available for forming dies, but no papers

have been presented yet on an accurate comparison of the different coatings for aluminum extrusion tools on the same geometries and specifically on the influence on friction [6,7]. Moreover, the studies already performed on tools used in forging cannot be directly extended to extrusion process in relation to the high temperature and high hydrostatic stresses characteristic of the extrusion process. Indeed the estimated reduction in friction coefficients is usually measured by means of standard tests (ball on disc, ring tests or double cup extrusion) far from the processing and frictional condition of the industrial extrusion [8,9,10]. So far, coatings are today used mainly in the production of large extrudate batches by the use of die inserts in the so called 'bearing zones' (the zones where the final profile shape is generated and wear is noticed first).

In order to clarify the influence of the die coatings on the process tribology, in the paper two different die coatings (PVD and CVD) are compared to the classical uncoated tools on a laboratory scale experiment in order to check the coating influence on process load, material flow and friction. The material flow, and consequently the friction, was investigated by means of visioplasticity techniques: the billets were prepared with rods of a dissimilar alloy then partially deformed; the billet rests were then cut along the rod's plane so as to reveal the final deformed pattern. The billets were deformed at typical extrusion conditions. The peculiarity of such test is related to the specific temperature and pressure field that acts on the billet-tool interface: only this kind of test allows to reproduce the high temperatures and high Pressure/Flow stress ratio typical of the extrusion process.

2 EXPERIMENTAL

Experiments were performed at laboratory scale on a tensile-compression test press ZWICK250 with a maximum load of 250kN. Containers and dies were designed purposedly for these experiments (Figure 1): a tool set (container and die) was produced uncoated so as to reproduce standard industrial conditions; a second set was coated with TiN by means of PVD process while the third set was coated with a TiC-TiN-Al_2O_3 layer through the CVD technique. The coating layer was applied on all the surfaces of the dies and of the containers thus varying of the friction conditions inside the whole deforming zones.

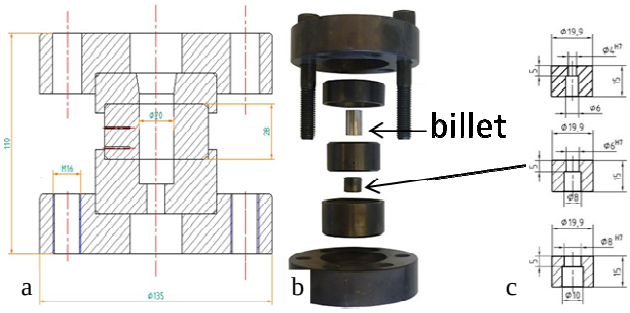

Figure 1: Tool sets: a) container, b) exploded, c) dies

Differently from industrial practice, containers were designed to be handled together with the die and the billet then placed from the oven to the press at each trial within few seconds. A ϕ0.8mm hole was also realized in the containers to allow a temperature monitoring near the billet-container interface by means of a ϕ 0.5mm K-type thermocouple. A heating system was also installed around the ram so as to keep the temperature at 400°C as monitored by a thermocouple.

Experiments were performed by deforming an AA6082 round billet of ϕ 19mm diameter and 25mm length into a round profile of three different diameters (4, 6 and 8 mm respectively) thus realizing dissimilar extrusion ratios. The billets were extracted from an industrial AA6082 (ϕ 140mm) billet by cutting discs of 25mm of thickness, which provided several blocks for the final turning to the required shape and dimensions. Five holes were transversally drilled in each billet in the diametric plane (Figure 2 a) and filled with rods of an AA5754 alloy: the AA5754 alloy was chosen as rod material because, at the tested conditions, it exhibits a flow stress behavior comparable to the AA6082 one.

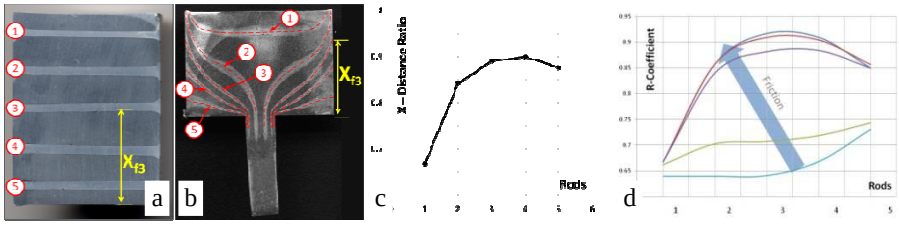

Figure 2: a) Section of un-deformed billet with rods, b)R-coefficient measurements on deformed specimen, c)R-coefficient plot, d)typical R-coefficient curves

A prepared billet, the die and the container were cold assembled without any lubricant and then placed in an oven for an hour in order to attain a homogeneous temperature; the oven temperature was generally set 50°C higher than the testing temperature. Once the assembly (container with die and billet) reached the required temperature in the oven, it was moved to the press and the temperature was monitored by means of the container thermocouple. Once the measured temperature reached the planned set value ram movement was started. A deforming ram stroke of 10 mm was performed so as to leave a butt inside the container of 15mm. Extruded profile was immediately cut and the assembly was water quenched within 3-5 [s]. Specimens were extracted from the tools and sectioned in the rod middle plane (as revealed by a short etch of the billet surface through caustic soda) by means of STREUSS-Labotom3 cutting wheel then polished till a 1000grid. After polishing, the rods were only slightly visible; in order to enhance such contrast the specimen was etched for around two minutes again with caustic soda (Figure 2 b).

The deformed grid was measured on a digitalized image of the specimen and compared in the several tested conditions (Figure 3). If the comparison of the different conditions is performed simply by an optical analysis of the deformed patterns, it seems that negligible differences arose. In order to realize a more accurate comparison of the results, the R-coefficient was introduced. The R coefficient was calculated for each rod

of a specimen as the ratio between the initial and the final distance of the rod from the die:

$$R = \frac{x_f}{x_i} \qquad \textit{(eq. 1)}$$

as shown in Figure 2b. It is important to note that measurements were performed on the billet surface where friction directly acted.

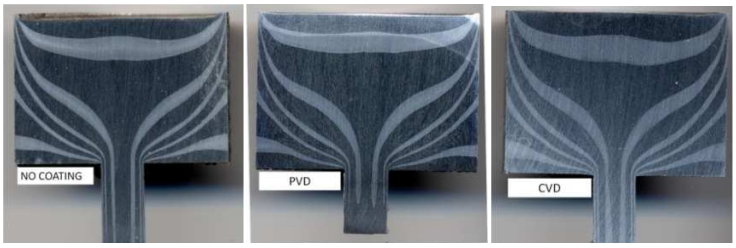

Figure 3: Etched section of φ4 mm deformed rod-added billets

The R-coefficient (eq. 1) can assume values in the range 0 to 1: the upper value of 1 means a perfect sticking since the distance of a rod from the die does not change during the whole ram stroke; conversely, a 0 value represents an ideal lubrication. If the R-coefficient is plotted on a graph for the several rods (Figure 2d), the resulting curve is very indicative of the tribological conditions: the shape and slope of a curve is related to the sliding or sticking phenomena as well as higher curves means higher friction conditions. In Figure 2 b-c is possible to observe that when the rods are severely deformed by the ram (i.e. rod 1 and 2) the R-value is low while the higher values (3,4 and 5) represent the desired friction behavior.

Preliminary tests were conducted with the uncoated tools at different billet preheating temperatures (480°C, 520°C, 560°C) and ram speeds (5mm/s and 0.5 mm/s): since such tests did not show any relevant difference in term of friction it was decided to focus the study on coatings effect at different pressure (i.e. different extrusion ratios) and in term of wear behavior (only for the highest extrusion ratio). The latter goal has been accomplished by interposing simple billets extrusion to series of rod-added billets as schematically reported in Figure 4 a. For each tool set, 3 rod-added billets were initially deformed (so to assure consistency of the data results) then 5 un-prepared billets were consecutively extruded. Rod-added billets were deformed by a ram stroke of 10 mm as previously described, the rest was extracted and the assembly was heated again, while un-prepared billets were subjected to 20 mm stroke thus allowing a continuous extrusion of the 5 billets without any stops. The sequence was then repeated till reaching 32 deformed billets. At the end of the trials container and die were cut and analyzed in order to evaluate the effect of the wear on the coating layer (Table 2).

Figure 4 b summarizes the experimental plan: the three die sets (No coating, CVD and PVD), three extrusion ratios (ϕ 4, 6 and 8 mm) and the wear sequence for the ϕ 4mm condition. Finally, in order to follow typical industrial conditions, the extrusion parameters for the trials were set at 520°C for billet temperature and at 5mm/sec for ram speed.

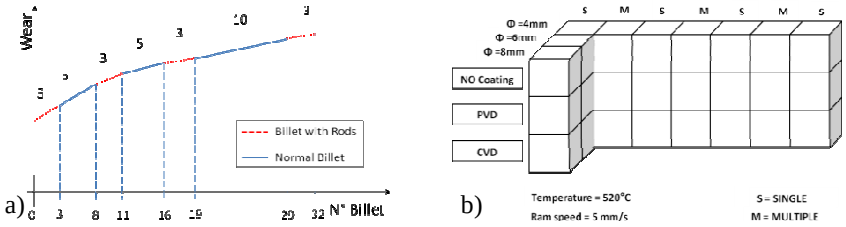

Figure 4: a) Wear sequence and b) Experimental plan

3 RESULTS

3.1 EXTRUSION LOADS

Figure 5 reports the load-stroke curves for the several tool sets at the three extrusion ratios; in each graph only the three initial repetitions for the rod-added billets are plotted.

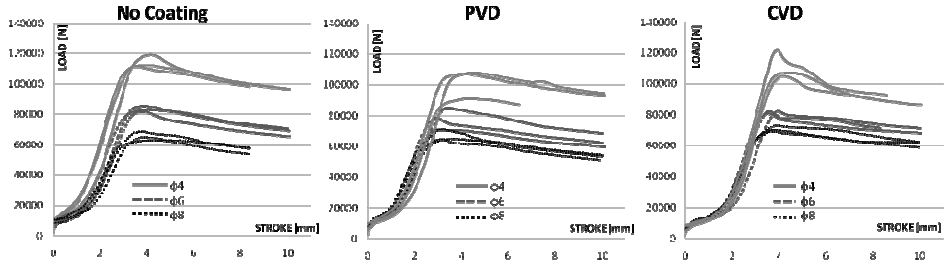

Figure 5: Load-stroke curves, different coatings, first repetition

For each tool set and diameter a good repeatability of the results was found and for all coating conditions, it is possible to notice the expected decreasing of the load with decreasing of the extrusion ratio. For all conditions the three coatings behave very similarly: for ϕ 4mm, for example, a 150kN peak load was found in all the conditions with slightly higher value for non coated tools. The load for successive repetitions is shown in Figure 6: it reports the trend of the maximum extrusion load registered for the different tool sets. The graph explains also the little differences described in figure 5. Indeed, for all three conditions there is a trend settling after the first three billets. While for the uncoated condition this was found to be related to the presence of residual of lubricant used during machining (that was not completely removed with the normal cleaning via alcohol used), the scattering for the PVD and CVD were related to small adhesion of very thin aluminum layers in some portions of the tools. In fact pure coating conditions can be achieved only in the real first trial that showed low values both for PVD and CVD. This effect is also confirmed by the optical analysis described later. Both CVD and PVD coating conditions showed a trend significantly lower than the uncoated condition, PVD more than CVD, and very stable.

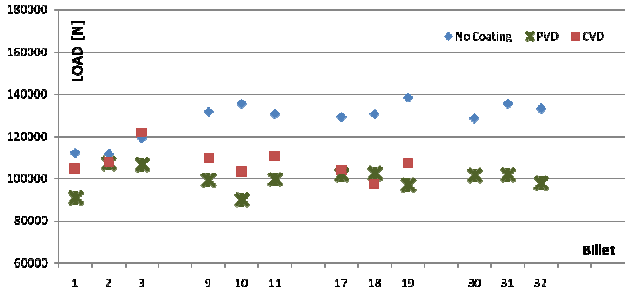

Figure 6: Trend of maximum extrusion load for all repetitions

3.2 R-COEFFICIENTS

In aluminum unlubricated extrusion the deformed rods generally follow the pattern as visible in Figure 3 [10]: a dead metal zone is located in the corner with the extrusion die, a very high friction acts on the billet surface thus generating very deformed rods that become thinner in the high deformation zones and, finally, the rods are packed in proximity of the ram where the scratching effect of the tool forces the deforming material to be detached from the container. The patterns obtained in the different conditions behaved similarly with minor difference in rod positioning on the billet surface. A more detailed description of the material flow and of the local friction conditions can be obtained by the analysis of the R-coefficient, calculated as previously described. In Figure 7 the results obtained for the ϕ 4mm extrusion ratio are fully reported for the several coatings and for all repetitions. Within a coating condition, curves are mostly coincident for the rods 1 and 2, then may differ in the last three which are more significant for friction measurement, in particular the value of rods number 3 and 4 are the most representative because the fifth rod is usually located inside the dead metal zone. Uncoated tools showed very high values always in the range 0,9-0,95 for the rod 4 with small variations unrelated to wear sequence. Surprisingly, PVD coating showed high R-values in the range 0,92-1 in the repetition 1 to 3 and a strong decreasing in repetition 4. Such values are comparable to uncoated tools, thus suggesting that similar friction mechanism occurred in the two conditions. Finally, CVD coating showed the lowest R-values in the range 0,85-0,95 thus evidencing a clear reduction of the friction on the billet surface; also with the progression of the billets the value remained low and inside such range.

Figure 8 compares the results of R-coefficient for the first repetition at each of the two other tested diameters: the ranges of R found for ϕ 4mm are confirmed also for ϕ 6 and 8mm. CVD coating showed the lowest values while PVD and no coating behaved similarly. Finally, the extrusion ratio seemed to have no influence on the friction condition, at least at the tested reduction as clearly visible in Table 1 that summarizes all the highlighted R-ranges.

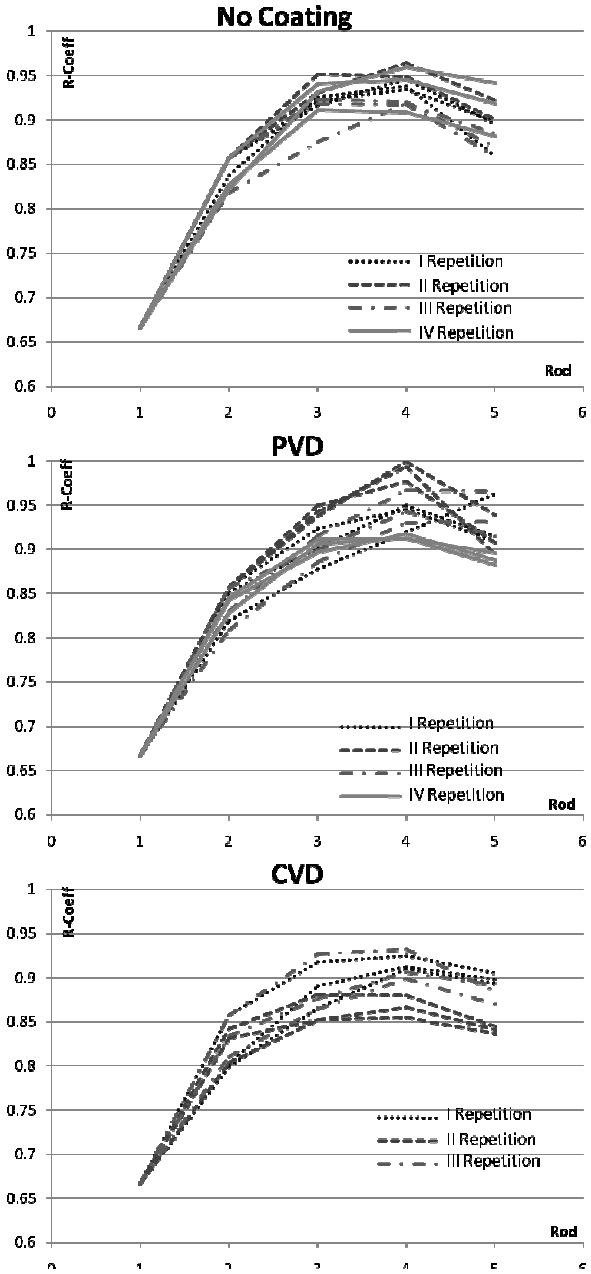

Figure 7: R-coefficient curves for all ϕ 4 repetitions

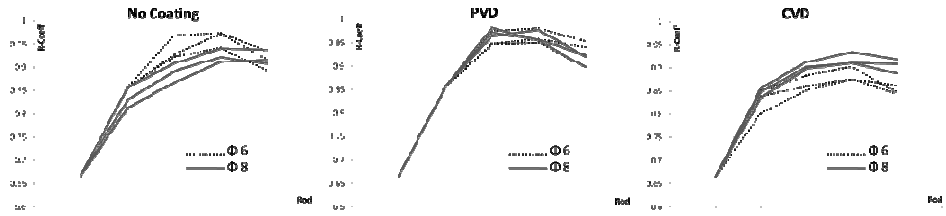

Figure 8: R-coefficient curves for first repetitions of 6 and 8 millimetres diameters

	No Coating	PVD	CVD
Φ4	0.9-0.95	0.91-0.97	0.85-0.95
Φ6	0.92-0.97	0.95-0.97	0.85-0.91
Φ8	0.87-0.97	0.95-0.97	0.9-0.93

Table 1: R-coefficients range for the different coatings and diameters.

3.3 TOOLS WEAR

At the end of the trials, containers and dies were cut along the axis and analyzed by means of optical microscope to verify the condition of coatings and to measure potential thinning. Three locations were observed for each container and two for the dies (Figure 9): for the containers two inside (dead metal zone 1, high shear zone 2) and one outside, that is not in contact with billet (zone 3), while for the dies, the die surface (zone 5) and the bearing (zone 4). A set of unused dies were also analyzed for all the coating condition for further comparison.

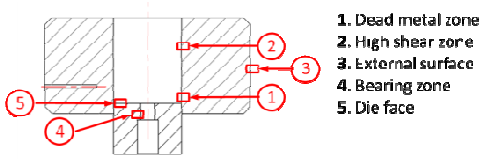

Figure 9: Location of coating measurements spots

CVD For new CVD coated tools, coating thickness was about 7.6µm. On used container (Table 2 and Table 3) coating thickness was about 7.5µm with good uniformity between inside and outside surfaces. In the areas of die contact and dead metal zone wear was completely absent with thickness value equal to unused condition. In the area surrounding the shear zone (zone 2), a layer of 20-40µm of aluminum was found stuck on coated surface. Also on the die, a coating layer of about 7.6µm was measured both on used and new tool, thus indicating absence of sensible wear.

PVD For new PVD coated tools, coating thickness was about 12.3µm. On used container coating was absent on the majority of tools surfaces thus indicating a very severe wear. This is in accordance with R-coefficient results, although surprisingly,

extrusion loads are always comparable with CVD coating tests. Exceptions are spots 3 and 1 characterized by a similar reduction of the coating layer thickness probably related to the thermal cycles carried out on the tools. A thick aluminum layer was again visible on the inner surface surrounding the zone 2 as in the CVD container; although in this case there was no coating layer between aluminum and container material. The same thick aluminum layer was found also in the bearing area, where usually the material slides on die surface.

Uncoated container showed minimal aluminum sticking mainly in the zone 2 and in the die bearing.

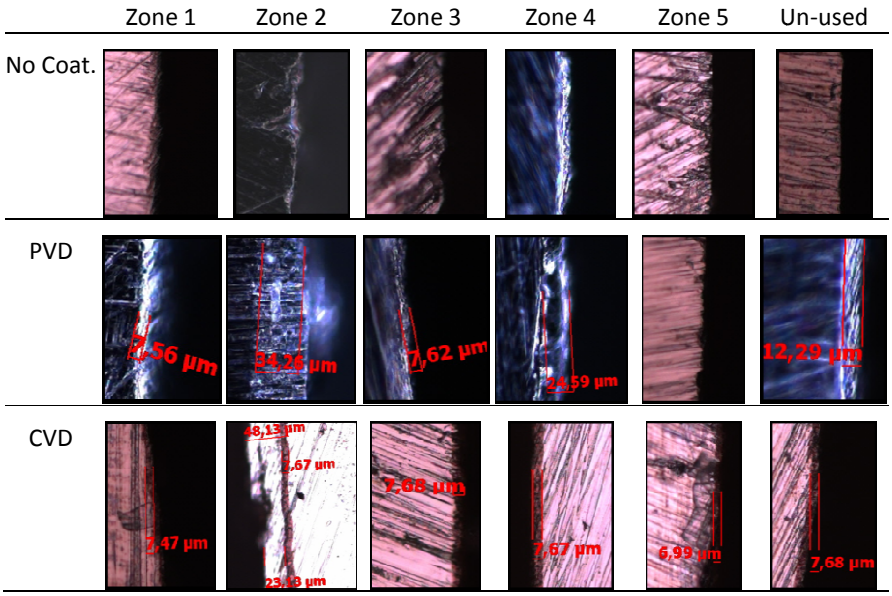

Table 2: Micrographs of container and dies

	Zone 1	Zone 2	Zone 3	Zone 4	Zone 5	Un-used
PVD	7.56	0 /34 Al layer	7.62	0 /*24.5* Al layer	0	12.3
CVD	7.47	7.67 /35 Al layer	7,68	7.67	6.99	7.68

Table 3: Thickness (µm) of container and dies

4 CONCLUSIONS

An experimental activity was designed to investigate the effect of PVD and CVD coating, technologies that are still not completely assessed in the extrusion practice. In particular, the investigation was aimed in providing measurements of friction and coating wear. Investigation was performed by means of visioplasticity on a small scale

direct extrusion. Trials showed comparable extrusion loads for CVD and PVD coating which are 30% lower than normal uncoated tools loads. Comparison of R-coefficient values indicate CVD as a better coating, with appreciably lower values than PVD and no coating conditions, which resulted comparable. This is also in good agreement with microscopical analysis of used containers, which indicate that CVD coating endured wear effect while PVD coating had almost completely disappeared.

5 ACKNOWLEDGEMENTS

This paper is based on investigations within the joint project "Alternative Paths for the Manufacture of Screw Rotors by Forming" (TE 508/3-3), which is kindly supported by the German Research Foundation (DFG). A sincere acknowledgement goes to eng. Roberto Antonaci for the great amount of work and enthusiasm exhibited during experimental activities.

6 REFERENCES

[1] N.C. Parson, J.D. Hankin, A. J. Bryant, "The Metallurgical Background to Problems Occurring During the Extrusion of 6XXX Alloys" Proceedings of 5th Extrusion Technology Seminar, Chicago, USA (1992) vol. 2, pp. 13-23;

[2] M. Schikorra, L. Donati, L. Tomesani, A. E. Tekkaya "Microstructure Analysis Of Aluminum Extrusion: Prediction Of Microstructure On AA 6060 Alloy" Journal of Materials Processing Technology 201 (2008) 156–162;

[3] B. J. Janoss, "Surface enhancement technology for Metal extrusion" Proceedings of 6th Extrusion Technology Seminar, Chicago, USA (1996) vol. 2, pagg. 201-206

[4] M. J. McCabe, "How PVD coatings can increase life and improve performance in aluminum extrusion" Proceedings of 7th Extrusion Technology Seminar, Chicago, USA (2000) vol. 2, pag. 305-311

[5] J. Maier, "CVD Coating Technology for Increased Lifetime of Aluminium Extrusion Dies", Light Metal Age Vol. 65 n.5 (October 2007) pp. 26-31.

[6] M. Sundqvst, T.Bjork, S.Hagmark, I, Srinivasan, "Tribological Evaluation of surface treatments for extrusion dies". Proceedings of 6th Extrusion Technology Seminar (1996) vol. 2, pag. 1-4.

[7] P.K.Saha, "Use of tribology to improve perormance and quality in aluminum extrusion". Proceedings of 8th Extrusion Technology Seminar (2004) vol. 2, pag. 277-287

[8] L. Wang, J. Cai, J. Zhou, J. Duszczyk "Characteristics of the Friction Between Aluminium and Steel at Elevated Temperatures During Ball-on-Disc Tests" Tribology Letters, Volume 36, Number 2 (2009), pp.183-190.

[9] A. Barcellona, L. Cannizzaro, A. Forcellese and F. Gabrielli, "Validation of Frictional Studies by Double-Cup Extrusion Tests in Cold-Forming" CIRP Annals - Manufacturing Technology, Volume 45, Issue 1, 1996, Pages 211-214.

[10] L. Donati, L. Tomesani, M. Schikorra, N. Ben Khalifa, A.E. Tekkaya, “Friction model selection in FEM simulations of aluminium extrusion”. International Journal Of Surface Science And Engineering. vol. 4, 2010, pp. 27 – 41.

Investigation And Prediction of Grain Texture Evolution in AA6082

A. Segatori[a], A. Foydl[b], L. Donati[a], N. Ben Khalifa[b], A. Brosius[b], L. Tomesani[a], A. E. Tekkaya[b]

[a]*University of Bologna, DIEM Department, Viale Risorgimento 2, 40136 Bologna, Italy*
[b]*Institute of Forming Technology and Lightweight Construction (IUL), Technische Universität Dortmund, Baropestr.301, 44227 Dortmund, Germany*

Abstract. Extrusion applications require a strict control of the mechanical proprieties of the extrudates, in particular when undergoing severe loading conditions like in the transportation sector. Profile mechanical properties directly depend on its microstructure and texture, which are the result of multiple mechanisms based on precipitation mechanism or on grain shape evolution (grain refinement, recrystallizations, recovery and grain growth). In this direction, predicting the final profile microstructure under specific process parameters in the die design stage is of great relevance. The present study involved experimental activity on grain size measurements of profile and butt during interrupted direct extrusion of an AA6082 round profile. The grain size measurements were coupled with simulation results in order to regress analytical models based on effective strain, strain rate and temperature. Finally, the developed model was implemented in the numerical code by means of a subroutine that can be used as microstructure prediction tool.

Keywords: Extrusion, Microstructure Evolution, Aluminum, Microstructure Prediction.
PACS: 81.05, 81.20, 81.40, 81.70, 83.10, 83.50, 83.60

INTRODUCTION

A study has been carried out to evaluate the relation between the strain the material undergoes during extrusion and its grain size. Results have been than used to regress an evolution algorithm implemented in a Finite Element (FE) code as a prediction model. Such an activity was driven by the high request of a control over the microstructure evolution during the process due to the significant relationship between microstructure and mechanical properties. During the extrusion, that is a manufacturing process for lightweight profiles of metals like aluminum or magnesium, the workpiece material experiences high deformation at temperatures. These cause changes in microstructure, that is in grain shape, size and in precipitations, that can therefore be adjust through a control of process parameters and the following heat treatment. In order to perform such a control it is necessary a knowledge on recrystallization and grain shape change during the extrusion process, which allows a direct correlation with process parameters as well as build of prediction models.

In literature is retrieved the influence of the process parameters on the recrystallization of the grains [1], supporting once again the responsibility of process parameters over mechanical properties through the microstructure.

Van Geertruyden [2] examined this correlation between state variables and material microstructure in detail. Also Doherty et al. [3] report the strong dependence that connects forms of recrystallization and the deformed state.

In general, the recrystallization is a process that occurs under thermal and-or mechanical stresses (e.g. forging, extrusion, rolling). When the mechanism occurs during the mechanical process, it is called dynamic or first, while when it occurs after the end of the mechanical process, it is called static or second. For aluminum, different descriptions of recrystallization are available in literature. The Dynamic Recovery (DRV) theory is well described by McQueen [5, 6]. During forming, both the subgrain size as well as the wall and internal dislocation densities are constant. Although the grains are elongated, the subgrains are still equiaxed. Hence, the length of high angle boundaries increases and the subgrains are continually rearranged. In addition, the Continuous Dynamic

Recrystallization (cDRX), described by Gourdet and Montheillet [7], is reported in detail in literature. The development of new grains occurs because of misorientation of the subgrain boundaries which increases during deformation. These occur inside already existing grains. The Geometric Dynamic Recrystallization (gDRX) is a subset description for the development of new grains during deformation. Several authors [2,3,8] have found gDRX in both the rolling and the extrusion process. It is a geometrical approach claiming that elongated grains become serrated and pin off, with the result that new grains have been formed.

In [4] a relationship for a rolling process between the grain thickness GS_{th}, the related strain ε and the initial grain size d_0 is formulated as:

$$GS_{th} = d_0 e^{-\varepsilon} \tag{1}$$

The gDRX occurs when the subgrain size becomes equal to the grain thickness [4]. According to De Pari [9] gDRX starts, if the grain thickness is reduced to 1-2 subgrain diameters.

This paper reports a study of the relation between strain, strain rate, temperature and grain size in an extrusion product by means of experimental and numerical investigations. The aim was to couple grain deformation at different extrusion parameters with numerically evaluated strain and strain rate. Hence, it was possible to correlate grain texture evolution to strain, temperature and strain rate. This correlation was then implemented in a FE code and grain shape was predicted.

MATERIAL AND METHODS

For the experimental activities, it was chosen to perform the extrusion process at a small scale by means of a tensile-compression test press ZWICK250 with a maximum load of 250kN. The billet was made of homogenized AA6082 with a diameter of 19mm and height of 25mm. FIGURE 1-a reports the tools used for the extrusion. Three dies were used to produce round profiles of three different diameters: 3, 4 and 6mm respectively, in order to have different extrusion ratios. It is important to note that all dies had the same bearing length. In order to have an homogeneity of material through all the specimens, the billets were extracted from a ϕ=140mm billet by first cutting discs of 25mm thickness, than extracting several blocks and finally turning to the required shape and dimension.

FIGURE 1. a) Tools: container, die and an extruded specimen (butt and profile), b) Experimental plan

All experiments were performed with a ram stroke of 10mm. FIGURE 1-b reports the experimental plan, that includes two different ram speeds of 5 and 0.5 mm/s and three different temperatures of 480°, 520° and 560°C. These, together with different extrusion ratios, allowed to investigate the effect of temperature, strain and strain rate effect on microstructure. For each combination of parameters a minimum of three repetition were planned in order to ensure statistically firm results. A tribological investigation was carried out on the same testing equipment with a simplified experimental plan by means of visioplatic analyses by insertion of an horizontal grid of rods with the aim to determine the correct setting of friction parameters in the numerical activities [10]

Contrary to industrial practice, tools were designed to handle container, die and billet all together: they were cold assembled (billet had been lubricated with boron-nitrate) and then placed in oven at 600°C for one hour. At removal from oven, the assembly was placed on the press within few seconds and a ϕ=0.5mm k-type thermocouple was inserted in the ϕ=0.8mm hole on the container to monitor the temperature as close as possible near the billet-container interface. Press ram was equipped with a heating system and monitored by a thermocouple in order to keep it at a 400°C.

As the container thermocouple reached the desired temperature, the ram movement was initiated. Immediately at end of the extrusion the profile was cut off and allowed to fall in water for immediate quenching; the assembly was

quenched by water immersion as well within 5-7 seconds after extrusion process end. A direct control of load-displacement curves allowed to evaluate the repeatability of experimental trials and to select the specimen for microstructure analysis or discharge of specimens.

Selected specimen were sectioned along diametric plane by means of a STRUERS-Labotom3 cutting wheel, polished up to a 1000grid and then processed on a -STRUERS LectroPol-5 for further electrochemical polishing and etching (Polishing and etching cycle details are shown in TABLE (1)).

TABLE (1). Polishing and etching parameters.

Action	Reagent	Time	Voltage
Polishing	A2 of Struers	60 s	20V
Etching	Barker reagent	70 s	20V

The etching method was chosen in order to allow a clear visualization of grain shape and boundaries under polarized light where grains appear in different bright colors, depending on their crystal orientation, and are therefore easy to identify.

Micrographical analyses were performed using a ZEISS Axio Imager. A detailed micrographical "map" of the entire section was generated through combining several high resolution images of small areas for each of the analyzed specimens (FIGURE 2). This "map" was built for the purpose of having a good overview of grain deformation distribution, ease of choice of spots where to numerically evaluate grain size and ease of localization of close up pictures for grain size evaluation. For each specimen the grain sizes were measured in ten spots (FIGURE 2) previously selected with the aim of having a wide range of deformation zones. These zones were consistently analyzed for all specimens.

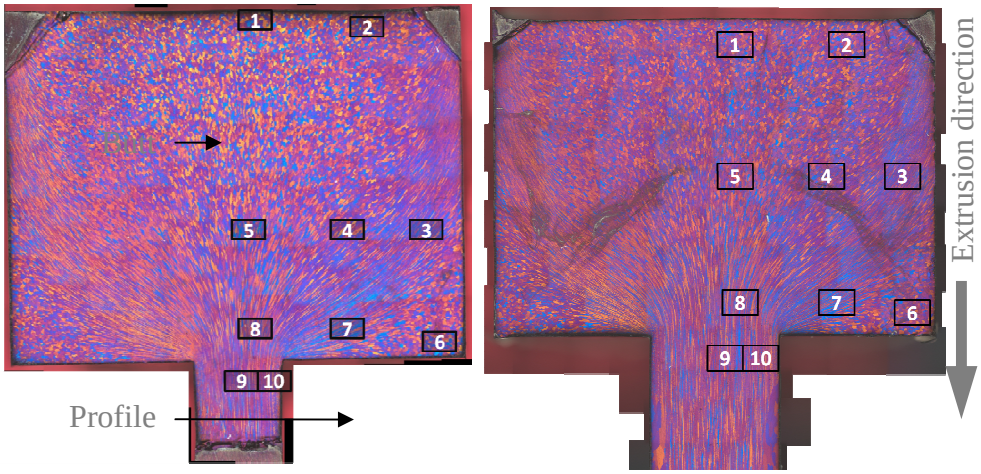

FIGURE 2. Overview of the grain structure of a butt, with measured spots. Spots 9 and 10 are on bearing section. Spot 6 refers to dead metal zone.

The grain size measuring was performed by means of the average linear interception of grains. In this method, an orthogonal grid is laid over the micrograph of a selected area where the measuring is intended. The mean of the ratios between the number of interceptions of grain boundaries and the line length provides the average dimensions of the grains in that direction, which is called grain size. Such a methodology requires a good selection of measuring spots, i.e. within the area to be examined the grains should have homogenous size and shape, and the grid should have a correct orientation (FIGURE 3). The grid should be oriented in the direction where grains show a deformation in order to be sure that the true thickness and length of grains are measured and not a mean value of the two. All measurements were performed on micrographs with the same magnification level and grid spacing of 5 to 7 grid lines to ensure a good mean value.

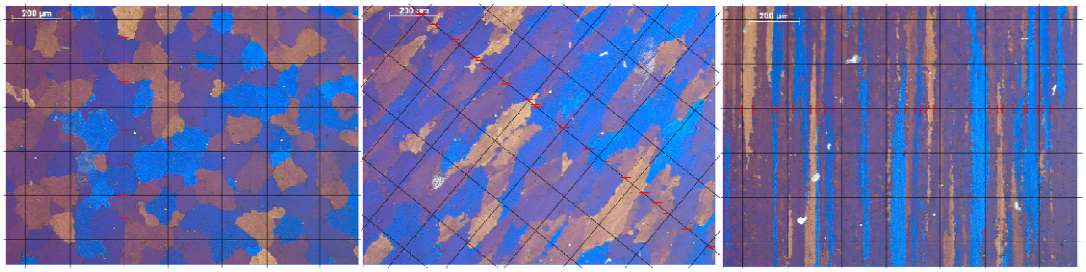

FIGURE 3. Grain counting for three different types of grain shapes.

Numerical simulations were carried out in order to predict the evolution of the state variables during the experiments. The simulation were performed by means of DEFORM 2D as a two dimensional model was used for ease of axisymmetric discretization. Container and die were discretized as a single object. Another set of simulations were also carried out to evaluate the best friction parameter to be used [12]. A friction factor of 1 plus sticking condition on container, punch and die face was set. Heat transfer coefficient between billet and container/die was set to 11 N/(s*mm*C). Validation and calibration of simulations were performed with the experimental loads and temperatures.

For experimental-numerical coupling effective strain was chosen. For each extrusion condition the measuring spots of the experimental specimen were localized on the corresponding simulation and the effective strain retrieved on that area.

Once data were coupled, it was possible to obtain graphs as in FIGURE 4 representative of grain thickness and length evolution over strain. These graphs were used to regress as evolution equation to be implemented in the simulation code. Once regression of equation was completed, the evolution algorithms were implemented in the FE code by means of sub-routines.

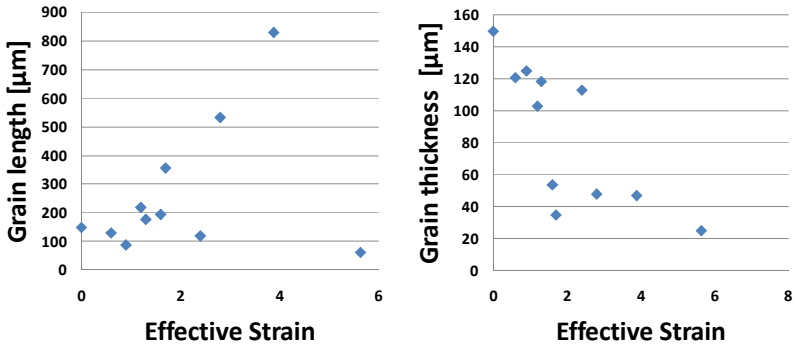

FIGURE 4. Grain length and thickness coupling for the ϕ=4mm specimen extruded at 480°C and 0.5 mm/s ram speed.

RESULTS

After coupling the numerical and experimental results, it was possible to observe the influence of the temperature and the ram speed ON???. As evident from FIGURE 5, there was no influence of such parameters.

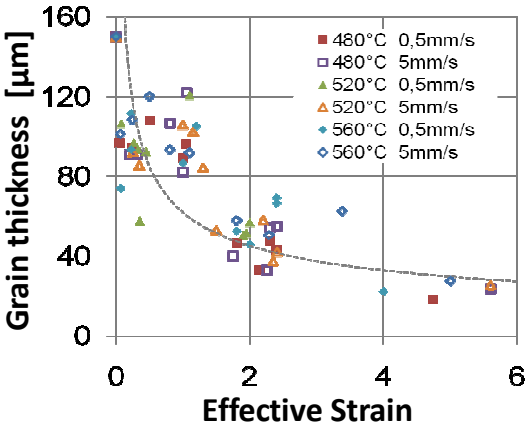

FIGURE 5. Coupling of strain with grain thickness for ϕ =6mm dies.

FIGURE 6 illustrates the evolution of grain thickness and length for all specimens. Spots with null strain show an undeformed state, that is no recrystallization under sole thermal solicitation. At increasing strain, grain thickness decreses till an asymptote at 25-30µm after a strain of 3.5. At about the same strain level grain thickness reaches a steady state followed by an abrupt decrease

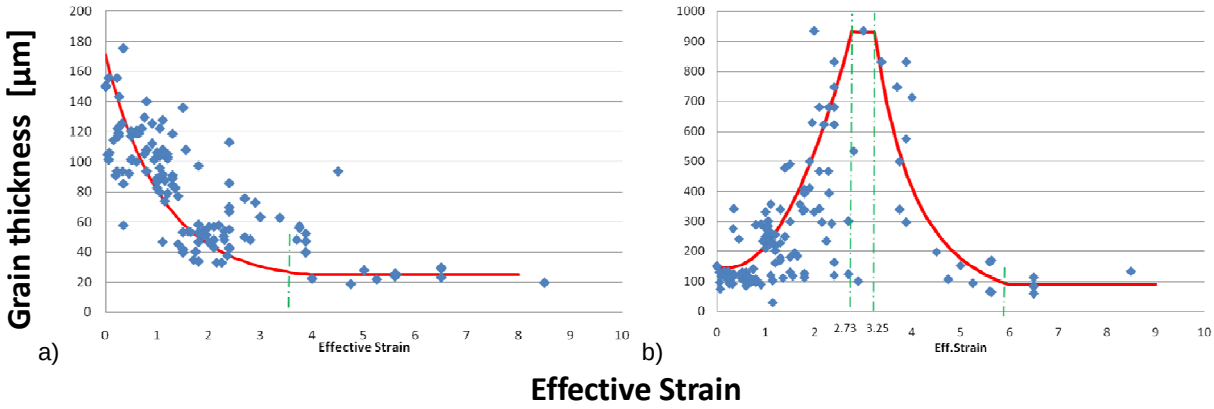

FIGURE 6. a) Coupling of strain with grain thickness; b) Coupling of strain with grain length.

Apparently, this is the value at which grains can not get thinner, because they reach 1-2 times the subgrain diameter and they undergo the pinch off phenomena.

Two algorithm were formulated for grain thickness and length prediction from regressed equation. TABLE (2) reports equation as implemented in the FEM code. Equation validity was set by strain intervals with the exception of initial grain thickness, which was kept constant at 150µm till the first equation reaches such a value.

Table (2). Equation of implemented algorithm

Grain thickness	
$GS_{thickness} = 62.07\varepsilon^{-0.45}$	$\varepsilon \leq 4$
$GS_{thickness} = 25$	$\varepsilon > 4$
Grain length	
$GS_{length} = 85.192\varepsilon^{2} - 14.88\varepsilon + 150$	$\varepsilon \leq 2.73$
$GS_{length} = 930$	$2.73 < \varepsilon \leq 3.25$
$GS_{length} = 80001\varepsilon^{-3.8}$	$3.25 < \varepsilon \leq 6$

$$GS_{length} = 90 \qquad \varepsilon > 6$$

Two variables were then evaluated and visualized by the code as in FIGURE 7. Although representative of a single dimension, together they give a good overview of dynamic grain shape evolution and gradients as the localization of recrystallization areas.

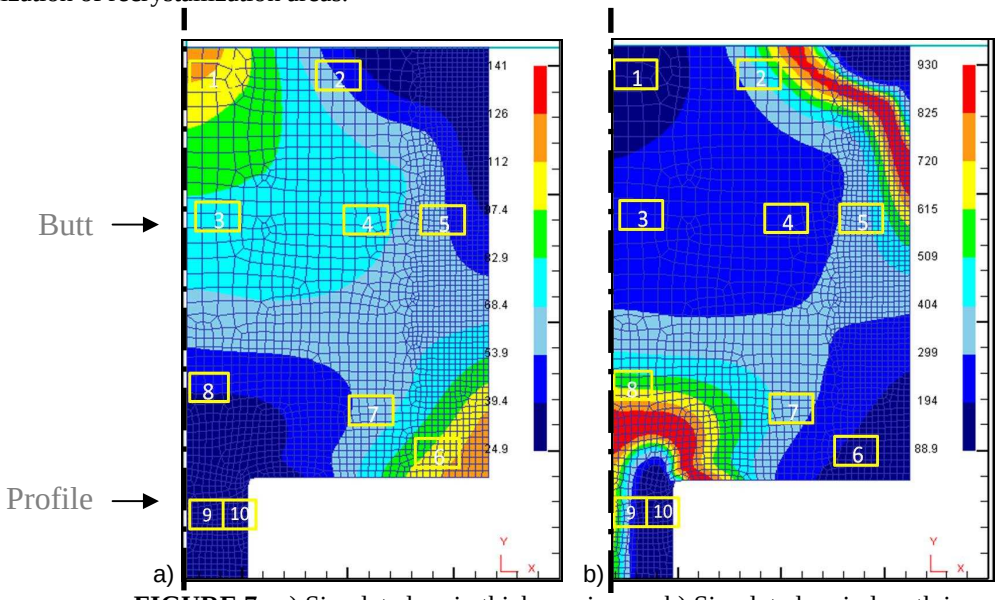

FIGURE 7. a) Simulated grain thickness in µm; b) Simulated grain length in µm.

CONCLUSIONS

A coupled experimental and numerical procedure was used to characterize dynamic evolution of the microstructure during hot extrusion process. No influence of process temperature and ram speed on dynamic grain evolution was found. A correlation between the two principal grain dimensions and the equivalent strain could be found, which allowed to propose an evolution algorithm. This was then implemented by means of a subroutine in a FE code that can therefore evaluate and predict grain shape over the entire extruded profile and butt.

REFERENCES

1. E. D. Sweet et al., *Effects of Extrusion Parameters on Coarse Grain Surface Layer in 6xxx Series Extrusions*, ET 2004.
2. W. H. Van Geertruyden, *The Origin of Surface Recrystallization in Extrusion of 6xxx Aluminum Alloys*, PhD-Thesis, 2004.
3. R. D. Doherty et al.: *Current issues in recrystallization: a review*, Materials Science and Engineering, Vol A238, 1997, pp. 219-274.
4. Humphreys, M. Hatherly, *Recrystallization and Related Annealing Phenomena*, ed. Pergamon, 2004.
5. H. Yamagata, *Dynamic Recrystallization and Dynamic Recovery in Pure Aluminum at 583 K*, Acta Materialia, Vol 43, 1995, pp. 723-729.
5. H. J. McQueen, W. Blum, *Dynamic recovery: sufficient mechanism in the hot deformation of Al (<99.99)*, *Materials Science and Engineering*, Vol A29, 2000, pp 95-107.
6. H. J. McQueen: *Deficiencies in Continuous DRX Hypothesis as a Substitute for DRX Theory*, Materials Forum, Vol 28, 2004, pp. 351-356.
7. Gourdet, F. Montheillet: *A model of continuous dynamic recrystallization*, Acta Materialia, Vol 51, 2003, pp. 2685-2699.
8. W. Blum, et al., *Geometric dynamic recrystallization in hot torsionof Al-5Mg-0.6Mn (AA5083)*, Materials Science and Engineering A, Vol 205, 1996, pp. 23-30.
9. L. De Pari Jr, W. Z. Misiolek, *Theoretical predictions and experimental verification of surfacegrain structure evolution for AA 6061 during hot rolling*, Acta Materialia, Vol 56, 2008, pp. 6174-6185.
10. A.Segatori, et al., *Effect of tool coatings on friction behavior during hot aluminum extrusion*, ICTMP 2010.

GRAIN SHAPE EVOLUTION ANALYSIS IN THE EXTRUSION OF 6XXX ALLOYS BY USE OF A LAGRANGIAN FE CODE

Lorenzo Donati*, Antonio Segatori* and Luca Tomesani*

***DIEM Department, University of Bologna, v. Risorgimento 2, 40136, Bologna, Italy**
l.donati@unibo.it, antonio.segatori2@unibo.it, luca.tomesani@unibo.it

ABSTRACT: A unified model is developed to study the grain shape evolution of 6XXX aluminum alloys during deformation and consequent static recrystallization in hot metal forming processes. In this model, effects of grain dynamic recrystallization (following continuous and geometric dynamic recrystallizations theories) during deformation, of dislocation densities distribution, of stored energy and of consequent grain static recrystallization are considered. Developed model has been implemented in the langrangian FE code Deform and validated over experimental trials performed at different forming temperatures and strain rates on a AA6060 aluminum alloy.

INTRODUCTION: Aluminum alloys and especially 6XXX series are widely used in the production of high performance and light weight components by means of bulk forming processes. An exhaustive review on the several aspects of recrystallization like nucleation and growth, the development of misorientation during deformation, continuous, dynamic (CDRX), geometric dynamic recrystallization (GDRX), particle effects and texture was realized by Doherty et alii, (1997) with a selected focus on grain and subgrain scale phenomena. In the extrusion of aluminum alloys the process chain involve the heating of an homogenized billet, the dynamic recrystallization of the grains during the deformation of the metal into high strain seams up to the final profile shape, finally followed by several degree of static recrystallization (from zero up to 100%) depending on the process quenching system. In defective cases, peripheral grain coarsening (PCG) may occur thus leading to profile scrapping. The implementation of a predictive tool able to simulate the whole complex sequence of phenomena involved in the extrusion process, at a macroscopic scale, consequently results of considerable interest (Aukrust 1997). In the paper a model based on the Kolmogorov–Johnson–Mehl–Avrami (KJMA) model (Avrami, 1941) and on the works of Vatne-Nes (1996) and Peng-Sheppard (2004) has been modified on the basis of aluminum alloys dynamic recrystallization mechanism and then implemented in the lagrangian FE code Deform. The several phases of the phenomena (deformation, dynamic recrystallization, static recrystallization and grain growth) were separately implemented and verified throughout two different experimental trials performed on AA 6060 alloy.

Materials and Methods

A test was set up for the investigation of the microstructure dynamic evolution by means of a small scale interrupted extrusion of a round profile. As described in detail by Segatori et alii (2011), the test was chosen in order to reach the high deformation levels

characteristic of the extrusion process, while, at the same time produces specimens that would present a wide gradient of strain within the same process conditions. The experimental plan combined three levels of temperature (480°, 520° and 560°C) and two levels of speed (0.5 and 5 mm/s) representative of typical industrial process.

Figure 1 a) Tools: container, die and an extruded specimen (butt and profile), **b)** Experimental plan

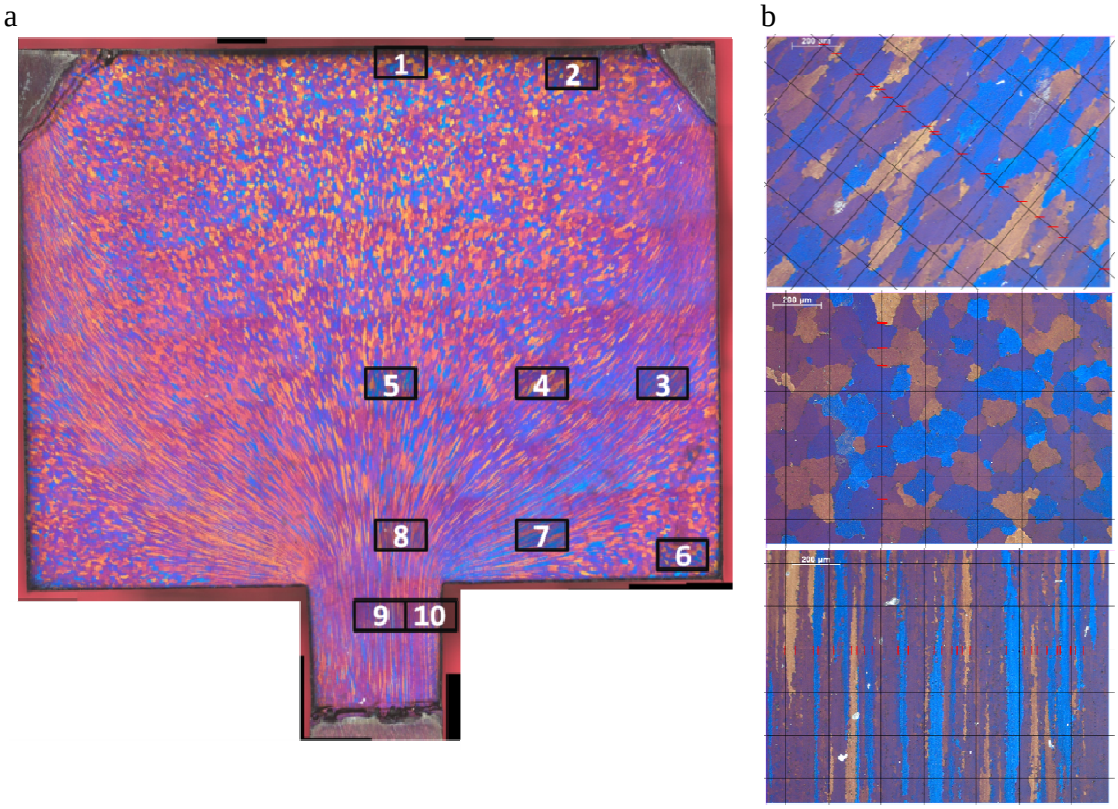

Figure 2 a) Overview of the grains of the longitudinal section of a specimens. The ten measuring spots are highlighted (9 and 10 are on bearing section). **b)** Grain measurements, by means of the average linear interception method, for three spots with different types of grain shape.

For each condition a grain size evaluation was performed in ten representative spots of the specimen diameter section (Figure 2). Measured sizes, that are grain thickness and length, were than coupled with the results of a FE simulation campaign conducted with DEFORM 2D. Coupling allowed to produce grain size-strain graphs for all conditions and retrieve microstructure behavior as in Figure 3.

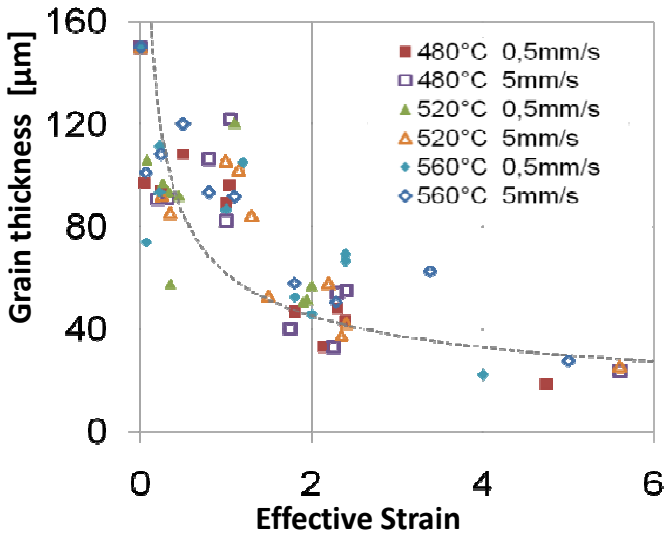

Figure 3 Coupling of strain (evaluated numerically) with grain thickness (retrieved experimentally) for φ =6mm dies.

A separate experimental campaign on a different test design was conducted for the evaluation of the static recrystallization. Such choice allowed also to validate the dynamic evolution model proposed and implemented in the FE code. A small scale inverse extrusion was set up to produce small cups from a billet of AA6060. The cylindrical specimen (ϕ 15mm and 10mm height) and the testing tools (bottom die and upper punch) were placed inside a resistance oven in order to reach the testing temperature (Figure 4).
Specimens were deformed at four different temperatures (250°, 350°, 450° and 550°C) and at two different ram speeds (0,1 and 5 mm/sec) then immediately quenched in water. This allowed to freeze the microstructure for the validation of the dynamic evolution model and to prepare the specimens for the following annealing process at 580° for 30 minutes.

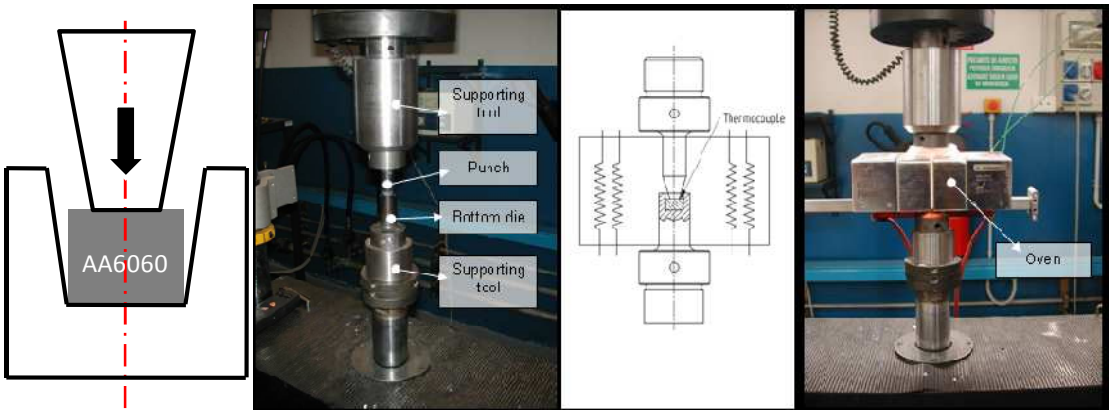

Figure 4 Draft of the experiment set up and real equipment with and without oven.

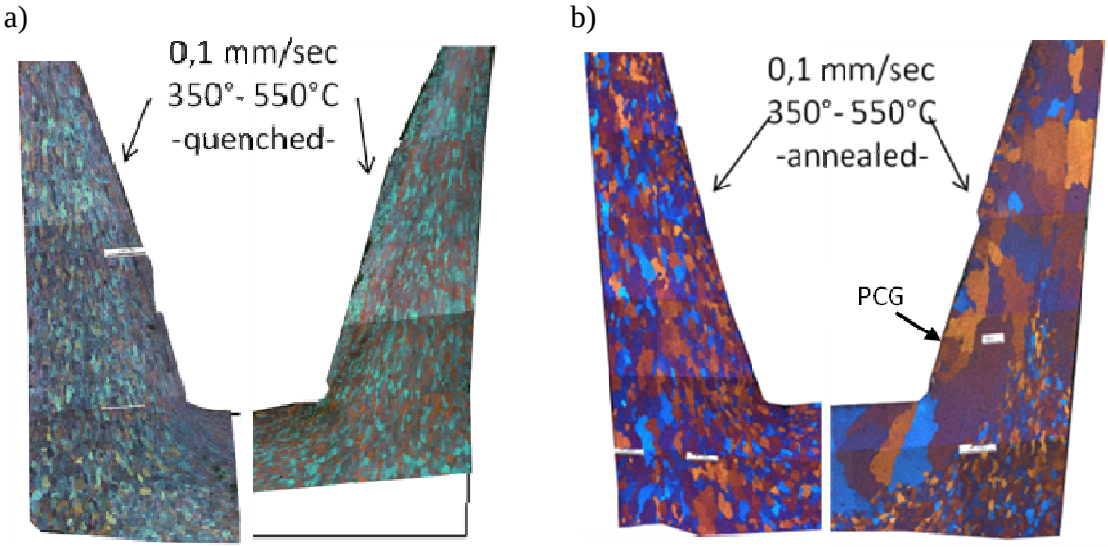

Figure 5 Different half sections of specimens from inverse extrusion for trials at 350°C and 550°C at 0,1mm/sec ram speed: **a)** quenched immediately after extrusion, **b)** after annealing.

The type of test was again chosen in order to produce specimens in a wide range of strain levels within the section of the specimen. Process parameters were selected to fit common industrial conditions.
Nine spots along the side of the specimen section were chosen for grain size evaluation. Measurements were performed again with average linear interception. Aside with the experimental activity, a simulation campaign of all tested condition was conducted with the FE code DEFORM 3D.
In evaluating the increment in grain size due to static recrystallization it is to be noticed that some specimens can undergo other phenomena such as Peripheral Coarse Grain (PCG) due to the particular combination of temperature, strain and strain rate. Such

phenomena must be distinguished from static recrystallization and has to be modeled apart. Figure 5 shows the different level of recrystallization and the occurrence of such phenomena, which is not modeled in the present work.

Theory

In casted billet with homogenized microstructure, the grains are equiaxed and the grain size is very uniform so as to express the grain dimension by a single value d_o (Donati et alii 2008). During forming, complex stress fields deform the material, being the change in shape mainly related to effective strain. If limited strain are reached (i.e. below 2 for 6060 alloys), final grains are simply elongated but if higher strain are reached, accordingly to GDRX or CDRX theories, new small grains are generated thanks to "pinch-off" effect or increasing of misorientation angles in subgrains, thus dividing a grain in two or more Such phenomena were illustrated by Segatori et alii (2011) as it is evident from Figure 6 were grain length is reported versus FE evaluated strain. After a certain level the length does not increase anymore but undergo an abrupt decrease. At similar level the grain thickness reaches a plateau.

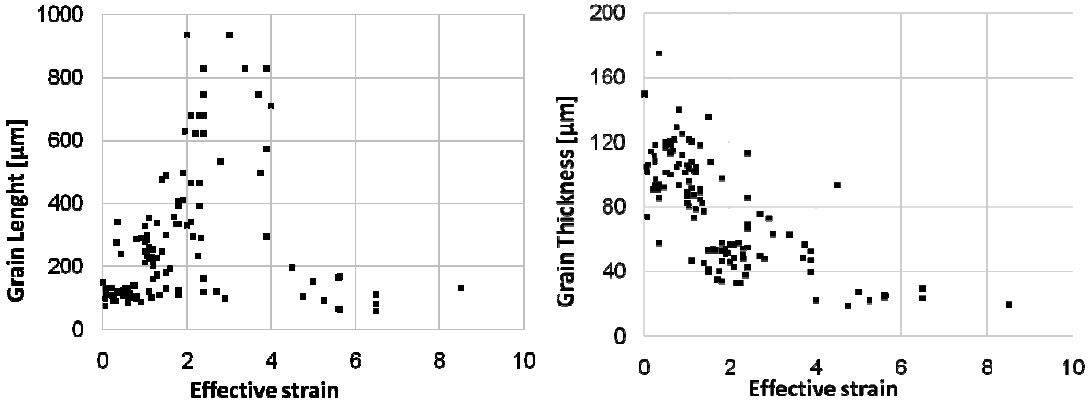

Figure 6 Grain length (left) and thickness (right) in dependence of strain. After a strain of about 4, length incurs in gDRX while thickness reaches a plateau of about 25 µm.

The grain thinning (d_t) and elongation (d_l) can be expressed by the effective strain dependent models proposed below:

$$d_t = d_0(k_1 + \bar{\varepsilon})^{-n} \qquad (1)$$

$$d_l = k_2\bar{\varepsilon}^2 - k_3\bar{\varepsilon} + d_0 \text{ for } \varepsilon < \varepsilon_c \qquad d_l = k_4\bar{\varepsilon}^{-m} \text{ for } \varepsilon > \varepsilon_c \qquad (2), (3)$$

where d_t and d_l are the grain thickness and length respectively, d_0 is the original grain diameter (137µm for the tested alloy), n, m and $k_{(1-4)}$ are constants to be experimentally

determined (n=1,2, m=3,8, k_1=0.75, k_2=85,192, k_3=14,88, k_4=8*10^4 for AA6060) and ε_c is the critical value of strain that corresponds to a grain thickness comparable to a subgrain size ($\varepsilon_c \approx 3$ for AA6060). The refinement of grain length is limited to a size of 90μm which occurs at strains of about 6. The model was implemented in the FE code DEFORM through preprocessing subroutine thus producing two variable respectively for grain thickness and length.

For the evaluation of static recrystallization subgrain size (δ) was included in the computational model throughout the entire process. The model proposed by Nes et alii (1996) and most used in literature evaluate as follow:

$$\frac{1}{\delta} = A \ln Z - B \tag{4}$$

$$Z = \dot{\bar{\varepsilon}} \exp\left(\frac{Q}{RT}\right) \tag{5}$$

with A and B coefficient to be experimentally determined (Castro-Fernandez et alii (1990) found A=0,165x10^6 m^{-1} and B=3,87x10^6 m^{-1} for hot deformed al alloys) and with Z the well known Zener-Hollomon parameter; $\dot{\bar{\varepsilon}}$ effective strain rate, R universal gas constant (R=8,341J/mol) Q Activation Energy (for AA6060 Q=265000 J/mol°K), and T temperature in °K. The initial subgrain size was considered at the same size of grain size till a critical level of Z is reached, that is, till a minimum deformation is imposed on the material.
In case of aluminum extrusion, the Z-range of processing varies from 1E+14 to 1E+05 as presented in Table 1. Both Nes model and Castro-Fernandez modification of it present a inapplicability for small values of the Zener-Hollomon parameter which are still in the range of the extrusion process as evident in Figure 7. A novel model was therefore proposed by the authors:

$$\frac{1}{\delta} = C(\ln Z)^n \tag{6}$$

with C=3,364E-9 [m^{-1}], n=5,577 and an upper limit to initial grain size (d_0=137μm for the specific alloy used in the present work). The model is based on the idea of a subgrain of initial size equal to grain, as proposed by Peng and Sheppard (2004). The proposed model shows good agreement with McQueen et alii (2011) experimental data on subgrain size evolution on hot torsion tests.

Table 1 Evaluation of typical Zener-Hollomon range of values for industrial aluminum extrusion process.

Temp [°C]	Temp [°K]	Strain rate [1/s]	Z [1/s]
400	673,15	30	9,48E+13
600	873,15	0,0001	4,33E+05

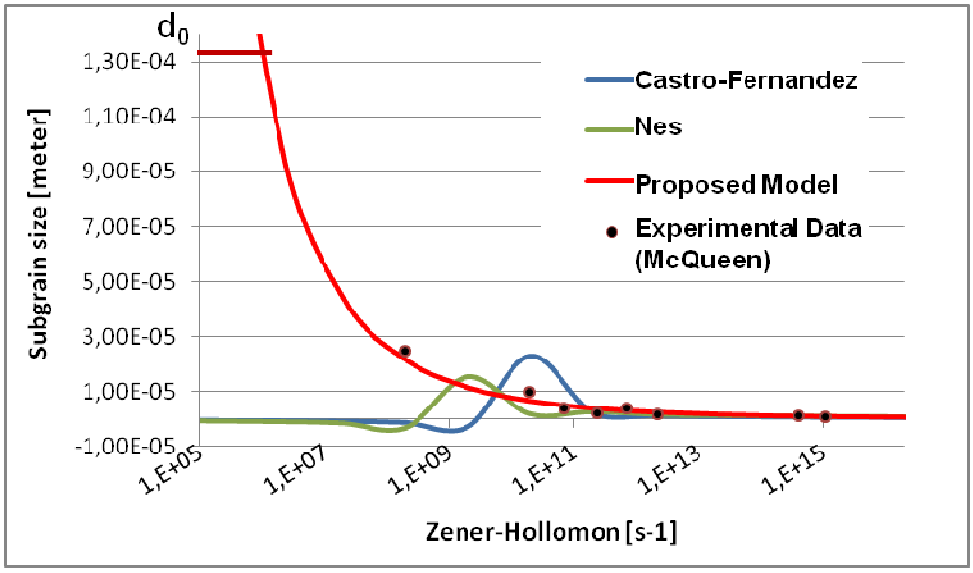

Figure 7 Subgrain size over Zener-Hollomon for different models (lines) and experimental evaluation (dots).

As reported by Doherty et alii, (1997) during deformation no static recrystallization phenomena occurs, but immediately at the end of the deformation (if no quenching is performed) grains start to recrystallize. Nucleation and growth of new grains can start from three different location as described by Vatne et alii (1996): i. from particles, ii. from pinched off grains and iii. from zones with high misorientation boundaries. When very high strains are reached like in extrusion (in the order of magnitude of ε=6), the authors realized that the second mechanism overcome the others, in relation to the huge number of pinched off grains.
The density of the recrystallization sites was then implemented as proposed also by Sheppard et alii (2004), :

$$N = \frac{4C_d}{\delta^2 \cdot (d_t + d_l)} \left[\exp(\bar{\varepsilon}) + \exp(-\bar{\varepsilon}) + 1\right] \qquad (7)$$

with C_d a calibration constant equal to $1{,}48 \times 10^{-4}$ (when grain size and subgrain size are expressed in meters).

The classical assumption for recrystallization kinetics of site saturation (Johnsen-Mhel-Avrami-Kolmogrov) and a random distribution of nucleation sites was used; the grain size (100% of recrystallized material) can be expressed by:

$$d_{rex} = DN^{-1/3} \tag{8}$$

with D a further calibration constant and N density of recrystallization as taken from eqn. (7).

The implementation of the subroutine in the FE code requires as only input the initial grain size d_0. Once the simulation calculation starts the strain rate will determine the presence of dynamic or static recrystallization. At positive strain rate the code evaluates Zener-Hollomon (eq. 5), subgrain size (eq 4) and grain thickness and length (eq 1, 2 and 3). For a null strain rate, that is at the end of the process, the code computes, starting from the values computed for the dynamic recrystallization, the density of recrystallization sites (eq. 6) and the statically recrystallized grain size (eq. 7).

The grain size after static recrystallization can be plotted in the section to obtain a map of easy comparison with experimental data as in Figure 8.

250°C - 0.1mm/s

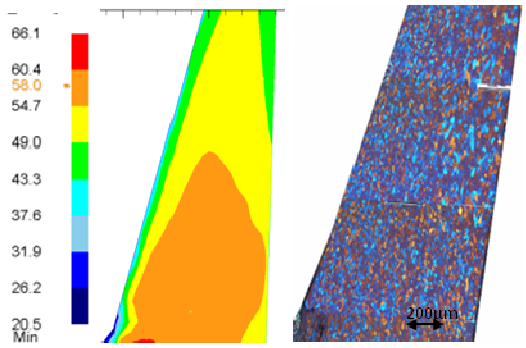

350°C - 0.1 mm/s

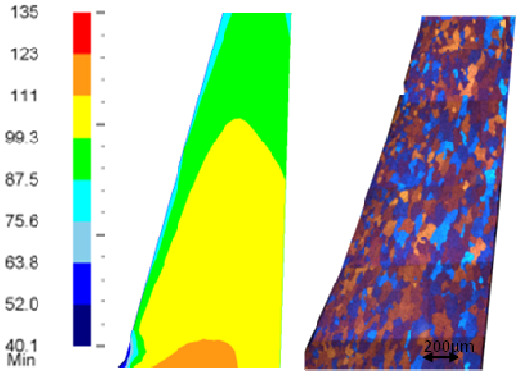

350°C - 5mm/s

450°C - 5 mm/s

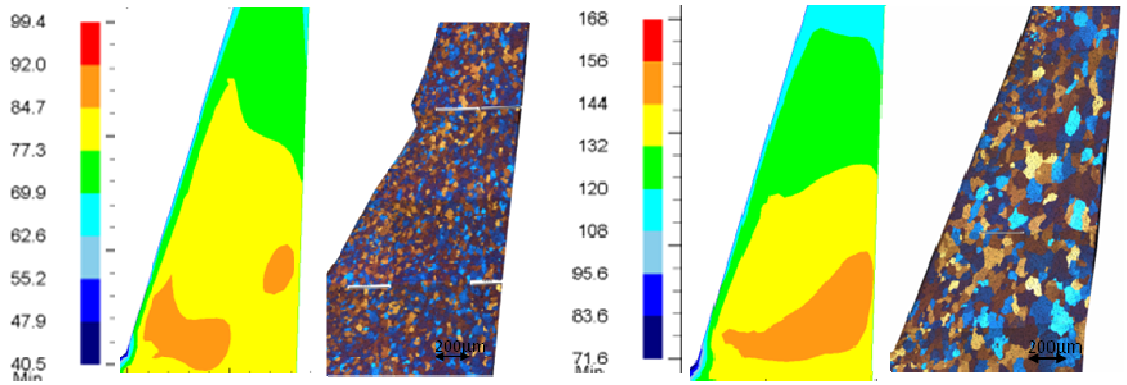

Figure 8 comparison between simulated grain size after static recrystallization and experimental specimen section for different temperatures and ram speeds.

Results

For inverse cup extrusion, grains dimensions were recorded in the quenched and annealed conditions. Figure 9 reports comparison between the experimental and the numerical grain size just after the quenching: only for few spots reports a slightly higher computed value. Figure 10 reports same data after the annealing with little underestimation of SRX from the code.

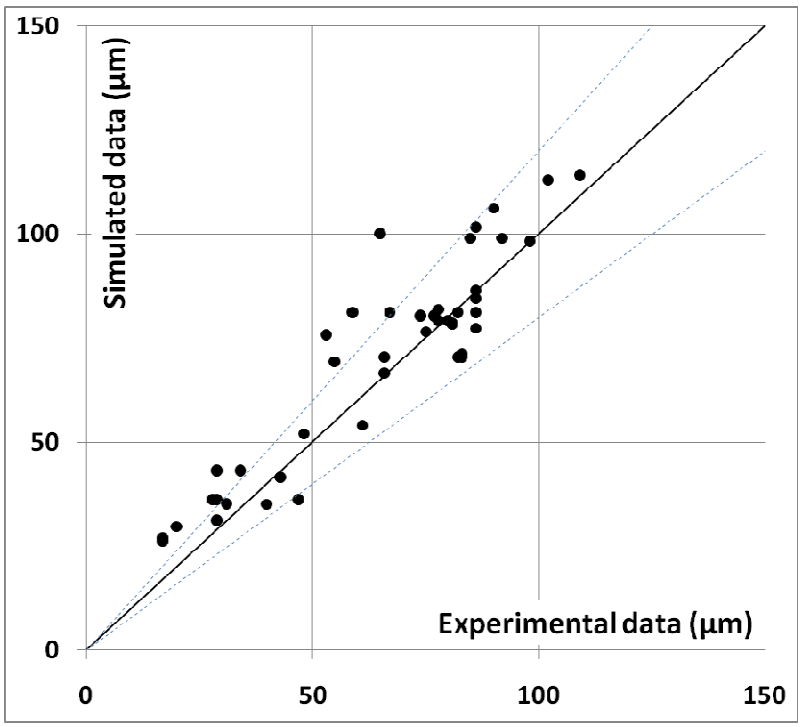

Figure 9 Comparison of computed and measured grain thickness after quenching. 20% error lines are reported as dashed line.

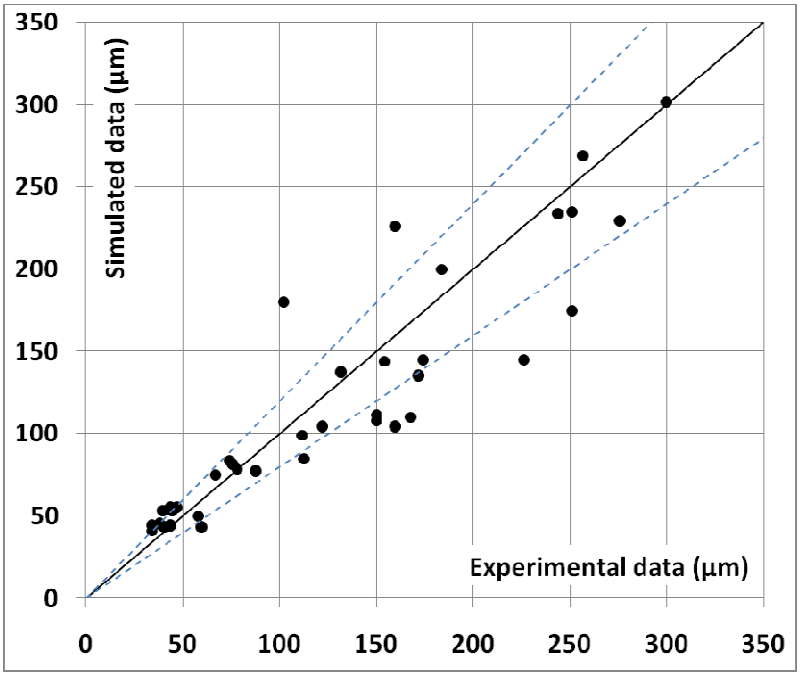

Figure 10 Comparison of computed and measured grain size after annealing. 20% error lines are reported as dashed line.

Conclusions

A combined dynamic and static recrystallization model was proposed based on experimental activities of mini direct extrusion and proposed models from literature. The model was implemented in the commercial software DEFORM 2D obtaining in output the characteristic size of grains during the deformation and after static recrystallization.
The model was then validated on a small scale inverse extrusion esperiment. A good agreement between the experimental and simulated size is found for both quenched (figure 2) and annealed (figure 3) conditions thus validating the developed model

References

Aukrust T., Tjotta S., Vatne H. E., Van Houtte P., 1997, “Coupled FEM and texture modelling of plane strain extrusion of an aluminium alloy” International Journal of Plasticity, Vol. 13, No. 1/2, pp. 111-125.

Avrami, M. ,1941, "Kinetics of Phase Change. III. Granulation, Phase Change, and Microstructure". Journal of Chemical Physics 9 (2): 177–184.

Doherty R. D., Hughes D. A., Humphreys F. J., Jonas J. J., Juul Jensen D., Kassner M. E., King, McQueen H. J., Rollett A. D., 1997, “Current issues in recrystallization: a review” Materials Science and Engineering A, Volume 238, Issue 2, Pages 219-274

Donati L., Dzwonczyk J.S., Zhou J., Tomesani L., 2008, “Microstructure Prediction of Hot-Deformed Aluminium Alloys” Key Engineering Materials Vol. 367. pp. 107-116

Vatne H.E., Furu T., Orsund R., Nes E., 1996,“Modelling recrystallization after hot deformation of aluminu” Acta mater., n. 11, pp. 4463-4473.

Peng Z., Sheppard T., 2004, “Prediction of Static Recrystallization during shaped extrusion”, Proceedings of ET conference 2004, vol I, pp.79-91.

Segatori A., Foydl A., Donati L., Ben Khalifa N., Brosius A., Tomesani L., Tekkaya A. E. (2011) “Investigation And Prediction of Grain Texture Evolution in AA6082” AIP Conference Proceedings (14th Esaform), 1353, 449-454.

McQueen H. J., Spigarelli S., Kassner M. E., Evangelista E., 2011. Hot Deformation and Processing of Aluminum Alloys, CRC Press.

The Streaks Formation in Hollow Profile Extrusion

L. Donati[1*], L. Tomesani[2] , M. Rompato[2], A.Segatori[1]
[1]University of Bologna, DIEM Department, Viale Risorgimento 2, 40136 Bologna, Italy, l.donati@unibo.it, luca.tomesani@unibo.it, antonio.segatori2@unibo.it
[2]Pandolfo Alluminio, Pandolfo Alluminio S.p.A.
Via della Provvidenza 143, 35030 Sarmeola (PD), Italy;
mrompato@pandolfoalluminio.com,
* Corresponding Author

Keywords: Extrusion, streaks, hollow profile, microstructure, AA6060.
Publication on: Industrial journal .

Introduction

In the last years the application of aluminum extruded profiles for the architectural market and for products with aesthetic requirements widely increased. A common concern related to the production of this type of profiles is the appearance of surface defects and in particular any difference in term of color homogeneity on the surface. Among the others, extruded profiles streaks represent one of the most difficult imperfections to deal with especially due to the lack of knowledge on the formation and evolution of this defect. Finally, an important industrial issue is related to the appearance of this kind of defects: immediately after extrusion it is often impossible to determine whether the profile surface is correct or faulty because the streaks usually appear only after profile anodizing thus generating the rejection of the whole batch at a late stage of the production chain with an obvious economical consequences.

A definition of the streak defect was made by Parson in 1992 [1] as "bands or lines appearing darker or lighter, brighter or duller, in color and tone than the remainder of the surface". Stating this definition, several aesthetical defects can be classified under the 'streaks' definition but their origin can be related to different phenomena or technological aspects of the process, from alloy chemical composition to profile temperature distribution, from homogenization cycle to changes in profile thickness for example.

Further classifications of streaks types and causes have been than proposed. Most of them, as that proposed by Takagi et al. [2], highlight a distinction between streaks due to profile surface and due to metallurgical structure. The analysis matter of this paper deal with the latter kind; although a brief analysis of both kinds will be proposed so as to provide a better understanding of the proposed industrial problem.

The correlation between microstructure and surface appearance is well described by Zhang et al. [3] who reports how visibility of streaks is due to a difference in the intensity and diffusing nature of reflected light. The presence of localized, thus non uniform, surface imperfections as those amplified by different response to anodizing etching increases the diffuse part of the reflected light. Going backwards in the die streaks defect formation process the origin of such a difference in response has to be analyzed, this leading to investigate the cause of an heterogeneous microstructure. Such heterogeneity may be induced by inhomogeneous grain size, intermetallic (particle) distribution, precipitate distribution or texture. These considerations show the direction that has to be taken when inquiring the defect causes in a specific industrial product.

In this paper, a rectangular profile shape for window frames produced in AA6060 by means of direct extrusion on a porthole die was analyzed. A thin bright streak was revealed after anodizing in the middle of the long edges in proximity of the seam weld (Figure 1 a), and the streaks were more clearly visible in the upper side of the profile with respect to the lower one (Figure 1 b and c), where upper and lower sides are referred to the positioning of the profile exiting from the extrusion press. The profile was investigated with three methods: by means of metallographic analysis, SEM (Scanning Electron Microscope) observations and EDS (Energy Dispersive Spectroscopy) estimation in order to understand the origin of the defect and the relation with process parameters and die design.

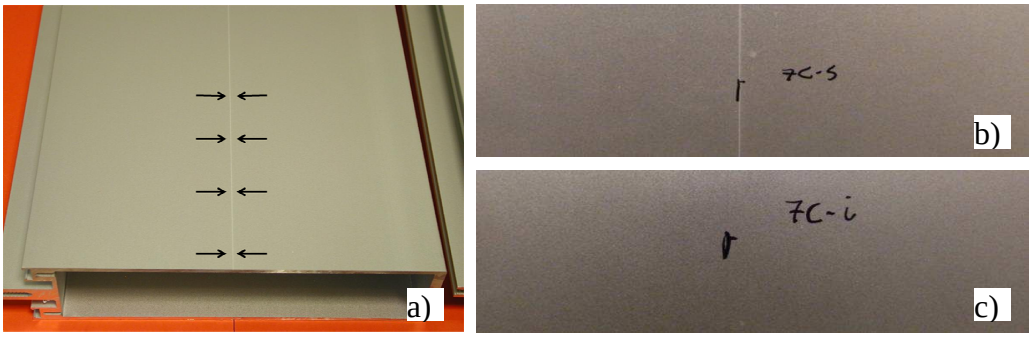

Figure 1 - a) Profile surface and streaks defect (upper side), b) upper side close up view, c) bottom side close up view.

Optical origin of defect. As previously mentioned, the appearance of streaks has to be related to a difference in the intensity and diffusing nature of the reflected light. Zhang et al. [3] report the Rayleigh criterion for smooth surface condition:

$$h \prec \frac{\lambda}{8\cos i} \qquad (1)$$

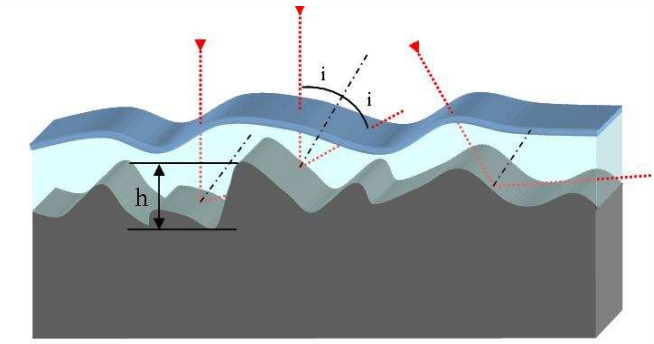

Figure 2 - Diagram of anodized profile surface, the actual reflecting surface with the roughness parameter h and the angle *i*.

in which *h* is the roughness height (Figure 2), λ the light wavelength (0.38-0.78μm for visible field) and *i* the reflection angle. For a reflection angle of 60° h≤0.2μm is obtained, which means that for roughness changes greater than 0.2μm there will be a visible effect. It is important to remember that the reflecting surface in an anodized aluminum surface is mainly that of the metal as the aluminum oxide is transparent. Changes in surface roughness grater than 0.2μm generated prior or during anodizing can therefore generate streaks defects. It is then evident how this kind of defect cannot be recovered after anodizing.

Billet metallurgical cycle. Going further back in the defect formation process it becomes evident how, to bare the cause of microstructure heterogeneity, the whole product process chain from billet casting to final anodizing has to be considered.

The 'theoretical' thermal cycle which the material undergoes is reported in Figure 3 described below along with the changes in microstructure [4]:

Casting. The DC casting process involves heating over the melting temperature and subsequent quick cooling. The type of procedure allows to obtain long billets but the solidification process is not quick enough to avoid segregation so to obtain generally a coarse distribution of big size intermetallics and precipitates.

Homogenization. It is a heat treatment after casting at very high temperature (500-550°C for AA6060 alloys remaining below melting temperature) within the single phase region in order to remove segregations and obtain a homogenous composition, removing some casting defects and allowing the dissolution of particles (MgSi) and intermetallics (AlFeMnSi). At the end of the treatment all the constituents (Mg, Si and impurities such as Fe and Mn) are in a single α phase (supersaturated solid solution, SSSS). A perfect treatment should tend to avoid the presence of such particles but industrial standard produce limited precipitation of particles and intermetallics. Process temperatures and permanence time influence the complete solution of alloying elements while cooling rate influences type and shape of particles [5].

Pre-heating and extrusion; this should be fast enough to avoid any substantial changes in particle dimension and number, although in industrial practice this is seldom the case. A solution soaking can therefore be performed after extrusion.

Solution soaking; it involves heating the material above the solvus temperature for sufficient time to dissolve any secondary phases that may have come out of solid solution during processing. As diffusion redistributes the solute from the precipitate phase to the matrix into a supersaturated condition, the material must be quenched to produce a super-saturated solid solution at low temperature. It is rarely applied and usually on critical alloys.

Quenching; if the alloy were slowly cooled, the β phase (mainly Mg_2Si for AA6060) would nucleate and grow at heterogeneous sites to form an equilibrium α+β structure. By quenching it is possible to reduce the time for diffusion and effectively 'freeze' the non-equilibrium α phase structure. Since the α phase contains now more solute than its equilibrium level, this solid solution is described as being supersaturated.

Ageing; the goal of this operation is to obtain a controlled decomposition of the SSSS so to have at the end a fine dispersion of precipitates (Mg_2Si). The precipitates type (GP, β', β) and precipitation distance are strongly dependent on precipitation temperature as well as precipitation time. An optimal fine and homogenous distribution of precipitates inhibits dislocation movements, thus producing best precipitation hardening effect.

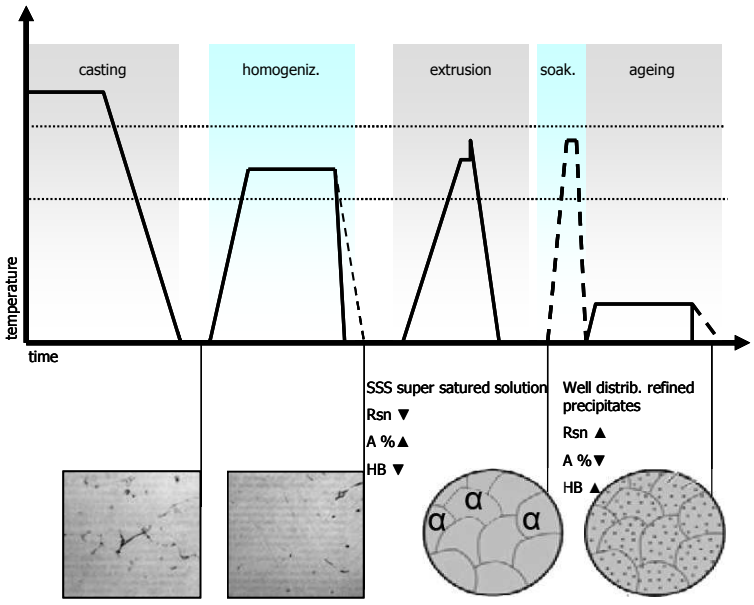

Figure 3 - Billet methallurgical hitory.

Streak types. In an attempt to collocate the investigated problem in the variety of streaks type, a brief description is hereafter reported. Referring to Figure 4 streaks defects can be classified into four main categories depending on their cause: billet structure, extrusion process and parameters, die design, and die performance.

- Billet structure streaks arise as a consequence of inherent bad quality of billet in its cast condition. This includes surface and bulk segregation, excessive coarse intermetallics and voids.

- Extrusion process & parameters streaks occur as a result of extrusion conditions; these not only involve ram speed and preheating temperature but also all the aside conditions, which can be both direct, like lubrication or back end lenght, and indirect, like container wear or deposits. The final product appearance is very dependent from all the above parameters. The product surface temperature is strongly bounded to extrusion speed and can overgo the solidus temperature. In this case, before the typical "speed cracking" the profile surface is already unacceptable due the onset of "pick-up" defects. The exit temperature is also limited by the precipitate distribution; it is therefore self evident how this parameter is bounded also to the billet structure -especially to it's homogenization process- and other elements so to create a very complex web of interactive parameters. The chemical composition of the material can be "polluted" by lubricant, oxide and skin elements which, dragged into the profile during extrusion, will create localized heterogeneities sometimes emerging to the surface (in this exposition the effect on mechanical properties has not been considered).

- Die design streaks are due to effects on deformation parameters (i.e. strain, strain rate, temperature) determined by die design, that is the way the final profile is attained. The geometry itself can imply T-junction, different wall thickness along the profile or seam welds which can all be cause of non-uniform material flow.

- Die performance streaks occur as consequence of mechanical action on the exiting profile. A damaged die can indeed scratch surface or modify geometry of the extruded profile; this can be produced by hard deposits (oxide or carbon) or local material dead zones. This category generation process is substantially different from the previous ones, where a web of parameters that affect metallurgical structure (i.e. grain size, precipitates, intermetallics).

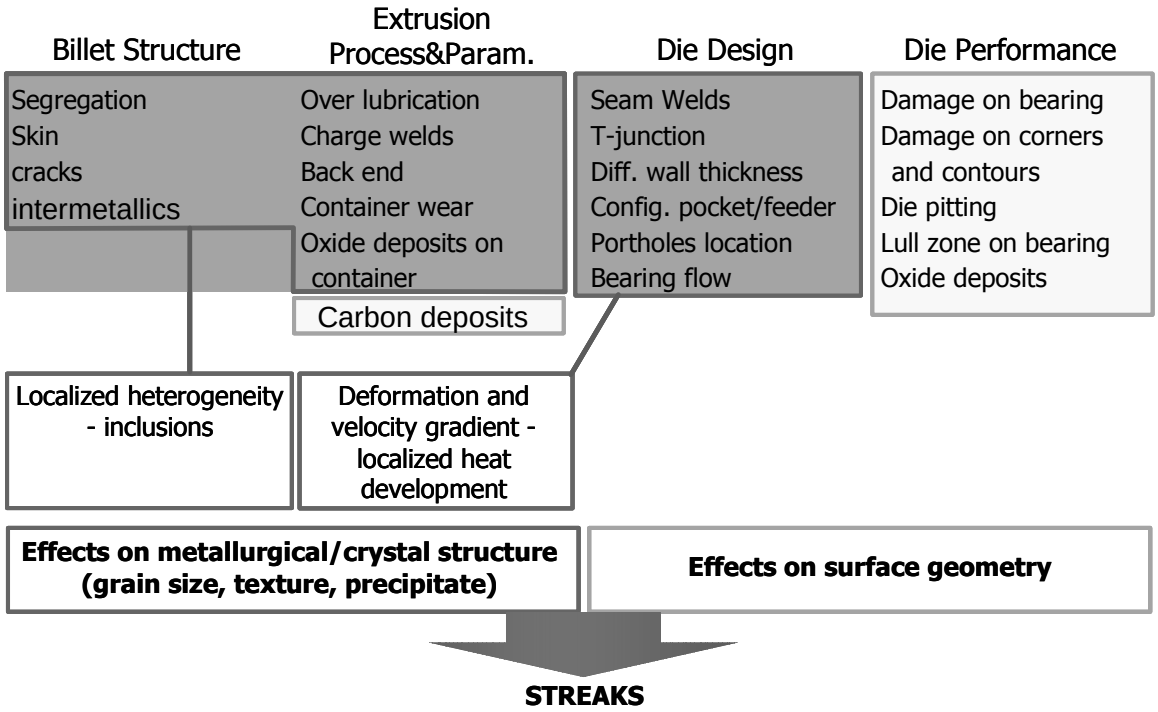

Figure 4 - Streaks cause classification diagram.

Welds. Among all the variety of causes exposed above, seam and charge welds are most likely two of the major "actors" in streak formation. They have quite different causes although they produce the same web of effects, this is the reason why they are also referred to as longitudinal and transverse welds.

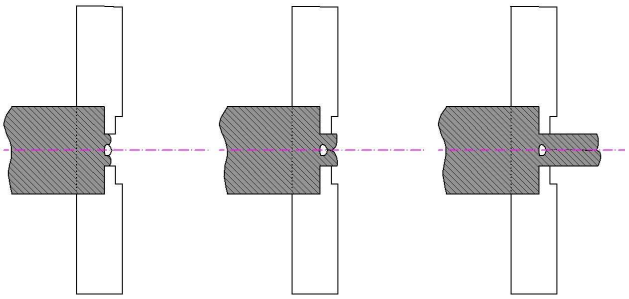

Figure 5 - Metal flow throughout the die ports and seam weld development.

Seam welds (or longitudinal welds) occur at the location of bridges as a consequence of metal flux merging together for welding trough adjacent ports; they are therefore present almost exclusively in hollow profiles, all along the length of the profile. Apart from their effects on mechanical properties it is important to point out that they imply an alteration in material flow, strain, strain velocity and temperature. If the two different fluxes participating to the weld also differ -even if slightly- in velocity or direction all the effects are magnified. This alteration leads to a different metallurgical structure from the rest of the profile. Depending from the severity of this microstructural unevenness a streak could turn to a visible defect: as a matter of fact a streak is always present even though not visible. This is represented in Figure 5 with a junction line halfway trough the section view of the profile.

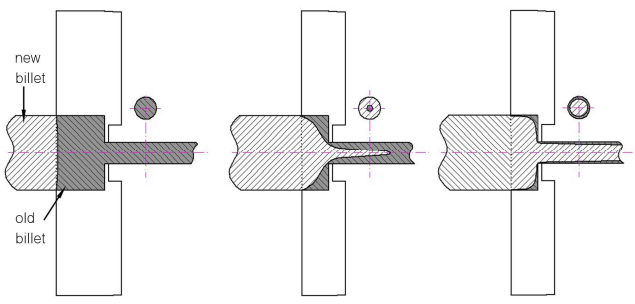

Figure 6 – Development of new billet metal flow in solid profile.

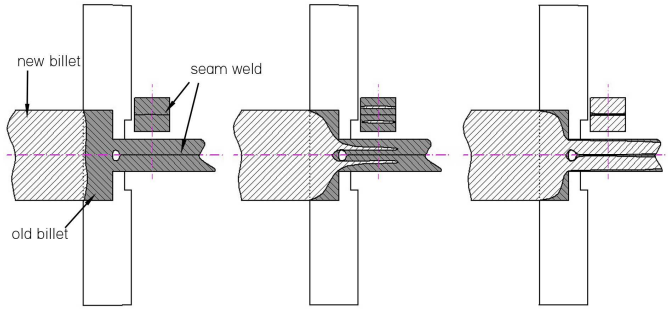

Figure 7 – Development of new billet metal flow in void profile.

Charge welds (or transverse welds) arise from the contacting surface of the new billet on the old one, at the end of the extrusion stroke. It starts as a plane surface, but the different flow speeds at different locations (inner points flow much faster than outer ones) soon stretches it longitudinally. A schematic representation is pictured in Figure 6 with a 3 steps development in a solid profile. The new material flows faster closer to the core while it is almost still at the container interface; this effect rebounds on the extruded profile carrying signs of the junction for a long extent before all the material from the former billet is "worn out". The image also shows, on the section views, the rise of the welding line-surface to the extruded profile surface.

In case of hollow profiles the same behaviour leads to an interaction of seam and charge welds as the charge weld surface it is carried through each of the die ports (Figure 7). In a section view this behaviour appears with a separate closed junction line for each port area that during the extrusion process merges towards the surface and the seam weld lines; this behaviour leads to the typical "three longitudinal welds" effect for each of the die bridges. The extent to which the charge weld line approximates to the profile surface was found to increase with the ratio of welding chamber area over section area [1].

The defect associated with charge welding has a further great parameter to be considered, which is the metallurgical history and compound of the previous billet back end. Leaving aside lubrication and wear of the container the butt is the zone where the major part of billet skin and surface layers are collected. Even though part of it is removed before the insertion of the new billet, a metallurgical inhomogeneous section is still present to be extruded with the consequent worsening of seaming interaction over precipitates, intermetallics and grain size.

Experimental

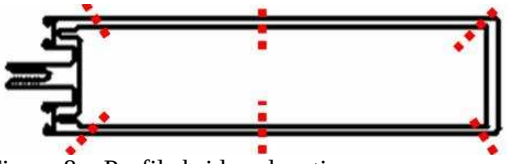

Figure 8 – Profile bridges location.

In the case studied in this paper, due to the dimension of the profile the die required the use of six portholes, thus producing four seam welds in the corners of the profile and two in the middle of the long edges Figure 8. This case study is of particular interest because the streak appeared only on the upper side of the profile in spite of the symmetry of the die and of the process, thus allowing a comparison of the material microstructure in the two symmetric sections.

Three spots of the profile were analyzed: two sections of the profile, upper and lower surface (1 and 3 on Figure 9), and one on the upper surface (2 on Figure 9). Investigation was carried out by means of optical analysis in bright field, optical analysis in polarized field, scanning electron microscope (SEM) and SEM with EDS probe.

All the data reported in this paper refer to the portion of extruded profile that revealed the greater defect, although other portions were investigated as well.

For **optical microscope analysis in bright field** the material was embedded, polished and etched with Keller reagent. This analysis highlights the presence and distribution of intermetallic and precipitate particles as AlFeMnSi and MgSi for the current alloy (AA6060). Their presence appears as a different color from the aluminum base matrix. From Figure 10 to Figure 13 they appear darker and distributed in a streak that cross the entire section. The streak is actually the composition of three lines; this is clearly visible closer to the profile surfaces where the three lines diverge. These lines are less visible on the lower section (Figure 13). If compared to Figure 7 it is well visible the similarity with charge weld lines behaviour.

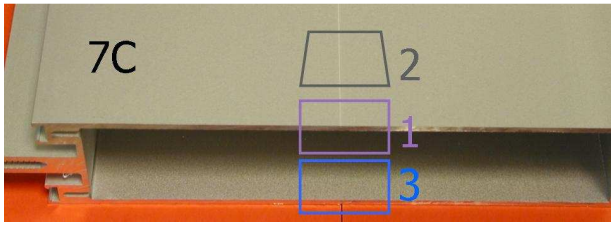

Figure 9 – Profile analysis spots.

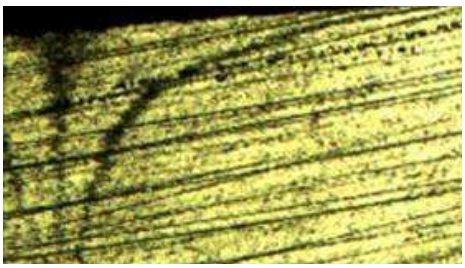

Figure 10 – Spot 1, upper surface zone.

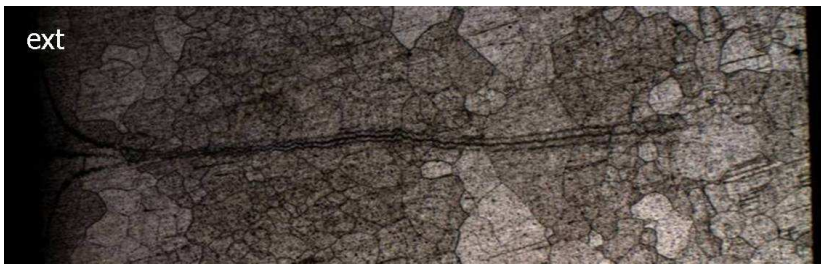

Figure 11 – Spot 1, entire section.

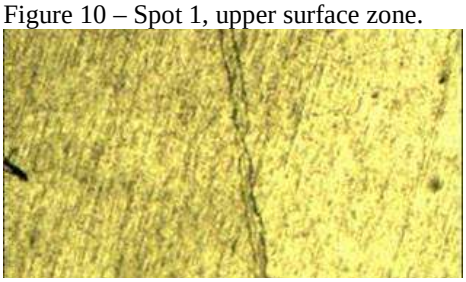

Figure 12 – Spot 3.

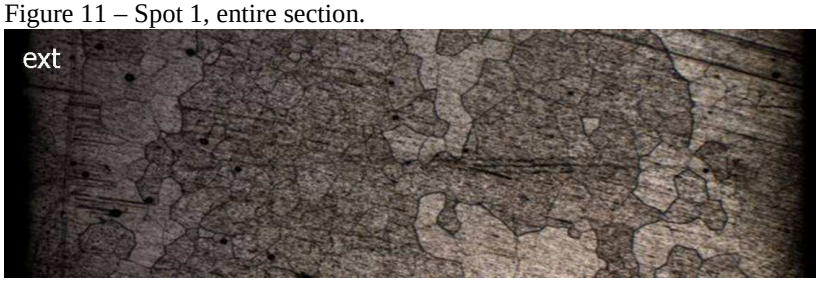

Figure 13 – Spot 3, entire section.

For **optical microscope analysis in polarized field** the material was embedded polished and electrolytic etched. The polarized view allows a better view of grain shape and their different orientation. In Figure 14 the same views of Figure 11 under polarized light is shows.

These two analysis show that the streak is the joint effect of three welding lines; these lines run across grains as well as between them. Grains have comparable size in the different areas.

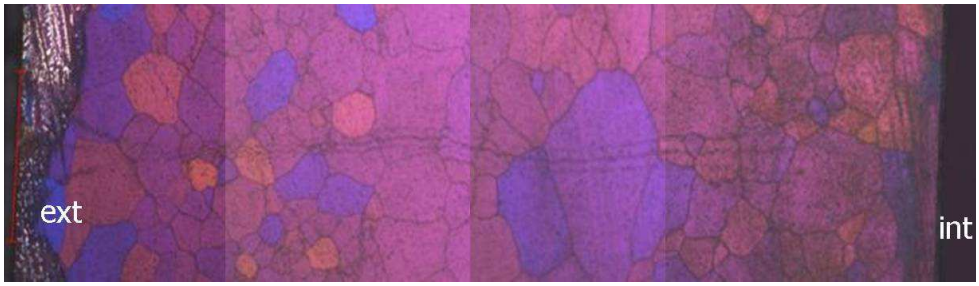

Figure 14 – Spot 1, polarized light view, entire section.

The **Scanning Electron Microscope** was performed with no etch -only the anodized state- on the surface (spot 2) and after Keller etching on the two sections (spot 1 and 3). This kind of analysis gives a more three-dimensional view of the material structure.

On section analysis the three lines visible in the previous views as darker areas are still visible and they appear as high density pits zones. With the EDS probe it is possible to analyse the chemical compounds of selected spots. Figure 16 shows different sizes analyzed spots and their chemical results. Besides the obvious major presence of aluminum the diagrams show traces of nothing more than the normal alloy elements thus excluding contamination by oxides or lubricants as the origin of streaks.

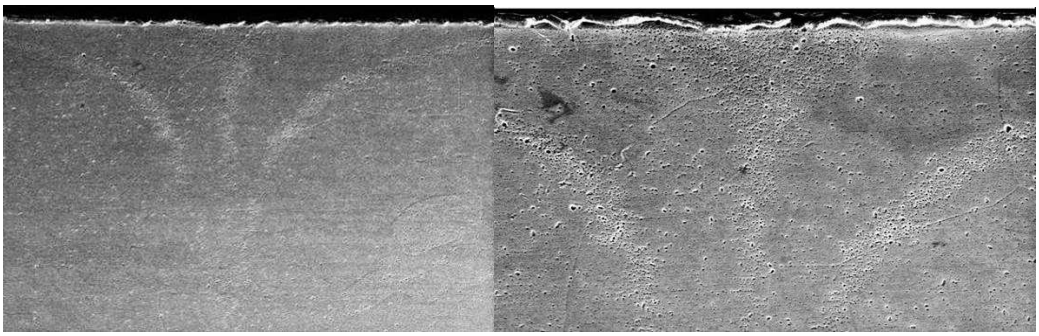

Figure 15 – SEM, spot 1, surface zone; two enlargements.

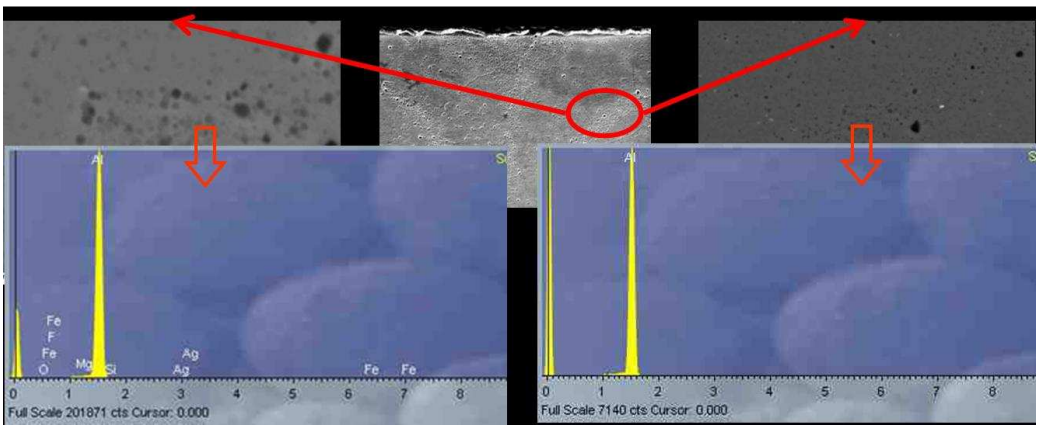

Figure 16 – EDS: chemical compund of welds.

The analysis performed on the surface (spot 2) revealed the streak defect as an etched "canyon" trough the more homogenous surface Figure 17. The pitted stripe is consequentially to the anodizing acid etch. Close ups of the stripe and out-stripe areas are visible in Figure 17, they reveal how the change in surface texture is very snap. The streaks zone has a rougher, coarser and etcher appearance if compared with the rest of the surface, which presents much more shallow and homogenous pits and grooves. If an evaluation of grain size on the profile surface was attempted, it would reveal the streak zone to be textured with grains of smaller size.

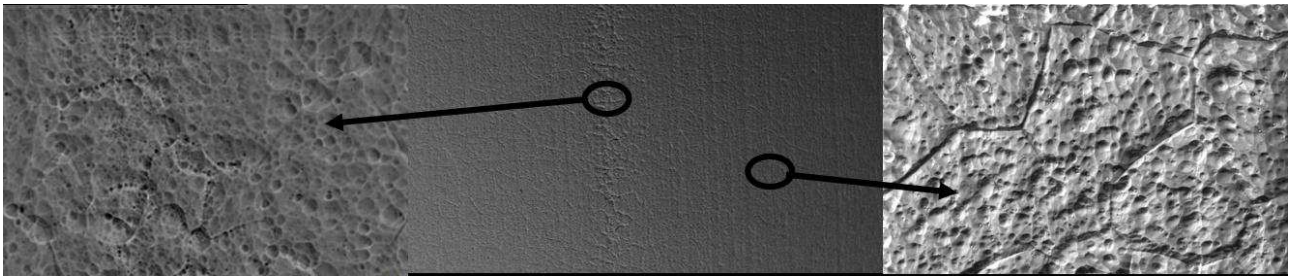
Figure 17 – SEM observation of surface at 75x magnification (center), streak canyon and enlargements of inner and outer streak regions at 1000x.

As exposed previously, the anodizing process is an etching process which can generate visible defects if an uneven microstructural distribution determines a sufficiently inhomogeneous attack. Two kinds of defects are visible in this analysis [3]: etch pits and grain boundary grooves.

Etch pits are cavities which formation has a direct relation to intermetallics distribution and size on surface. They are consequence of intermetallics adjoining aluminium matrix dissolution or by intermetallics direct dissolution; it depends from the different electrochemical potential. During anodizing the higher potential of Fe rich intermetallics compared to the Al matrix boosts the anodic dissolution of particles and intermetallics. In Figure 18 it has been highlighted the extent of this defect on both inside and outside streak zones.

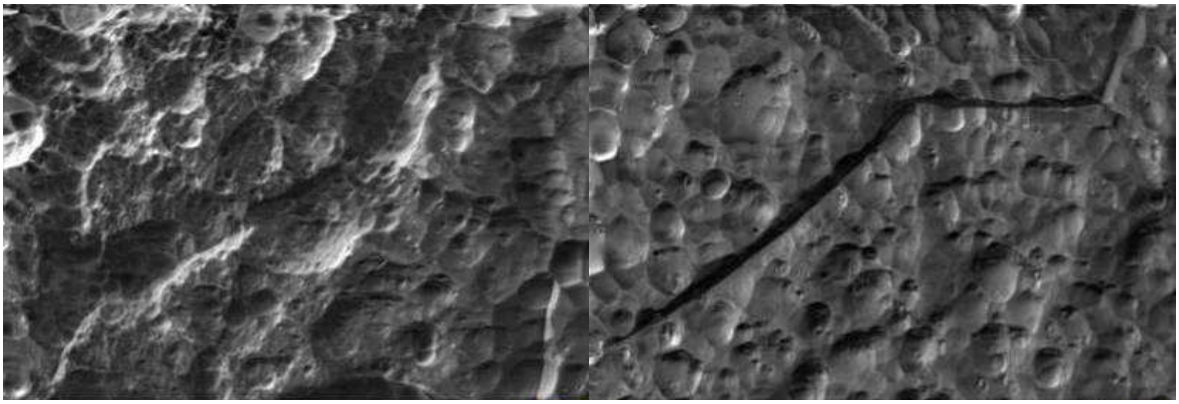
Figure 18 – SEM observations at 2000x, inside (left) and outside (right) streak area.

Boundary grain grooves are ruts along grain boundaries caused by a preferential etching along them during anodization. Their formation is directly related to Mg_2Si precipitates and $Al_{15}(MnFe)_3Si_2$ distribution in grain interior and grain boundary.

In Figure 18 the defect entity in inner and outer streak zones is shown. In the surface part not affected by streak defect the grain boundary grooves are well visible and deep. In the streak area they are not well recognizable, if present, as their size is comparable with that of the grain size and the etch pit defects.

An EDS analysis was carried out on spots inside and ouside the streak areas on the surface. For the inner area close ups were performed. Results of these tests are reported in Figure 19. Differently from the results on the section view, the presence of Oxygen and Sulphur was reported as a consequence of the interaction with anodizing solution. More localized checks lead to equal results. The comparisons of the different spots do not reveal differences in the chemical composition.

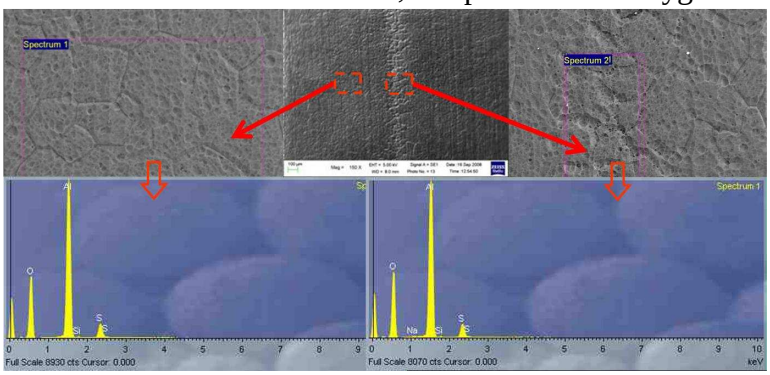

Figure 19 – EDS results for inside and outside streak areas.

SEM analysis showed that the seam welds are zones of preferential etching during the anodizing process, thus in relation to the local microstructure of the material and in particular relation with concentration of precipitates and iron-based intermetallics.

Conclusions

An overview on principal cause and developing phenomena of streaks was initially proposed. Then the analysis of an industrial extruded profile was performed revealing how interactions between seam and charge welds produce inhomogeneous metallurgical distributions which are loci of preferential etching during anodization. In particular these seam and charge welds interactions resulted quite sensible to the thermo-mechanical process evolution thus producing a more intense defect on one side of the profile despite die and profile symmetry. The result of the asymmetry in the thermo-mechanical behaviour is a distribution of particles and intermetallics more suitable to etching in the upper part of the profile respect to the lower one.

References:

[1] N.C. Parson, J.D. Hankin, and A.J. Bryant, “The metallurgical background to problems occurring during the extrusion of 6XXX alloys”, ET Seminar 1992, vol.2 (1992) pp. 13-23;

[2] S.Takagi and H.Hamzah, "Extrusion Defects - Streaking" Proceedings of Extrusion Technology Seminar (ET 2008), 2008, vol. 1 pag. 261-270.

[3] X. Zhang, H. Zhu, A.K. Dahle, M.J. Couper “Mechanisms of streaking on anodized 6XXX series extrusions” ET Seminar 2008, vol.2 (2008) pp. 455-464;

[4] Porter D.A. and Easterling K.E., "Phase transformations in metals and alloys", Chapman & Hall

[5] R. Shahani, R. Tirard-Collet, C. Sigli, “Optimized 6XXX alloy billet performance: a structural approach” Proceedings of Extrusion Technology Seminar (ET 2000), 2000, vol. 1 pag. 13-22.

[6] T. Ramanan “Helping the Customer” ET Seminar 1992, vol.2 (1992) pp. 35-42;

[7] L.Donati and L.Tomesani, "Evolution of particles and intermetallics during hot plastic eformation of AA6060 alloy" AMPT International Conference, Manama, Barhain, Oct. 2008.

Prediction of Position and Extent of Charge Welds in Hollow Profiles Extrusion

Antonio Segatori (*University of Bologna, Bologna, Italy*),
Barbara Reggiani (*University of Bologna, Bologna, Italy*),
Lorenzo Donati (*University of Bologna, Bologna, Italy*),
Luca Tomesani (*University of Bologna, Bologna, Italy*).

Abstract
In billet to billet direct aluminum extrusion the high hydrostatic pressure field produces the joining of the material, however the mechanical proprieties of the profile are lower in the welded region compared to the adjacent ones thus requiring the scrapping of the welded segment. The computation and localization of the segment to be discarded is a complex matter. Aim of this work is to investigate the interaction between the different welding phenomena inside an industrial multi-profile die, in order to determine the exact position and the minimal profile length to be discarded. Experimental investigation were performed on an industrial extrusion of four hollow profiles in EN AW-6060 alloy through a multi-hole die. Location and dimension of charge weld was retrieved and compared with finite element simulations of the process thus evaluating the possibility to use the code as reliable tool for the localization and determination of the scraps, in particular if new die design strategies has to be evaluated also in term of reduction of the zone extension.

Introduction
Aluminium extruded profiles are today extensively used in several types of applications in civil and industrial engineering, furniture design and in the whole transportation sectors (motorbikes and automotive frames, buses, trucks and trains, up to airplane primary structures). The proprieties and quality of the profiles are strictly related to their final application: if for aesthetical applications (i.e. windows frames or interior design structures) the surface aspect is of primary importance, in more severe loaded conditions (like automotive or aerospace) the mechanical proprieties of the profiles remains of critical importance. In particular transportations standards (EN 13981-1:2003 [1]) require 100% production testing at the beginning, middle and end of each extruded bar. These tests are necessary because both extremities of an extruded bar may be corrupted by defects that affect the final profile proprieties [2]. Parson et al. [3] classified and described the most common extrusion defects: pick-up, blistering, streaks and back end defects play a primary role on the surface aspects while in term of mechanical proprieties the most critical problems are incorrect heat treatment, seam welds failure and presence of charge welds inside the profile. Such defects often mutually interact but the studies available in literature usually analyze each imperfection singularly. In particular for an accurate understanding of the extension of the defective segment it is important to focus the attention on three phenomena: back end effect, seam welding and charge welding itself.
Back end Defect: it is also often called contamination by billet skin because it consists in the presence of billet skin inside the final profile (figure 1). In the direct hot extrusion of aluminum profiles a complex material flow is generated in the container and in the die in relation to the high friction conditions generated at the billet-container interface. The friction produces an imbalanced material flow that on one side positively affects the process (reduction of contamination by billet skin) but on the other side generates dead metal zones and complex material flow inside the die. The skin of the billet usually is characterized by a different chemical composition or microstructure respect to the inner material; this difference can be the results of an altered chemical composition (as consequence of cooling from casting) or of a contamination due to impurities (oxides, dust, oil, etc) during billet shipping, pre-heating and loading in the press. The key parameter used for controlling the billet skin contamination is the dimension of the discarded butt: a longer butt allows holding more billet skin and consequently it guarantees a contaminated free profile, while shorter butts represent a profit because less material is discarded. Figure 1 shows the evolution of the billet skin during a typical un-lubricated hot extrusion processing of an aluminum alloys: in relation to the high

friction factor with the container, the billet skin is accumulated in proximity of the ram and, if an adequate butt length is used, it is entirely discarded (Figure 1a), while, if a too short butt is used, the billet skin can flow inside the die up to the welding chambers and eventually also in the profile (Figure 1b). The phenomenon has been extensively investigated in literature [4, 5, 6]. In order to understand if the butt length is adequate microstructure analysis of the profiles in proximity of the profile end has to be performed. More in detail, when the ram is stopped the profile stick to the bearing zones thus creating a very evident mark on the profile surface called "stop mark"; the stop mark is a permanent shape marker on the profile that indicates the end of a billet stroke. If the billet skin overcome the stop mark the contaminated part of the profile has to be cut and discarded, while if the skin remains inside the die (eventually up to the welding chamber) the profile can be considered as skin free. In the industrial environment this type of analysis is actually performed by cutting several slices of profile on the right and left side of a stop mark, grind and etch them in order to verify the complete absence of skin contamination.

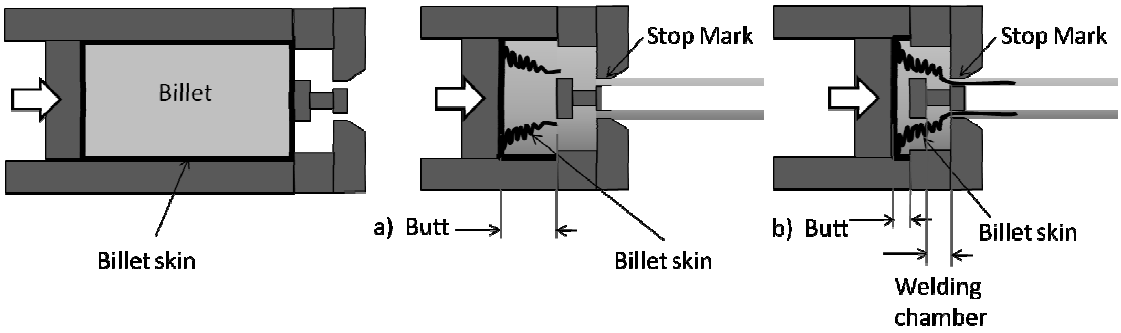

Figure 1: Billet skin contamination in the extrusion of a tube (schematic): a) long butt (no contamination), b) short butt (contamination).

Seam weld: while open-shape profiles can be easily produced by a flat die, hollow profiles require a porthole die that is split into two parts, the mandrel and the die (Figure 2). The mandrel realizes the shape of inner cavities while the die the outer shape. The billet is initially divided around the mandrel legs then it rejoins in the welding chamber at high hydrostatic pressures thus realizing a solid state welding all along the profile length; such weld is called "seam or longitudinal weld". These welding lines are generated in the profile section all along the extrudate length [7, 8]. Previous studies [9, 10] showed that such welds, when the die design and the extrusion process are conveniently optimized, can exhibit a resistance equal to that of base material, but a lack of knowledge on the interaction between billet charge and seam welds is still present.

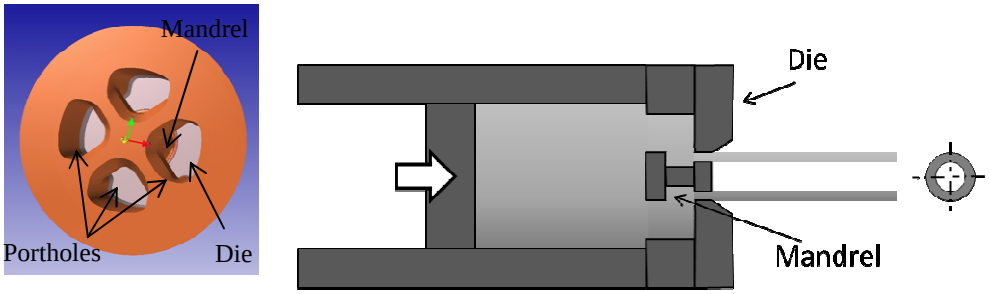

Figure 2: Schematic representation of porthole die and seam weld localization.

Charge weld: the material flow becomes even more complex when multiple billets are consecutively loaded into the press, as usually happens during continuous extrusion. Indeed at the end of a process stroke although the butt is removed the die remains completely filled by the material (figure 3a); this condition can be easily identified on the profile by the stop mark. When a new billet is loaded in the press a new speed gradient is generated in the material being in relation with friction. The old and the new billet start interacting producing on the profile a wide transition zone located on the left side of the stop mark: it is the so called "charge or transverse weld" often called as 'carrot' in relation of the shape of the new material in the old one. As visible in figure 3 c) and d), this transition is not localized in a single profile section but

extends itself along the profile to a variable length depending on die design and processing parameters [11]. The charge weld is generated at high hydrostatic pressure too, but differently from seam welds, it is usually contaminated by oxides, dust deriving from billet skin or by lubricant received during loading into the press. As consequence, the charge weld has to be discarded from the final profile because it attains lower mechanical proprieties. It is to be noted that, from an industrial point of view, two data are of critical importance: the position of the transition zone on the profile respect to the stop mark (which is usually different form hole to hole in multiple holes dies) and its extent.

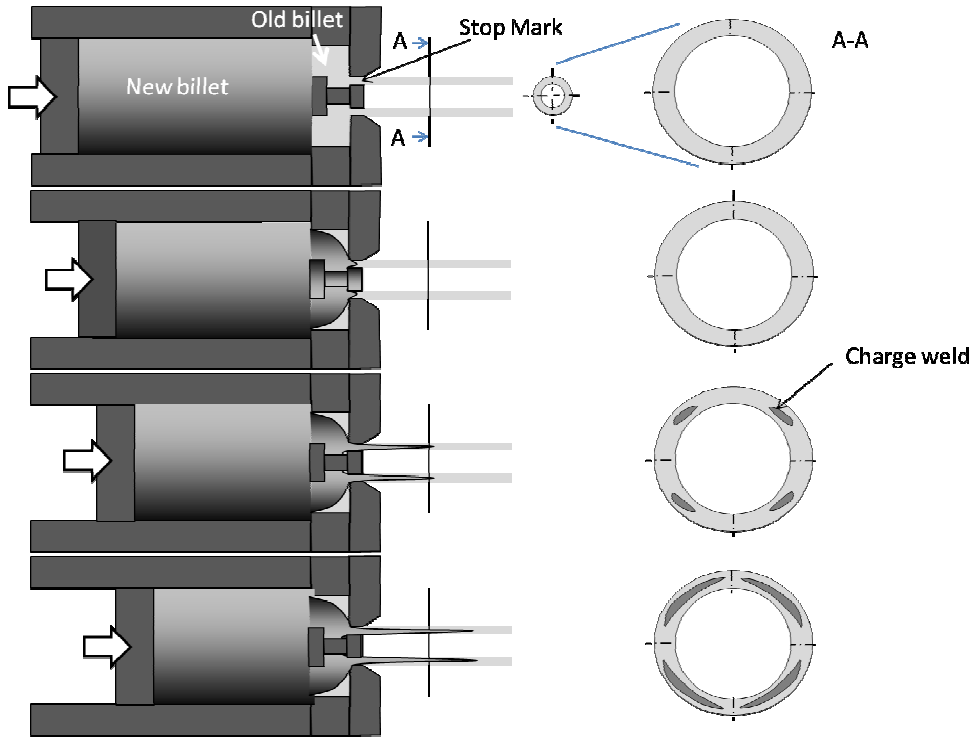

Figure 3: Sequence of a charge weld formation in a longitudinal and transverse views.

The three aforementioned phenomena have a deep interaction on the defect magnitude and extent. As a consequence, a wide segment of the final profiles has to be discarded due to lower mechanical proprieties. In industrial practice, the determination of the zone to be discarded is usually performed by means of rule of thumb or, in the more critical applications, by labour intensive microstructure investigations at the beginning and end of each extruded lots. The phenomena interaction produce considerable process inefficiency, since either a large portion of profiles have to be discarded or a great amount of time has to be spent for scrap reduction. It is worth noting, in addition, that the possibility to reduce this defect through a dedicated die design is actually never considered.

Finite Element Modelling (FEM) has been used to optimize the extrusion process saving expensive and time consuming trial and error experimental procedures. In the last decade, in a number of works in literature the extrusion process of aluminum profiles has been simulated by means of FE codes [12, 13, 14, 15]. The common effort is to improve the computational tools in order to limit the role of expensive experimental campaign. However, while the evolution of seam welds has already been modelled by means of a number of numerical models [16, 17, 18, 19, 9, 20, 21, 15], no studies, to the knowledge of the authors, report the experimental validation of a FEM-predicted charge weld evolution.

Aim of the present study is, first, to investigate the evolution of charge welds inside an industrial multi-profiles die, in order to determine their exact position and extent, thus determining the minimal profile length to be discarded. The convergence of the charge welds towards the seam lines is also considered in order to give a deeper focus on the interaction mechanism between these two types of welds.

Then, the evaluation of the numerical simulation capabilities on such a real industrial application is carried out by means of the commercial code Altair HyperXtrude®. To this aim, numerical predictions were

compared to experimental data with a particular focus on the computation of charge weld position and extent.

Experimental investigation

Experimental set-up

The experiment was performed on an industrial 1600 tons extrusion press at Alutitan plant. The porthole die consisted of eight cavities to produce four hollow profiles (Figure 4a). The profile geometry presents a massive part with a thin long tongue (Figure 4b). The inner cavity is produced by a mandrel supported by two bridges, so that seam welding will occur. A non symmetrical position of the profiles, with respect to the horizontal axis of the die, allowed to investigate the influence of the holes placement and orientation on the metal flow (profiles A-D have the massive part of the section toward the centre of the billet, while C-B have the thinner) while the vertical symmetry allowed the FEM computation of half model. The minimum profile thickness was 1.4 mm, the section area of each profile was 135 mm^2 and the maximum bearing length 11 mm.

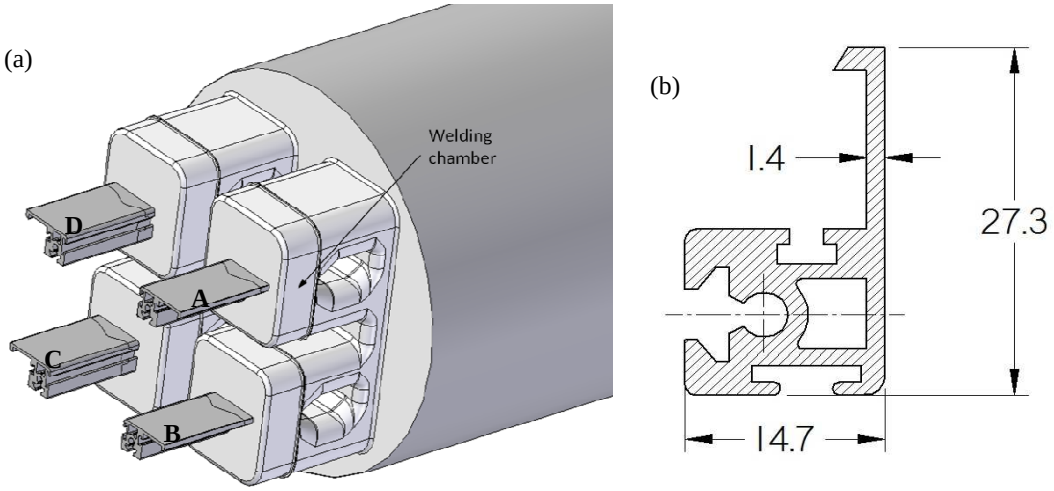

Figure 4: (a) The die used in the experimental design with the profile labelling (press exit view), (b) profile shape

Four billets made of a AA6060 alloy were consecutively extruded during the experimental investigation. The temperature of the container was kept at 410°C and that of the ram at 450°C. The die and the billet were preheated at 468 °C and 478 °C respectively. Table 1 reports the initial thermal and geometrical conditions of the experimental set-up.

Table 1: Initial temperatures and geometries of the billets and tools involved in the experimental set-up.

	Temperature [°C]	Lenght [mm]	Diameter [mm]
Billets	478	500	178.0
Die	468		
Container	410	1150	186.0
Ram	450	150	185.5

The temperature of the profile A was continuously monitored by means of a pyrometer (accuracy of ±5°C) pointed in the middle of the flat profile portion at 1 m from the die exit. xtrusion load, ram speed and profile velocity were registered as well in order to validate subsequent FEM simulations. The four profiles were sequentially marked in order to track down profile correspondence with die hole (A to D) and the billet number. The profiles clearly showed the “stop marks” (Figure 5b), thus allowing a stable position referencing in the several profiles independently of the process stoke. Indeed, these marks permit to roughly identify the position of the segment to be discarded: the charge welds appear at a distance d_0 (Figure 5b) from the stop mark that depends on the die design and on process parameters; after a distance d_f from the stop mark the transition is completely finished and the profile is made of 100% new billet

material. In Figure 5 are also showed the four extruded profiles (Figure 5a) and the labelling method used to track the sections of the profiles (Figure 5c).

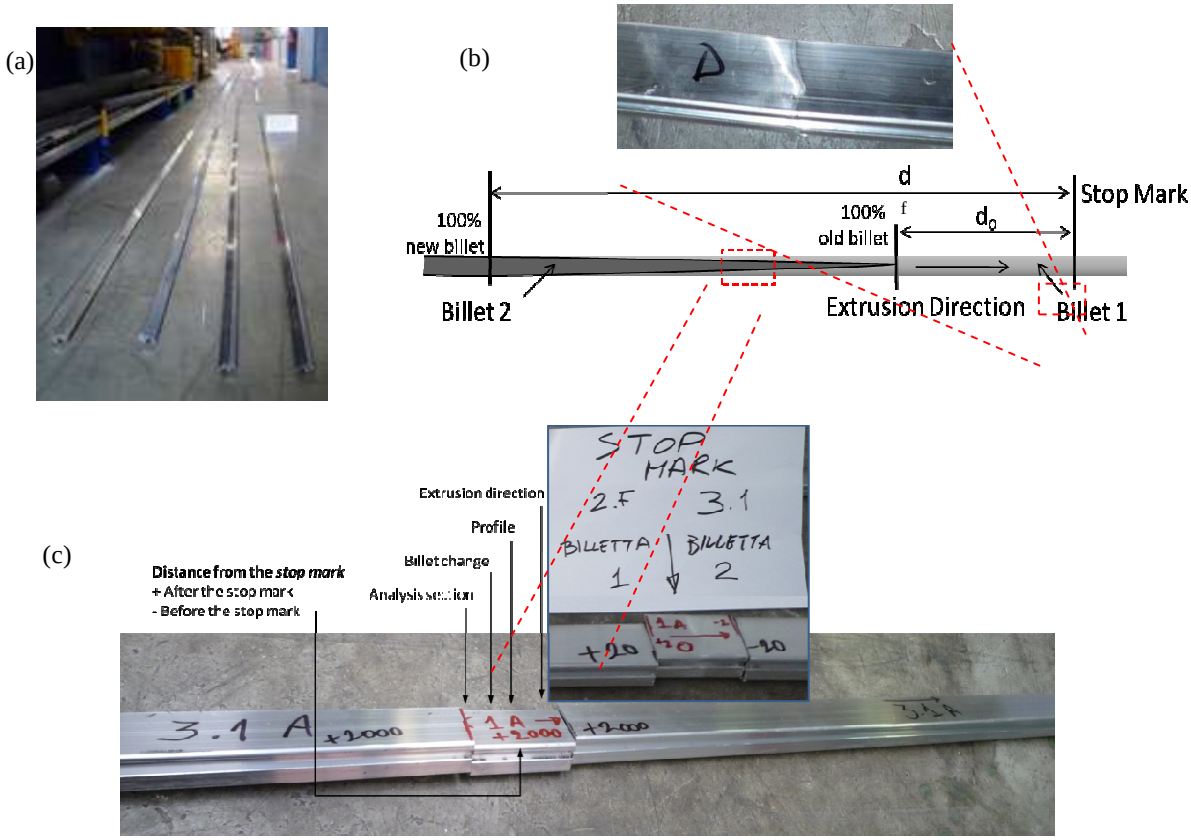

Figure 5: (a) The four extruded profiles; (b) Stop mark evidence in one of the extruded profiles and (c) the experimental sample labelling.

The transition between the first two billets was chosen to explore the welding phenomena interaction, this in order to limit the interference of previous billet material deposits. The four extruded profiles were analyzed by cutting slices every 50 mm on the left side of the stop mark (figure 2 b))for welds investigation. Each specimen was grinded, etched by fluoride acid dilute in water, HF 10%, and observed at the optical microscope. For each slice, the percentage area of the new billet was computed by means of image analysis software (AxioVision). The analysis was carried out till complete exhausting of charge welds. Analogous activity was performed on the right side of the profile from the stop mark to check the presence of back end defects.

Experimental results

In the following two figures process parameters monitored during the experiment for the four extruded billets are reported.

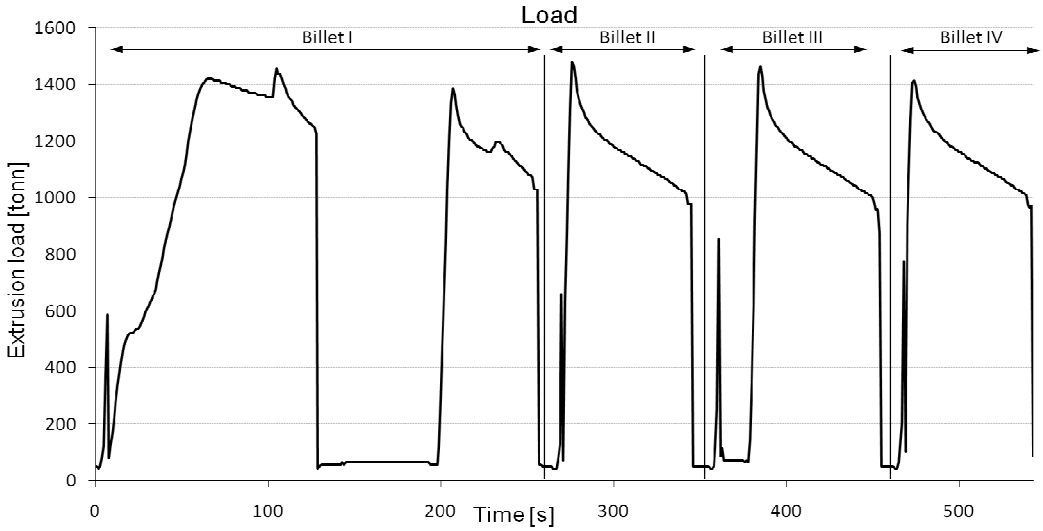

Figure 6: extrusion load.

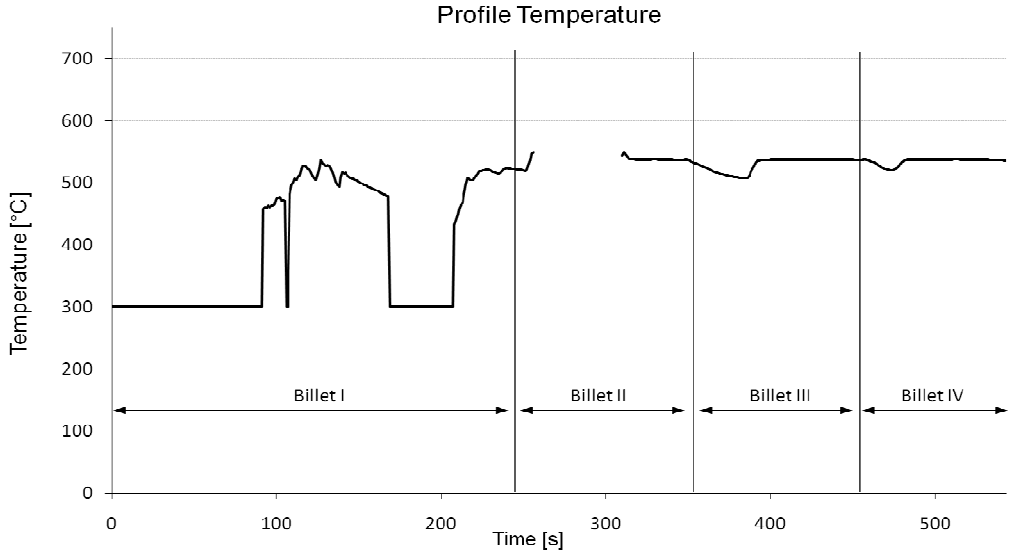

Figure 7: profile temperature acquired by pyrometer.

Table 2: Difference in length after the first 7 m of extrusion compared to profile D.

Profile A	-660 mm
Profile B	-770 mm
Profile C	-610

Since profiles were supported by a puller, the speed was stable and only the first recording was performed with free profile prior to tip cutting. This resulted in a different profile speed only for the first recording even if with a higher ram speed of 6.2 mm/s versus the initial 5.3 mm/s. Before the puller was activated profile D showed to be the fastest: difference in length of tips, after the first 7 m of extrusion, for each profile compared to profile D is reported in Table 2. Similarly the extrusion load of the first billet was still influenced by the initial thermal transient with the die at a lower temperature that increased the flow stress of the material.

At first it was investigated the trend and quality of the seam weld in the real early portions of the extruded profiles. For this activity the tips of each profile were sliced and analyzed from 50mm out from the tip. Welds were well evident as a dark line (Figure 8). They were localized, as expected, close to the two bridges although not perfectly straight and a bit shifted toward the thinner part of the profile. Figure 6 also shows their position in respect to the bridges axes. This effect is most likely to be associated to a faster flow in the more massive part, also in good agreement with the results of the charge welds shown below.

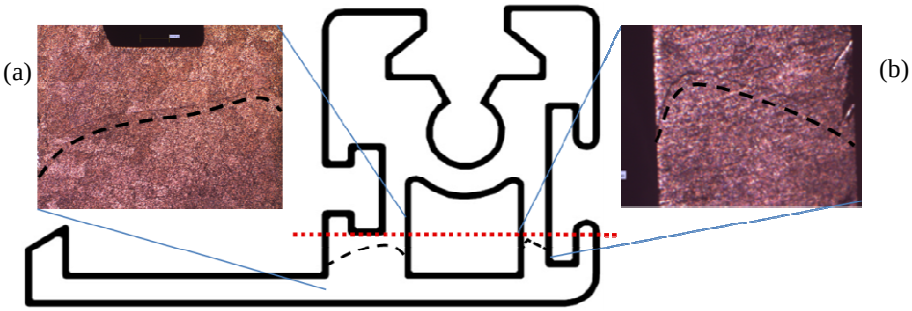

Figure 8: Position of the theoretical seam weld on the bridge axis (dotted line) and experimental seam weld (dashed line). (a) Left seam weld for profile A at 200mm from tip – bright field, (b) right seam weld for profile A at 200mm from tip – bright field.

Once seam weld position was retrieved, analysis moved to the first billet change. The investigations of back end defect did not reveal any contamination of the billet skin in the profile. Both the profile section before and after the stop mark did not show the typical variation in microstructure color (mostly lighter) associated with oxide or carbide contamination.
The analysis of the charge weld produced micrographs as the one shown in Figure 9, were multiple micrographs have been composed to recreate a complete view of the weld over the profile section. Once the image was composed, it was then possible to carry out a measure of the area enclosed by the weld line and therefore the percentage of new material at a specified point of the profile, that is, the exhausting of the old billet material. Along with this activity the starting and ending point were looked for. With both this information it was possible to retrieve extent, position, and trend of charge weld for each of the four profiles.

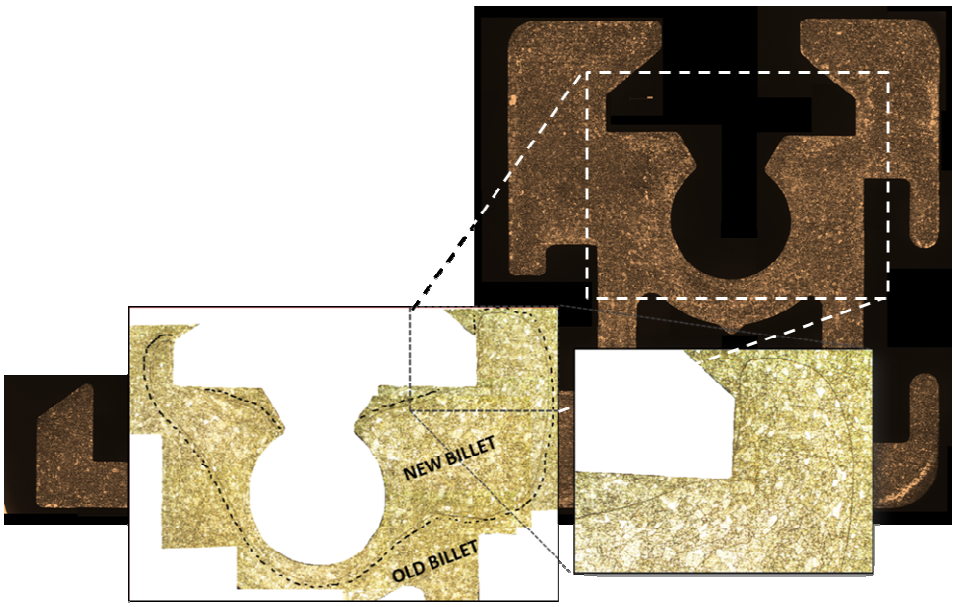

Figure 9: Composition of complete micrographical profile section

Figure 10 shows four steps of the sequence required to assess the evolution of the transition within the profile section. In particular, the different sections analyzed for profile B at increasing distances *d* from the stop mark are reported with the weld line highlighted. Figure 10a shows the starting point of the charge weld that always appears as a small closed loop on the section. Figure 10b indicates how the new material replaces the old one within the profile section. It is well apparent in Figure 10c how the new material has nearly filled the thicker part (flow X) and, at the same time, has just appeared in the thinner part (flow Y) of the profile. Both flows converge on the two seam welds (Figure 8) and in Figure 10d there is no residual trace of charge weld in the upper part of the profile, while the lower flow is not complete yet. The way the profile section is filled depends on the particular die design: aluminium flows faster in the upper part due to the bigger die feeder, thus producing a faster charge weld transition with respect to the bottom region. The filling of the lower region ends only at 1900 mm after the stop mark.

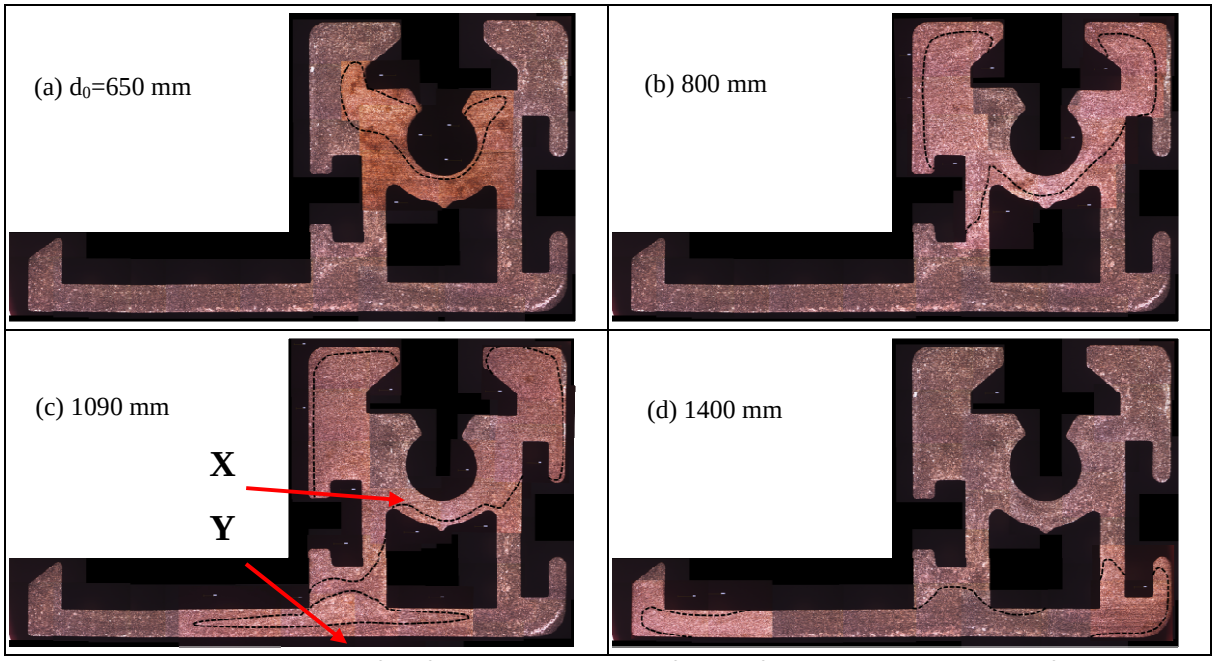

Figure 10. Charge weld evolution of profile B: image analysis of the profile at increasing distance d from the stop mark.

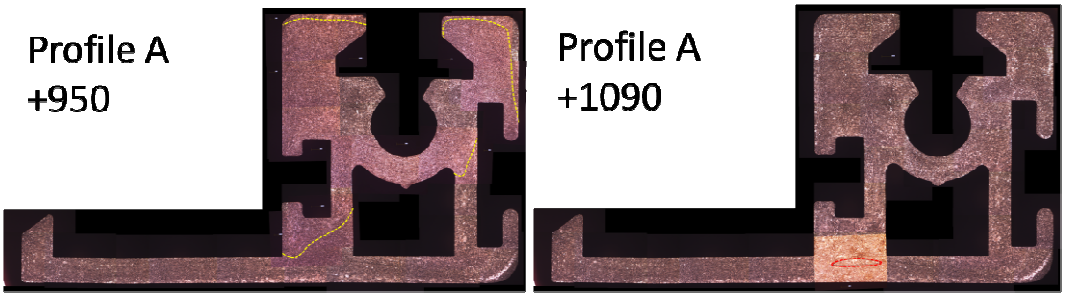

Figure 11. Profile A, end of charge weld in flow X and begin in flow Y.

For profile A, two results are of evidence. First, the filling of the two parts of the profile by the new billet is disjoined (Figure 11), i.e. only when the upper part is completely filled the new billet material starts flowing in the lower part, thus increasing the final extent of the charge weld (Figure 4-profile D). Second, the lower flow presents a charge weld extent (950 mm) equal to the upper one even if a smaller and thinner area has to be replaced.

Figure 9 reports the percentage of the new billet over the stop mark distance for the X and Y flows for the four profiles. Graph representation allows an immediate overview of the charge weld over a single profile as well as between profiles. It can be noted how for all the profiles the charge welds start at different distances d_0 (in the range 400-550 mm) and always at the more massive part (X) of the section. On the

other hand, the complete transition length of the phenomenon strongly varies from 1550 mm on profile C to the 2100 mm on profile D. Moreover, for profiles A and D the filling of X and Y parts are completely disjoined and in particular the D profile shows about 100 mm distance between the exhausting of the upper weld and the onset of the lower one, thus producing the greater transition distance. On the other hand, in profiles B and C the two transitions partially overlap; this is particularly relevant in profile C, where the shortest transition is seen. The die design, in particular the feeding port dimension or the localization of the profiles on the die, together with their orientation, has a great effect on the velocity unbalance; it’s clear that such transition is too complex to be analytically modelled even with rule of thumb thus requiring massive metallurgical analysis for charge weld extent determination that has to be repeated for every new die design.

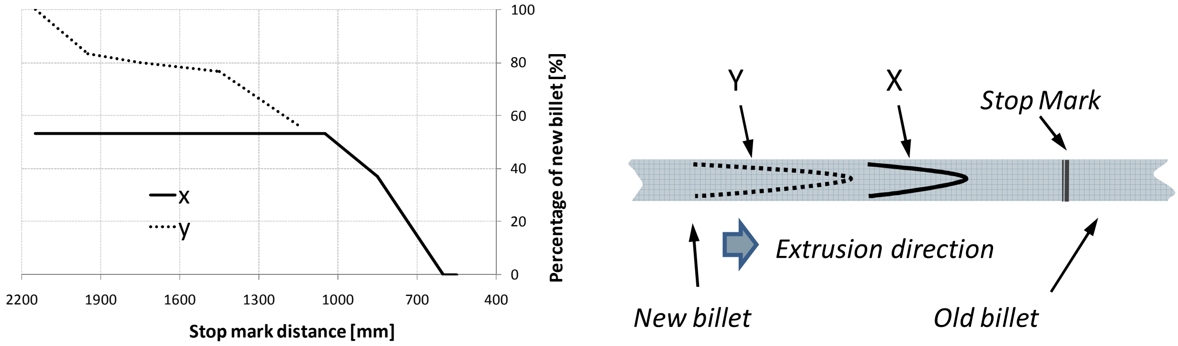

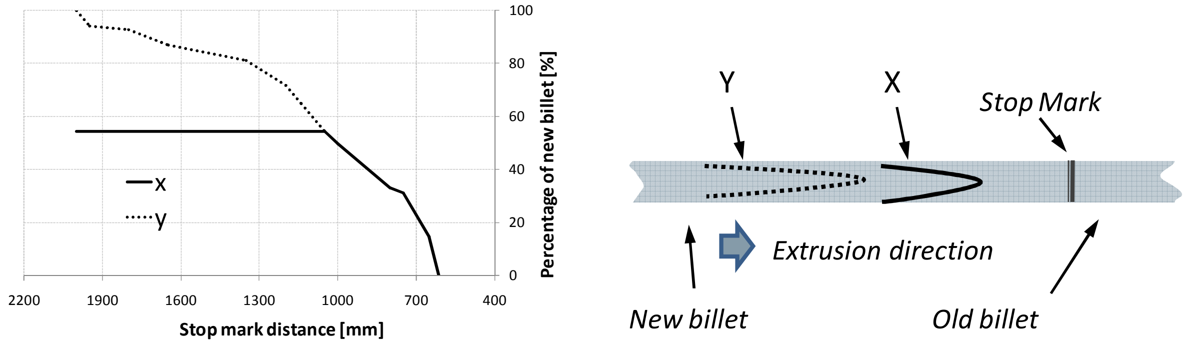

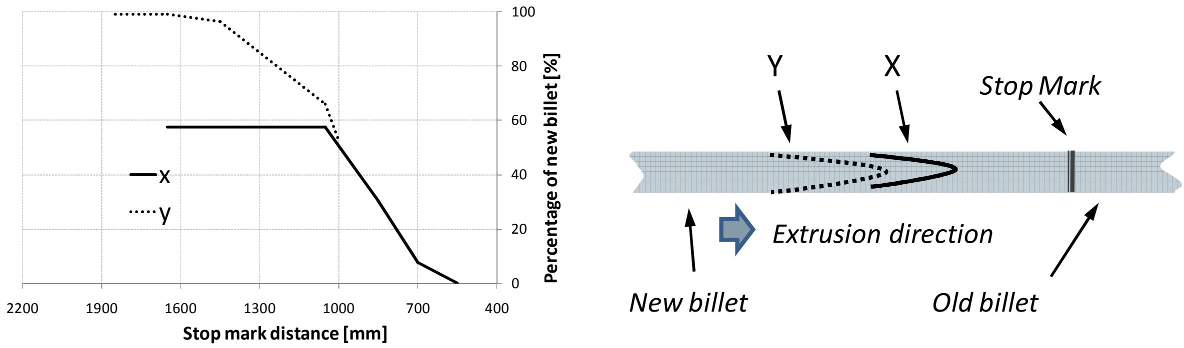

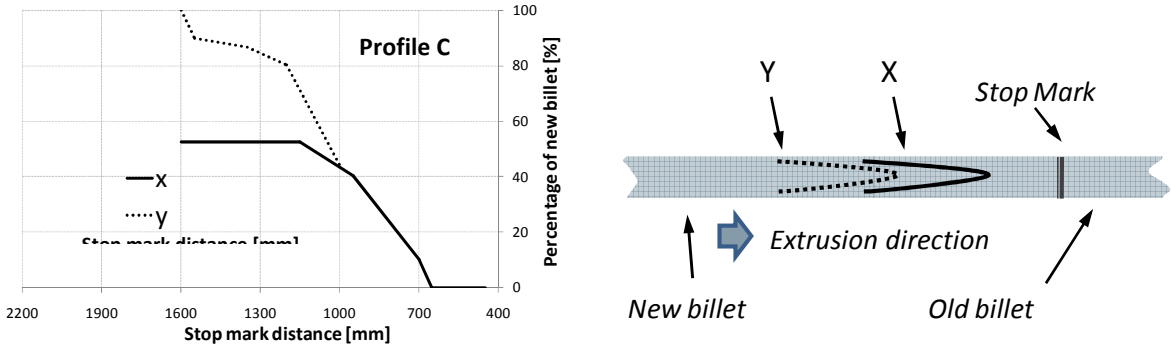

Figure 12. Percentage of new billet material, divided for X and Y flows, in the profiles over stop mark distance and corresponding schematical representation.

Profiles A and D have the greatest transition length because their thinner sections are located at a greater distance from the die centre (which causes a slower material flow). In order to minimize such transition, the different flows should emerge at the same time inside every feeder for all the profiles and, possibly, at a minimum distance from the stop mark, which represents a scrap itself.
Table 3 reports the precise starting and ending measurements of the charge weld. Data are also reported for the each of the two flows (massive, X, and thin, Y)

Table 3: Charge weld starting and ending points.

Profile	Start-stop distance from stop-mark [mm]	X	Y
A	1950-565	1000-565	1950-1090
B	1600-500	1000-500	1600-900
C	1550-400	1150-400	1550-950
D	2100-500	1000-400	2100-1080

Numerical analyses

FE model

The evolution of the charge welds in the investigated extruded profiles was simulated by means of Altair HyperXrude® (HX) (Altair Engineering, Inc., Italy). HX is a commercial FE simulation code for the analysis and optimization of the extrusion process and dies, based on a fluid dynamic approach for modelling incompressible flows, including non-Newtonian fluid behaviour [22].
According to this type of modelling technique, the model of the aluminium billet had to copy the final shape of the extruded profile. It was therefore derived as the Boolean subtraction between a cylinder and the 3D CAD model of the die (Figure 13a).

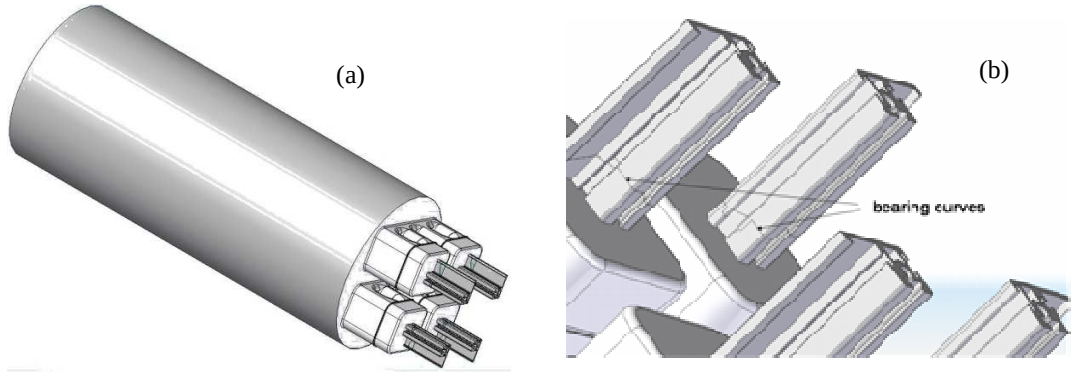

Figure 13: (a) The 3-dimensional CAD model of the billet as required in input in HX; (b) magnification of the bearing curves.

The bearing curves were extracted by the 3D CAD model of the die and then projected on the billet surfaces (Figure 13b). As explained before, due to the symmetry of the profile, only half of the model was simulated focussing on profiles A and B, thus reducing the number of mesh elements and computational times. The resulting model was divided in 4 components due to the different boundary conditions involved: billet, porthole, that included the welding chamber, bearing and profile (Figure 11). The computation of the transverse welds evolution did not require the simulation of the tools that were not included in the model. However, the heat exchange at the tool-billet interfaces was accounted for by setting proper values of the convective coefficients and reference temperatures for a third kind of boundary conditions for the heat diffusion equation at the surfaces.

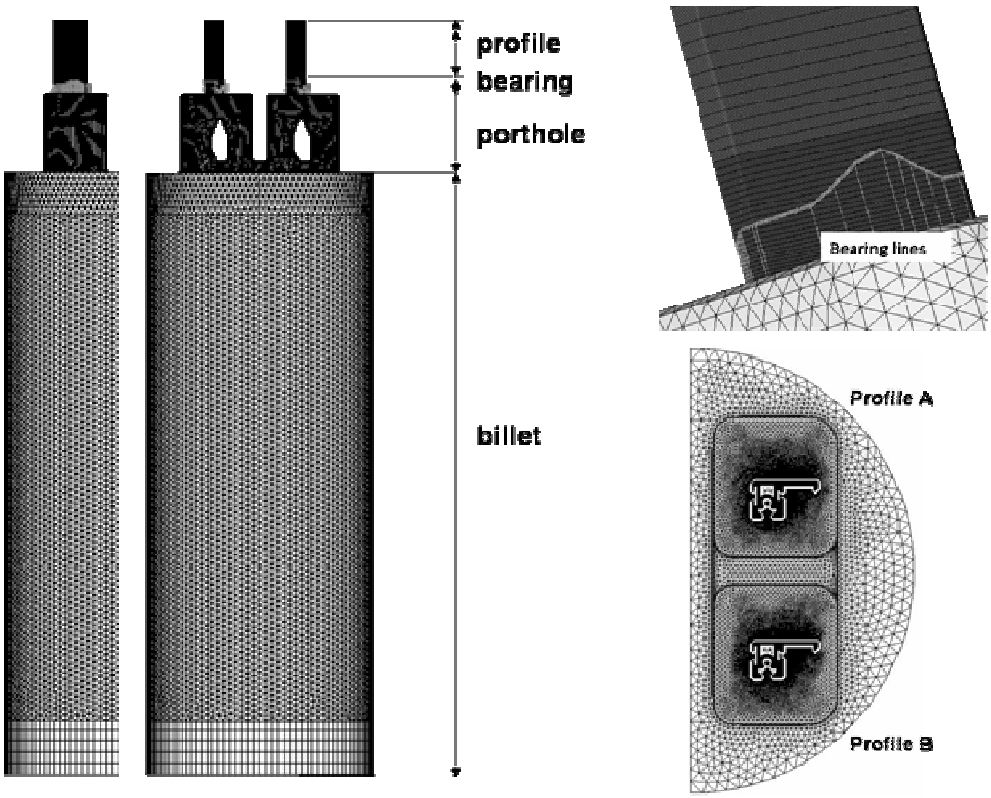

Figure 14: FE model of the billet with the defined components.

The billet and porthole components were free meshed with 3D tetrahedral 4-noded elements. Due to the higher accuracy required in the bearing and profile regions, 3D prismatic 6-noded elements were used for these regions. The final model consisted of 1323583 elements and 538026 nodes.
The temperature of the billet at the exit of the preheating oven was set as the initial values in the FE simulation (i.e. 478°C). The process parameters of the fourth billet recorded during the experimental campaign were used as the reference values for the ram speed setting and the results comparison. Thus, a ram speed of 6.2 mm/s was used producing a mean profile speed of 19.2 m/min.
At the two exits, zero normal stress boundary condition was specified. A full sticking condition was set all around the billet surfaces except on the bearings where a viscoplastic friction model with a coefficient value of 0.3 was used accounting for the material sliding that occur in these regions [22]. A convective coefficient of 3000 $W/m^2C°$ was set between aluminium and the tool system (container, die and ram), while the initial values of the tools were used as reference temperatures. Heat flux was set equal to zero for the free surface condition at the profile surfaces. The ram speed was imposed by applying the prescribed velocity of 6.2 mm/s at the billet back. The scheme of the applied boundary conditions is reported in Figure 15.

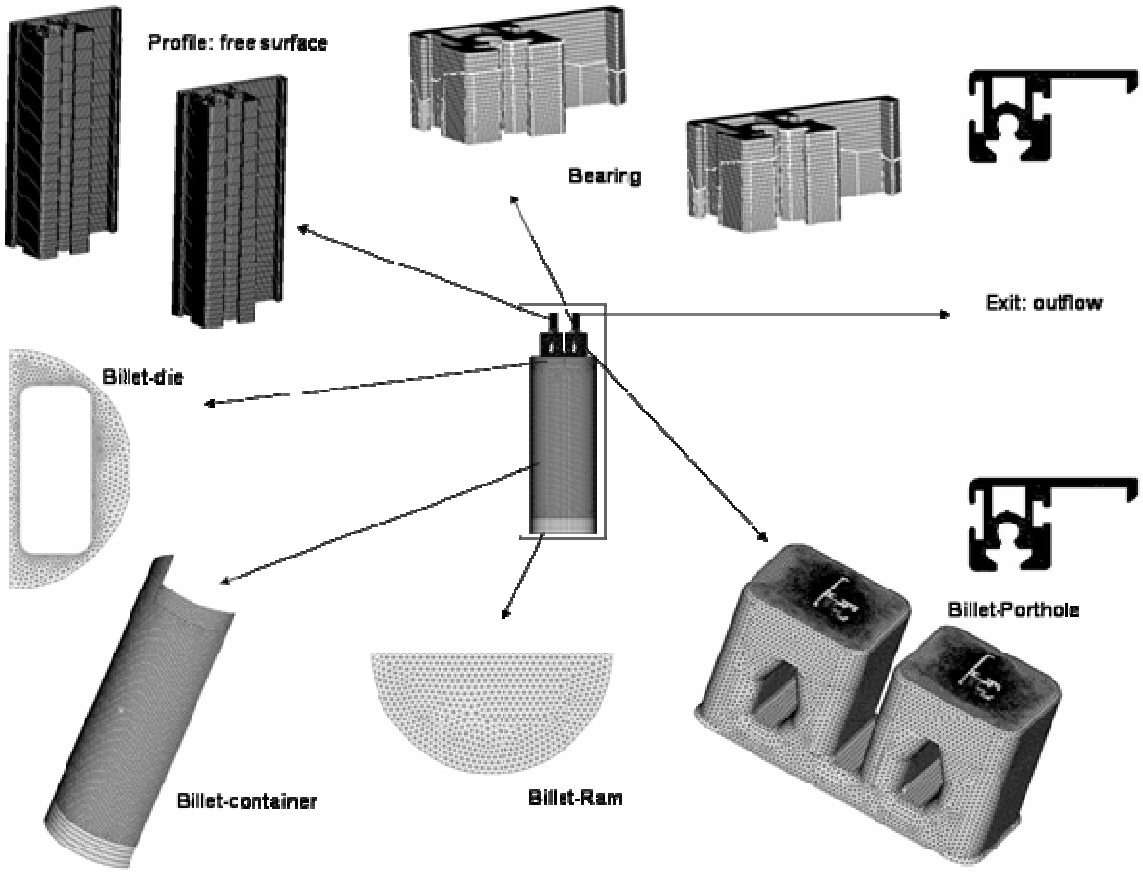

Figure 15: The boundary conditions applied to the 3D FE model of the extruded billet.

The flow of aluminum at elevated temperature exhibits a viscoplastic behaviour and is thus non-Newtonian. The effective flow stress of the AA6060 alloy was expressed by the Sellars-Tegart inverse sine hyperbolic model [23] to yield the steady-state effective deviatoric flow stress:

$$\bar{\sigma} = \frac{1}{\alpha}\sinh^{-1}\left[\left[\left(\frac{Z}{A}\right)\right]^{\frac{1}{n}}\right] = \frac{1}{\alpha}\sinh^{-1}\left[\left[\frac{1}{A}\cdot\dot{\varepsilon}\cdot\exp\left(\frac{Q}{RT}\right)\right]^{\frac{1}{n}}\right] \qquad (1)$$

where Z is the Zener-Hollomon parameter [24], n=3.515, Q=144000J/mol, $A=5.91052\cdot10^{9}s^{-1}$, R=8.314 J/(K°·mol), $\alpha=3.464\cdot10^{-8}$ m^2/N and T is expressed in K°.
The physic, thermal and mechanical properties used for the AA6060 alloy are reported in Table 4:

Table 4: Physic, thermal and mechanical properties of the AA6060 aluminum alloy used in the present study.

Density (Kg/m^3)	2685
Specific heat (J/Kg·K)	878
Conductivity (W/m·K)	200
Coefficient of thermal expansion (1/K)	1e-5
Young modulus (MPa)	40000
Poisson ratio	0.35

The weld length calculation was performed by means of a transient analysis with moving boundaries. In this type of problem, the boundary conditions for the flow and heat transfer equations are treated as time-dependant and the position of the billet back and of the billet-container interface tracked during the simulation time. The mesh in the profile, bearing, porthole and welding chamber remain fixed, but in the

billet region the elements scale down linearly in the extrusion direction at each time step. HX uses an Arbitrary Lagrange-Eulerian description of motion in problems with moving boundaries since it coalesces a good numerical stability and convergence properties with a robust mesh moving technique.
A variable decreasing number of time steps was defined starting from the first 10 seconds, in which the transverse welds were supposed to evolve and the velocity and thermal fields to reach the regime values, to the remaining 70 sec of simulation, used to evaluate the load-stroke history. The maximum number of nonlinear iteration was set equal to 25 with a convergence tolerances on velocities taken to be 10^{-3}. Even the tolerance for iterative equation solvers was set at 10^{-3} for velocities. A 90% of the deforming work was considered to be converted in heat. The total simulation time was 132 hours (on a Dell T7400 with 4 Intel Xeon processors at 3 GHz, 20 GB of ram).

Numerical results
In Figure 16 the evolution of the transition between the new (grey) and the old (black) billets for the two profiles is shown. The FE code correctly predicted the replacement of the billet that first affected the massive part (X) of the profile (steps 12 to 14) and then the thinner part (Y). In addition, as experimentally observed, the code was found able to capture the faster filling of new material in the thicker part for the profile A than in B and the contrary for the thinner part.

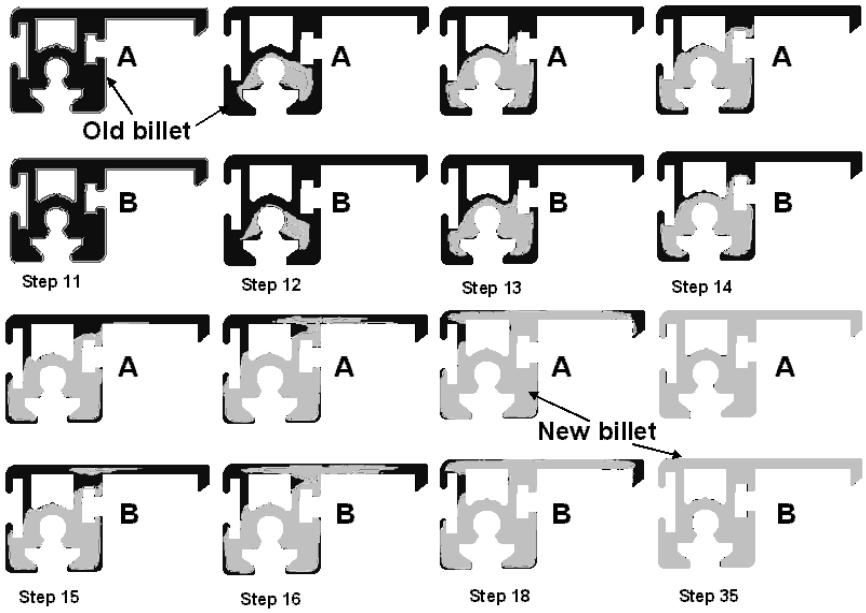

Figure 16: Evolution of the transverse weld at various subsequent time steps.

Figure 17 shows the percentage of the new billet as a function of the stop mark distance with the detail of the replacement of the new to the old billet for four simulation steps.

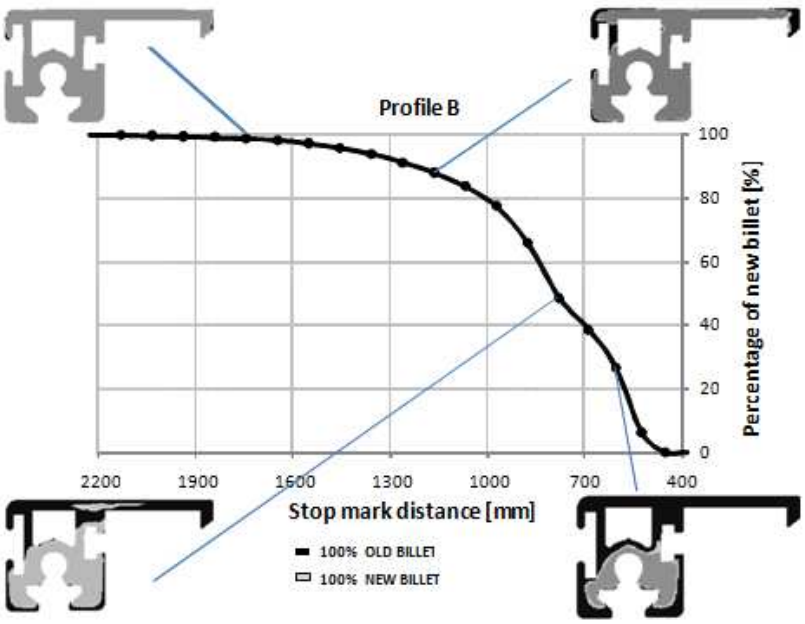

Figure 17: Simulated percentage of new material as a function of the distance from the stop mark.

Minimal differences were observed between the prediction of the profiles A and B charge weld evolution, especially at the beginning of the old billet replacement (Figure 18).

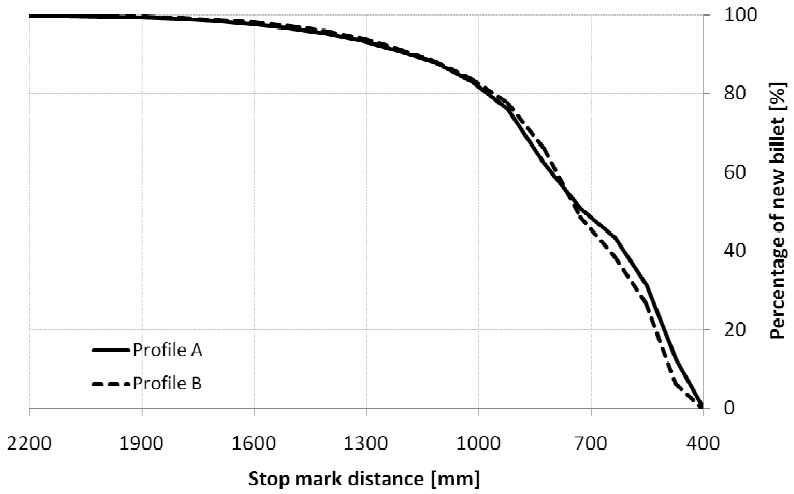

Figure 18: Comparison of the computed percentage of the new material history for the profiles A and B.

Comparison with experimental results

A fine agreement was found between experimental results and numerical prediction in terms of profile exit velocity with a peak error at the steady state less than 3% (Figure 19a).

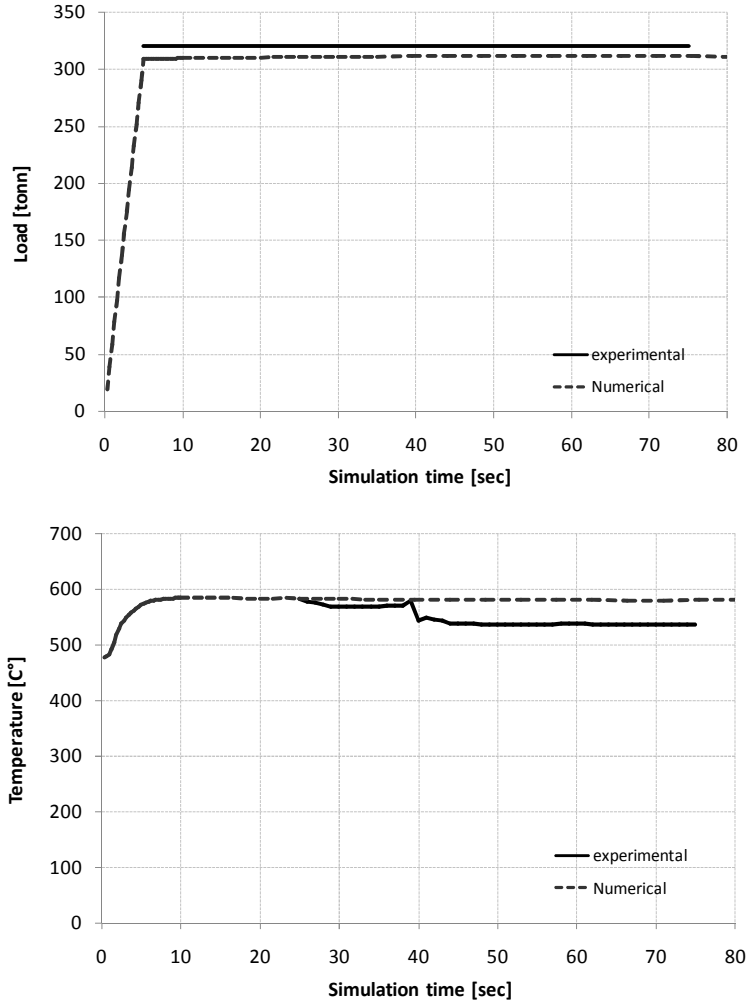

Figure 19: Comparison of the experimental vs. numerical results for the profile A in terms of exit velocity (left) and temperature (right).

A similarly accordance was observed for the profile exit temperature after the initial experimental thermal transient with a peak difference of 7.8% (Figure 16b). Numerical predictions were always higher than experimental ones. This latter difference is consistent with the effect of heat exchange (which was not simulated) between the profile and the surrounding air in the travel from the die exit to the temperature monitoring point.

A more detailed analysis over the charge weld evolution showed a very good agreement on the trend of profile filling by the new material. Figure 20 reports a comparison of numerical and experimental results for profiles A and B. The discrepancy of 150 mm between the experimental and numerical onset of the charge welds curves is to be partially related to the upsetting of the billet in the container (which delays the profile exit in the range of 120-170 mm) and cannot be computed by the FE code.

In addition, the simulation clearly evidenced, although not apparent from Figure 14, the overlapping of the charge weld transition for the two flows X and Y in profile B and the corresponding separation in profile A.

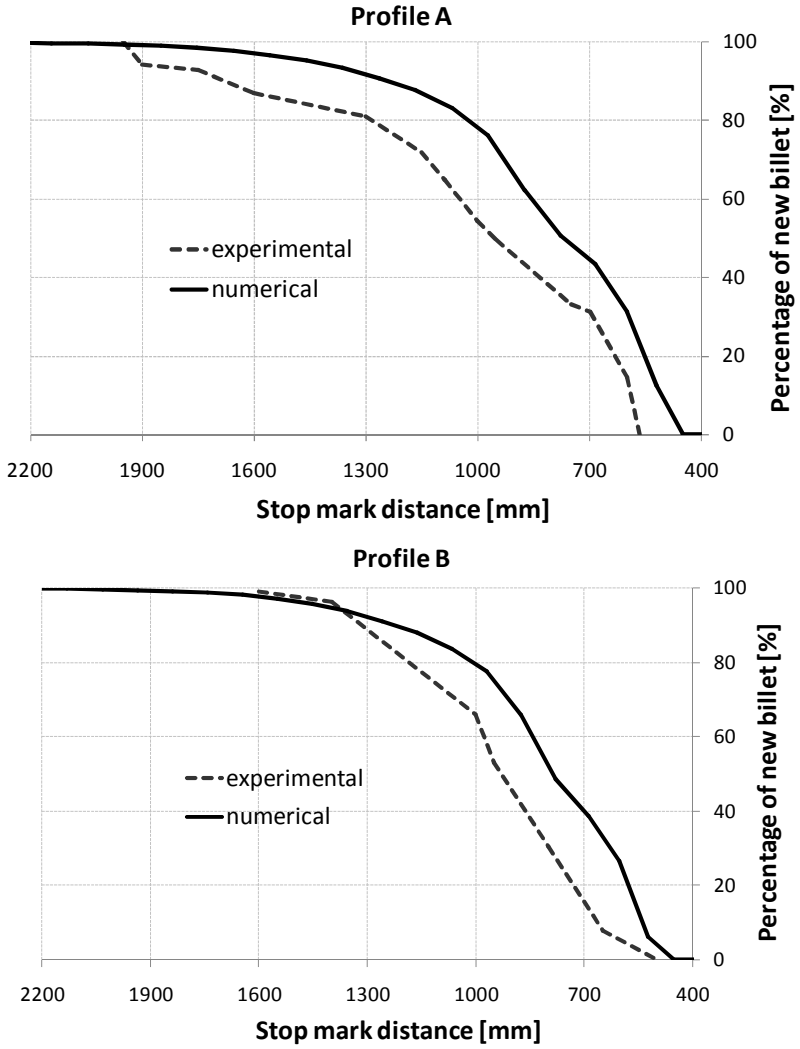

Figure 20: Comparison of the experimental vs. numerical results for percentage of new material over the stop mark distance for profile A (left) and B (right).

With the results showed above and a comparison with the industrial process parameters, it was possible to perform an evaluation of the die-process efficiency. First, the company was scrapping 2000mm by rule of thumb after the stop mark for weld contamination, which is a 8.7% of billet material. Above results showed that 2100mm is the extent that grant complete weld scrap, that is a 9.1%. Moreover, it was normally scrapped 1000mm of profile before the charge weld for skin contamination while keeping a butt of 20mm; these adding up to 8.7% of billet material. Experimentally no trace of skin contamination was found in the profiles neither before than after the stop mark, thus suggesting that no scrap was necessary before the stop mark and that butt length could be reduced to 12mm, hence reducing the material waste to 2.6% of billet material. Adding up the above results, the company process scrap index of 17.4% could be lowered to the die-process efficiency index of 11.7% (retrieved by experimental activities).

Conclusions

Three typical extrusion problems have been investigated for a multi-hole die in a industrial environment. Most of the attention was directed to the charge weld as the seam welds are not visible after 250mm nor show any defect. The charge weld was investigated by means of image analysis both in terms of extent, onset and evolution behaviour, thus comparing the influence of the section shape and its localization on the die. Aside welds investigation, skin and butt defect were also inquired.

A numerical simulation of the process was performed by means of the FE code HyperXrude® with the aim to evaluate the code capability to predict the charge weld evolution. The comparison between experimental and numerical results showed a good agreement both in terms of general trend and exhausting points of the new material charge weld over the stop mark distance. As consequence, the codes can be successfully applied during the die design stage in order to select the optimal porthole channels shape able to reducing profile scrap during billet to billet transition. This can be used to compare two different die designs and theoretical and practical process parameters (e.g. butt and scraps length).
The advantages of the simulation is double: at the die design stage it can be used directly to maximize the material flow overlapping, thus minimizing the whole charge weld extent; on the plant, it allows to discard the minimum amount of material while avoiding expensive optical analyses over the profile section.

Acknowledgements
The authors would like to thank Eng. Floriano Bagagli of Alutitan S.p.A. San Marino, RSM, for the interest, support and for his help in experimental trials.

References
[1] EN 13981-1:2003, Aluminium and aluminium alloys. Products for structural railway applications. Technical conditions for inspection and delivery. Extruded products;
[2] Akeret, R.,1992. Extrusion Welds-Quality Aspects are now centre stage. In the Proc. of the 5th ET Seminar, vol II, 319-336;
[3] 13 Parson, N.C., Hankin, J.D., Bryant, A.J., 1992. The metallurgical background to Problems Occurring During the Extrusion of 6XXX alloys. In the Proc. of the 5th International Aluminum Extrusion Technology Seminar, Chicago, USA, vol II, 13-24;
[4] Lefsta, M., Reiso, O., Johnsen, V., 1992. Flow of the billet Surface in Aluminum Extrusion. In the Proc.of 5th International Aluminum Extrusion Technology Seminar, Chicago, USA, vol II, 503-518;
[5] Valberg, H., 1988. Physical Simulation of Metal Extrusion by Means of Model Materials. In the Proc. of 4th International Aluminum Extrusion Technology Seminar, Chicago, USA, vol II, 321-328;
[6] Valberg, H., 2010. Understanding Metal Flow In Aluminium Extrusion By Means Of Emptying Diagrams. International Journal of Material Forming, Vol. 3, issue 1, 391-394;
[7] Bariani P.F., Bruschi S., Ghiotti A., 2006, Physical simulation of longitudinal welding in porthole-die extrusion, CIRP Annals-Manufacturing Technology 55/1, 287-290;
[8] Valberg H., 2002, Extrusion welding in aluminium extrusion,Int. J. of Materials & Product Technology, 17/7, 497-556;
[9] Donati, L., Tomesani, L., Minak, G., 2007. Characterization of seam weld quality in AA6082 extruded profiles. Journal of Materials Processing Technology 191, 127–131;
[10] Nanninga N., White C., Mills O., Lukowski J., 2010, Effect of specimen orientation and extrusion welds on the fatigue life o fan AA6063 alloy, International Journal of fatigue 32, 238-246;
[11] Finkelnburg W, 1992, Some investigations on the metal flow during extrusion of Al alloys, Proceedings of 5th ET Seminar, vol II, 475-484;
[12] Reggiani, B., Donati, L., Tomesani, L., 2010. Effect of different FE simulation codes in the stress analysis of extrusion dies. In the Proc. of the 13th International ESAFORM Conference on Material Forming, University of Brescia, Brescia, Italy, 7-9 April;
[13] Sommitsch, C., Sievert, R., Wlanis, T., Günther, B., Wieser, V., 2007. Modelling of creep-fatigue in containers during aluminium and copper extrusion. Computational Materials Science, 39, 55–64;
[14] Tomesani, L., Reggiani, B., Donati, L., Khalifa, N.B., Tekkaya, A.E., 2010. Experimental evaluation and numerical analysis of speed-related effects in aluminium extrusion. In the Proc. of the 60th CIRP, Accademia Internazionale di Ingegneria della Produzione (http://www.cirp.net), 22nd-28th August, Pisa, Italy;
[15] Zhou, J., 2003. 3D FEM simulation of the whole cycle of aluminium extrusion throughout the transient state and the steady state using the updated Lagrangian approach. J. Mater. Proc. Technol., 134, 383-397;
[16] Ceretti E., Fratini L. Gagliardi F., Giardini C., 2009, A new approach to study material bonding in extrusion porthole dies, CIRP Annals-Manufacturing Technology, 58, 259-262;
[17] Bourqui, B., Huber, A., Moulin, C., Bunetti, A., 2002. Improved weld seam quality using 3D FEM simulations in correlation with practice. In the Proc. of the First EAA, European Aluminum AssociationVol. 27-2 - Ed. 2009 Metallurgical Science and Technology 29 Extruders Division, Brescia, Italy;

[18] Donati, L., Tomesani, L., 2004. The prediction of seam welds quality in aluminum extrusion. Journal of Materials Processing Technology 153–154, 366–373;
[19] Donati, L., Tomesani, L., 2005. The effect of die design on the production and seam weld quality of extruded aluminum profiles. Journal of Materials Processing Technology 164–165, 1025–1031;
[20] Liu, G., Zhou, J., Duszczyk, J., 2008. FE analysis of metal flow and weld seam formation in a porthole die during the extrusion of a magnesium alloy into a square tube and the effect of ram speed on weld strength, J. Mater. Process. Technol. 200,185 – 198;
[21] Schikorra M., Tekkaya A.E., Kleiner M., 2008, Experimental investigations of embedding high strength reinforcements in extrusion profiles, CIRP Annals-Manufacturing Technology, 57, 313-316;
[22] Reddy, M.P., Reddy, J.N., Akay, H.U., 1991. A 3-D penalty finite element model of forming processes. Adavances in Finite Element Analysis in Fluid Dynamics ASME 123, 61-76;
[23] Sellars, C.M., Tegart, W.J.McG., 1972. Hot workability. International Metallurgical Reviews, 17(1), pp. 1-24;
[24] Zener, C., Hollomon, J.H., 1944. Effect of stran-rate upon plastic flow of steel. Journal of Applied Physics 15, pp. 22-32.

[25] 3
[26] 4
[27] 5
[28] 6
[29] 7
[30] 9
[31] 11
[32] 12
[33] 14
[34] 15
[35] 16
[36] 17
[37] 18
[38] 19
[39] 20
[40] 21
[41] 22
[42] 23
[43] 24

Appendix A

Considering the possible strain model, effective strain (eq. 1) was chosen versus Von Mises strain (eq. 2) as it is dependent from the deformation history during the process, which is the base for a correct evaluation of recrystallization energy and values. Due to the inner definition of the two, the effective strain is always greater or equal to Von Mises strain.

$$d\varepsilon_{eff} = \sqrt{\frac{2}{3}\left(d\varepsilon_r^2 + d\varepsilon_z^2 + d\varepsilon_\theta^2 + \frac{1}{2}d\gamma_{rz}^2\right)} \quad (1)$$

$$\varepsilon_{Von\ Mises} = \sqrt{\frac{2}{3}\left(\varepsilon_r^2 + \varepsilon_z^2 + \varepsilon_\theta^2 + \frac{1}{2}\gamma_{rz}^2\right)} \quad (2)$$

At a first comparison of the microstructure with the strain field is evident how, Figure 1, grain shape is not in agreement with strain distribution as, for instance, spot 7 and 3 show similar grain deformation but different simulated strain: 1,54 vs 0,157.

Moreover spot 2 shows undeformed grain while the simulation estimates a strain of 1,75 (greater than spot 7.) This is although not considered a problem as it could be related to a backflow effect present in real extrusion but not simulated (no space between ram and container in the FEM model)

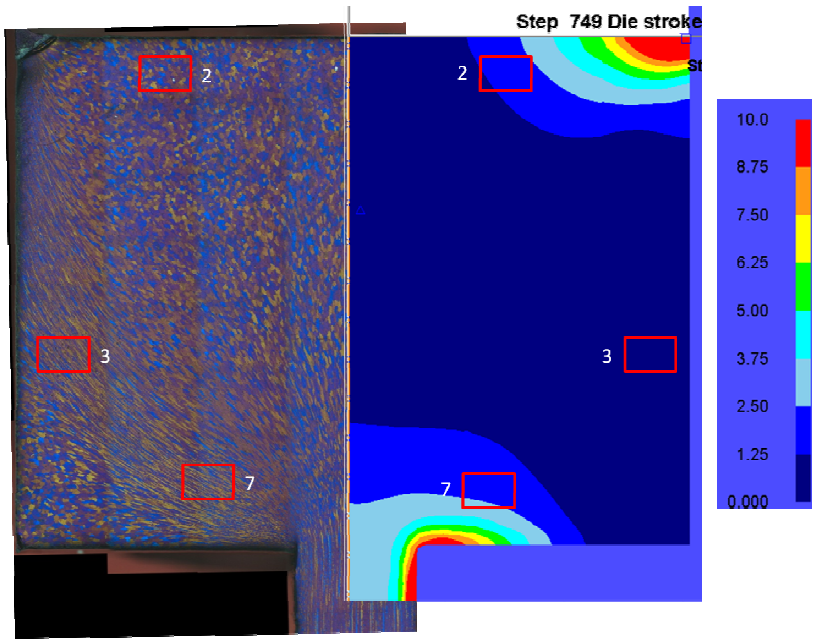

Figure 1. Microstructure coupled with simulation strain distribution for a ϕ4mm, 520°C extrusion.

Also for the ϕ3mm rod extrusion, figure 2, there is no shear zone. Spots 3,4,5 display different grain deformation (figure 3) but similar FEM strain. Moreover, as visible in figure 4, spot 10 shows little deformation gradient along the radius and small strains compared to the grain deformation.

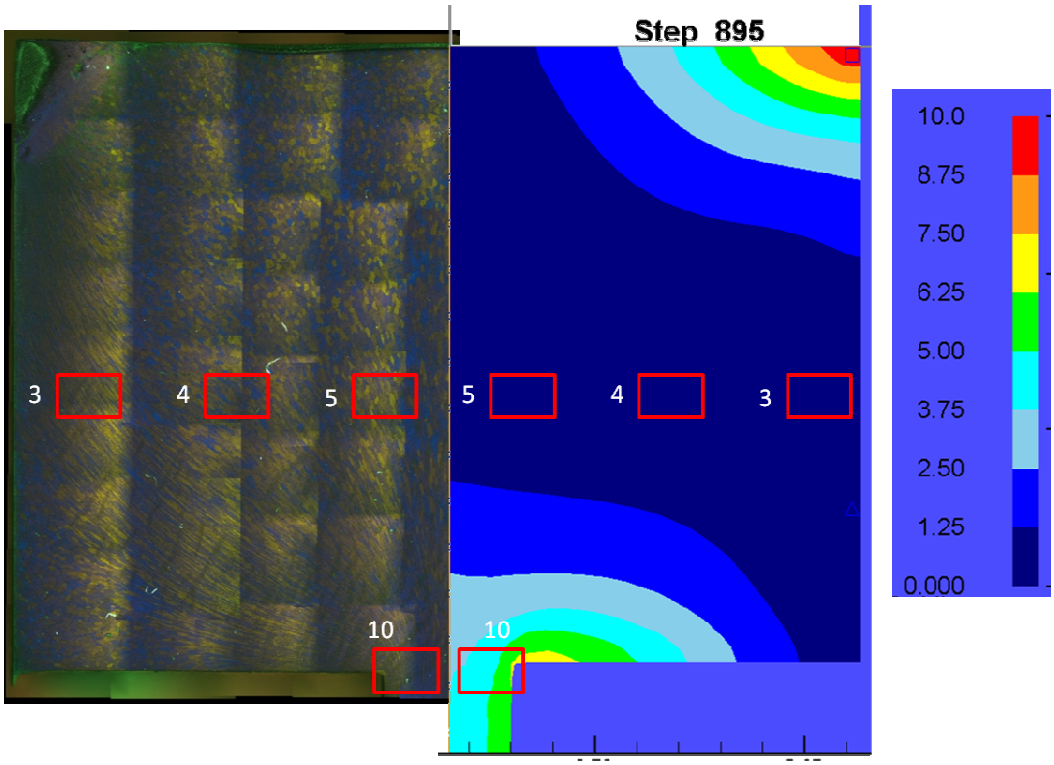

Figure 2. Microstructure coupled with simulation strain distribution for a ϕ3mm, 520°C extrusion.

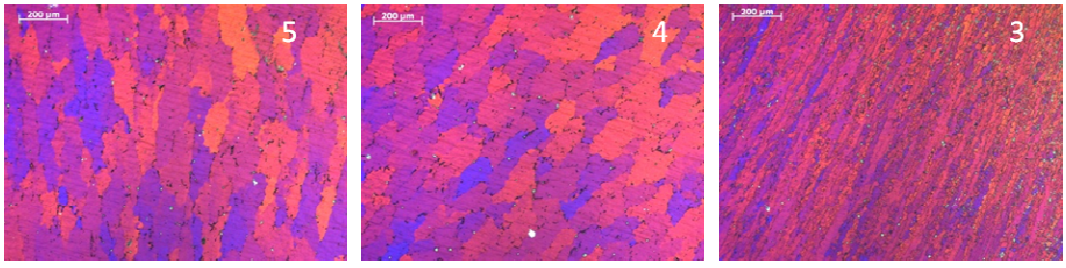

Figure 3. Enlargements of spots 5, 4 and 3 of specimen extruded at 520°C for a ϕ3mm showed in figure 2.

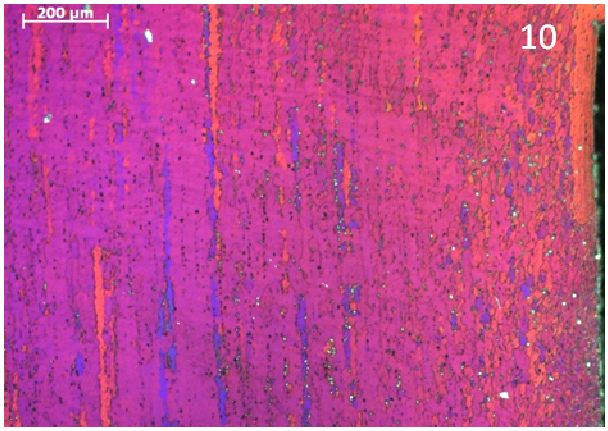

Figure 4. Enlargement of spot 10 of specimen extruded at 520°C for a ϕ3mm showed in figure 2.

The software DEFORM allows use of a *flownet* tool, that is drawing a rectangular or circular grid joined to the material and therefore giving a visual representation of the local deformation. Despite that strain is not in accordance in ϕ3mm and ϕ4mm test, the flow net is in good agreement with microstructure. A circular flow net has been performed for both simulation with the same grid definition.

Figure 5 and figure 6 show a comparison of the *flownet* with the microstructure. *Flownet* is negligible different for the two simulation. Differences are mainly on the upper part (red area) while the rest has a similar behavior and is in accordance with microstructure.

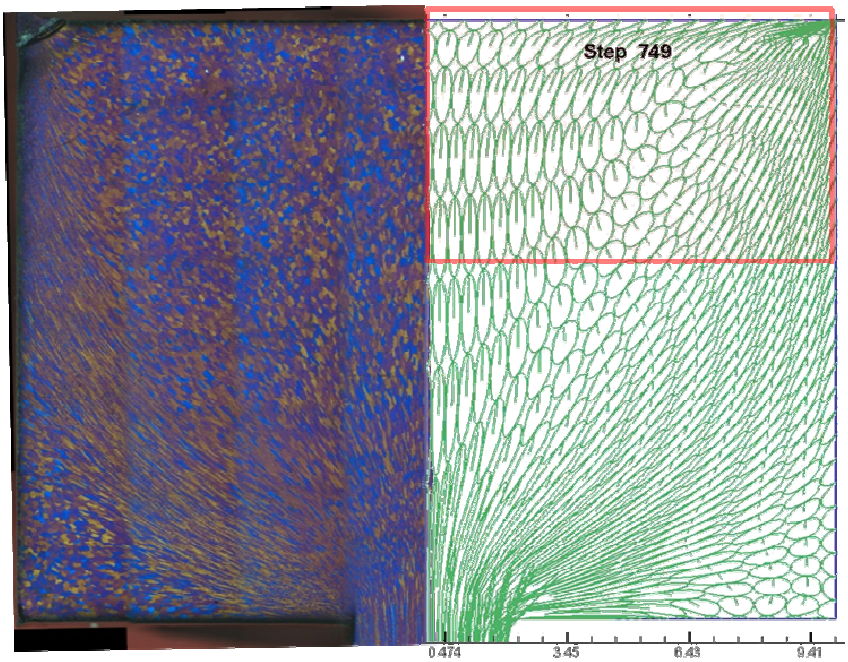

Figure 5. Flow net comparison with experimental microstructure for ϕ4mm 520°C extrusion. Flownet was set up with 15 circles along the x-axis, 100% diameter.

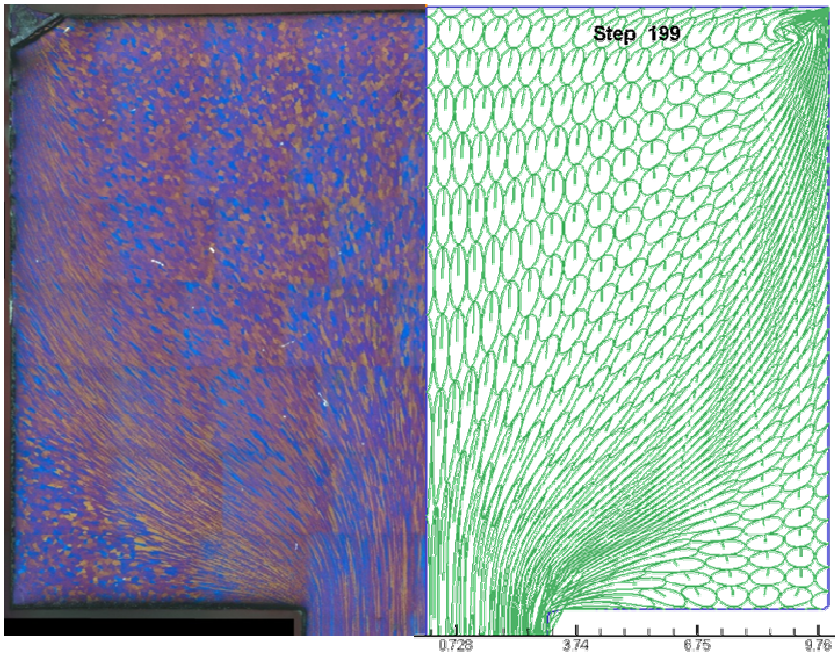

Figure 6. Flow net comparison with experimental microstructure for ϕ6mm 520°C extrusion. Flownet was set up with 15 circles along the x-axis, 100% diameter.

A direct comparison between *flownet* and effective strain has been done. Figure 7 repots such comparison for ϕ4mm and ϕ6mm with the enlargement of spot 3. The reported effective strain is strongly different (0.165 for ϕ 4mm and 1.75 for ϕ6mm) while flow net shows similar distortion and deformation (length of flow circle 1.9 for ϕ4mm and 2 for ϕ6mm).

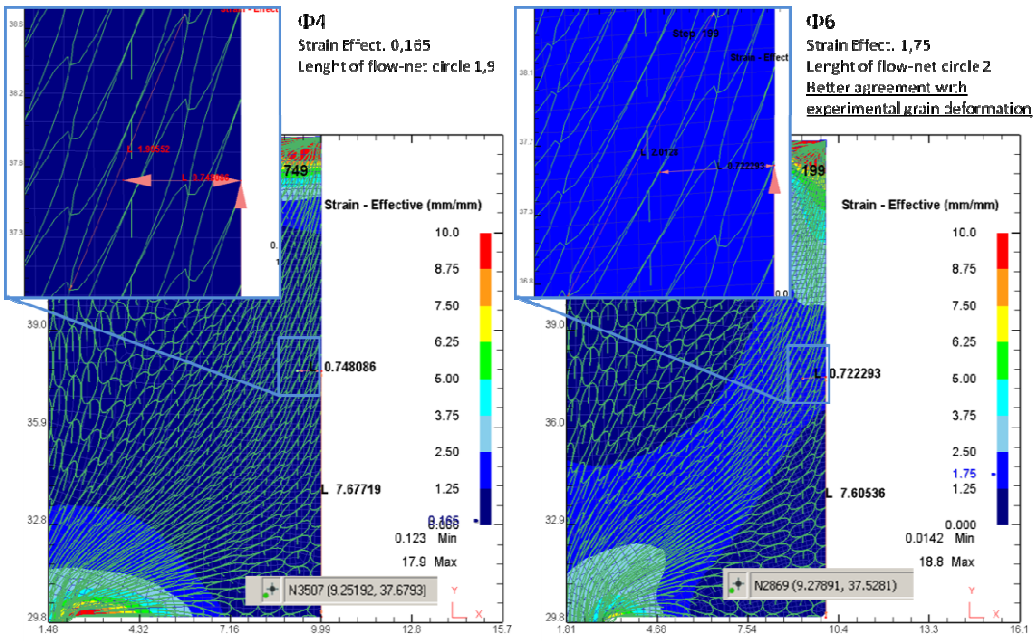

Figure 7. Flow net comparison with effective strain for ϕ4mm and ϕ6mm at 520°C extrusion.

Considering the above results a user evaluation of effective strain was implemented as a pre-processor subroutine following eq. 1. The subroutine, insert in the code file usr_msh.f, is reported below:

```
C CALCULATION AT THE BEGINNING OF THE STEP, THAT IS STATUS=0
      IF (ISTATUS.EQ.0.AND.NUMEL.GT.0) THEN
       A=0.8165
        IF (KSTEP.NE.(-1)) THEN
          IF (KSTEP.NE.USRVE(27,1)) THEN

            USRVE(27,1)=KSTEP
            DO  I=1,NUMEL,1
C Just copying deformation components
                  USRVE(1,I) = TSRS(1,I)
             USRVE(2,I) = TSRS(2,I)
         USRVE(3,I) = TSRS(3,I)
                  USRVE(4,I) = TSRS(4,I)
C Start of evaluation
            USRVE(11,I)=TSRS(1,I)**2+TSRS(2,I)**2
            USRVE(33,I)=TSRS(3,I)**2+0.5*TSRS(4,I)**2
            USRVE(34,I)=USRVE(11,I)+USRVE(33,I)
            USRVE(9,I) = A*(USRVE(34,I))**0.5

C  Copying values of previous step so to keep values at STATUS 0 and STATUS 1 for each step
            USRVE(21,I)=USRVE(19,I)
            USRVE(24,I)=USRVE(23,I)
            USRVE(35,I)=USRVE(20,I)
            USRVE(22,I)=USRVE(25,I)
           ENDDO
          ENDIF
         ENDIF
       ENDIF
C CALCULATION AT THE END OF THE STEP, THAT IS STATUS=1
       IF (ISTATUS.EQ.1.AND.NUMEL.GT.0) THEN
         IF (KSTEP.NE.(-1)) THEN

        A=0.8165
        DO  I=1,NUMEL,1
C Just copying deformation components
          USRVE(5,I) = TSRS(1,I)
          USRVE(6,I) = TSRS(2,I)
          USRVE(7,I) = TSRS(3,I)
          USRVE(8,I) = TSRS(4,I)
C Evaluation
          USRVE(31,I)=TSRS(1,I)**2+TSRS(2,I)**2
          USRVE(12,I)=TSRS(3,I)**2+0.5*TSRS(4,I)**2
          USRVE(32,I)=USRVE(31,I)+USRVE(12,I)
          USRVE(10,I) = A*(USRVE(32,I))**0.5
          USRVE(13,I) = (USRVE(5,I)-USRVE(1,I))**2
          USRVE(14,I) = (USRVE(6,I)-USRVE(2,I))**2
          USRVE(15,I) = (USRVE(7,I)-USRVE(3,I))**2
          USRVE(16,I) = 0.5*(USRVE(8,I)-USRVE(4,I))**2
          USRVE(17,I) = USRVE(13,I)+USRVE(14,I)
          USRVE(18,I) = USRVE(15,I)+USRVE(16,I)
          USRVE(19,I) = A*(USRVE(17,I)+USRVE(18,I))**0.5
          USRVE(20,I) = ABS(USRVE(10,I)-USRVE(9,I))
C USRVE(25) = Von Mises STRAIN
          USRVE(25,I)=USRVE(22,I)+USRVE(20,I)
C USRVE(23) = TOTAL EFFECTIVE STRAIN
          USRVE(23,I)=USRVE(24,I)+USRVE(19,I)
```

```
      ENDDO
    ENDIF
  ENDIF
RETURN
END
```

A first validation of the subroutine was through the point tracking of the three critical points presented in figure 2 (i.e. on shear zone, in the middle area and close to the axis). For all three points at the three diameter of extrudate, a plot is reported for code and user computed effective strain, and for Von Mises strain and is reported in figure 8. Subroutine calculated effective strain (red line) is always greater than Von Mises, as expected from theory, while code one presents some discrepancies.

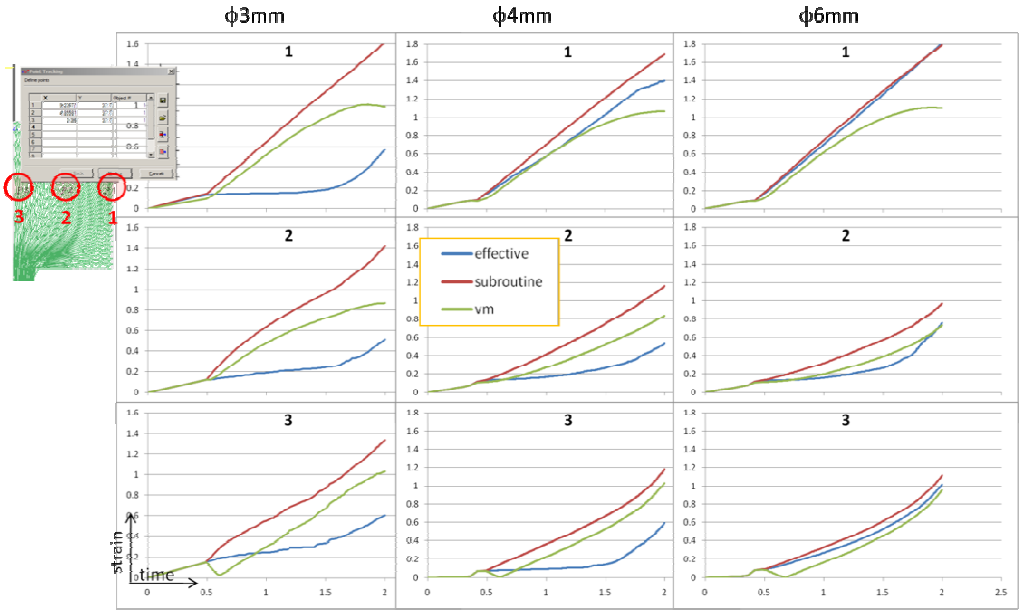

Figure 8. Point tracking results in three spots for extrusions at 520°C.

The implementation of the user evaluated effective strain had an evident positive impact on the experimental grain size and numerical evaluated strain coupling results. Figure 9 and figure 10 show the coupling performed on two different specimens, for both grain thickness and grain length. While some spots do not present any change, others move toward higher strains this showing a tendency of strain dependant evolution which was not retrievable otherwise.

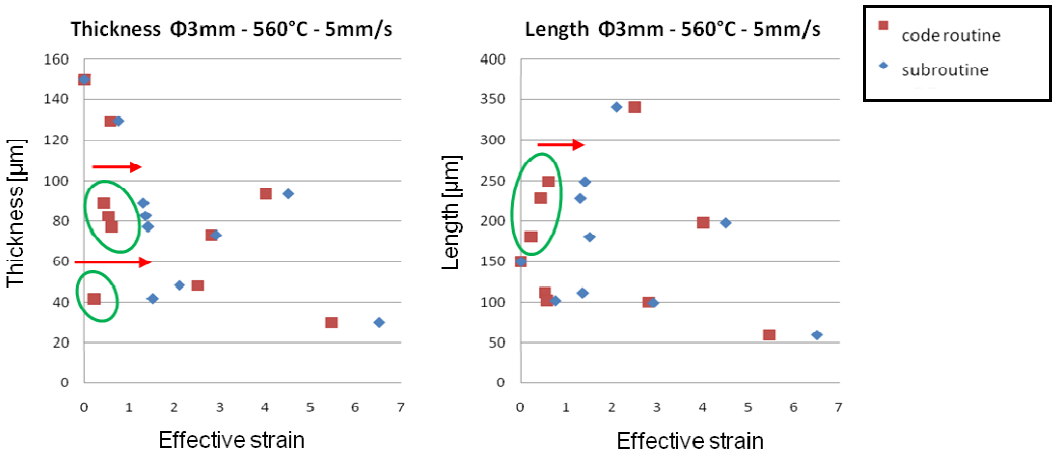

Figure 9. Coupling of experimental grain size (thickness and length) with effective strain evaluated by original code routine and user implemented routine for ϕ3mm specimen extruded at 560°C and 5mm/s.

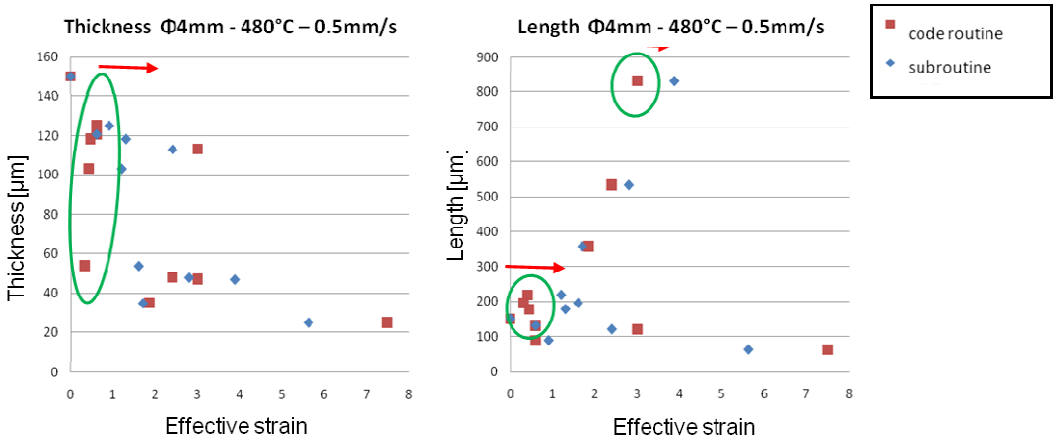

Figure 10. Coupling of experimental grain size (thickness and length) with effective strain evaluated by original code routine and user implemented routine for ϕ4mm specimen extruded at 480°C and 0.5mm/s.

The overall effect of such correction is clear if all condition are plot together as in Figure 11, where it is of immediate notice how the implementation of the user-routine reduced enormously the dispersion of data, allowing to achieve better regression of the dynamic grain evolution and recrystallization, as well as provide correct data for the static recrystallization. In all the works presented in this thesis, the user-routine evaluated effective strain was used for the evaluation of grain evolution.

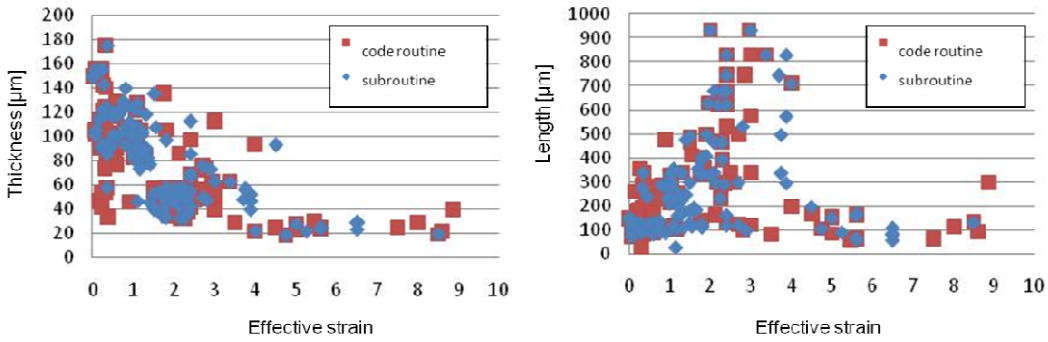

Figure 11. Coupling of experimental grain size (thickness and length) with effective strain evaluated by original code routine and user implemented routine for all specimens.

Conclusions

In the present work a study of the microstructure evolution for 6XXX aluminum alloys and building of a tool for its prediction to be used in the industry was carried out. The focus of the thesis was to develop the model for the extrusion process and to provide all the contour knowledge for the correct calibration of a FEM code and interpretation of results.

In such direction the work was developed in three sections.

A primary phase involved the calibration of the commercial code for the correct simulation of the extrusion process. This brought not only to investigate the correct contour parameters but also the reliability of the code itself and the results were beyond the simple tuning of the software. An investigation on the friction parameter brought to understand the tribology of the extrusion process as well as the possibility to use different coatings (whose effects in extrusion were not yet completely clarified in literature). During the work a critical approach was kept in the use of the code, which brought to the development of a proper subroutine for the evaluation of effective strain, thus allowing a greater control of the FE code itself, useful in the implementation of the following microstructure model.

The core phase of the work was the development of a specific set of tests to investigate the microstructure evolution and validate the model. A mini extrusion experiment was designed and the results of the microstructure analysis compared with a campaign of simulation. This allowed to retrieve the development of the microstructure during the dynamic evolution and implement the corresponding model in the code as a pre-processor subroutine. A model for the static recrystallization was developed starting from the model proposed in literature. The novelty of the proposed static recrystallization model lies on integration with the dynamic evolution. A second test, of small scale inverse extrusion, was used to validate the integrated module.

An activity of building critical knowhow on the interpretation of microstructure and extrusion phenomena was carried out during the entire doctorate study. It is believed, in fact, that the sole analysis of the microstructure evolution regardless of its relevance in the technological aspects of the process would be of little use for the industry as well as ineffective for the interpretation of the results. Studies were conducted on those issues, characteristic of the extrusion process, that can arise defect bound to microstructure as the streak formation or the charge weld evolution. Streaks on extruded profiles is a common cause of scrap, but little knowledge is available. From this a deep

analysis on an industrial was performed, leading to understand the causes and link them to the microstructure. The charge weld phenomena, first analyzed from the microstructural side with the streak defect, was then investigated in his full complexity by means of an experimental activity thus allowing to retrieve the influence of tool and process design on charge weld evolution.

As a final comment, it was possible to develop an combined dynamic-static recrystallization model which has never been proposed before thus allowing the implementation of a tool that allows to predict the evolution throughout the extrusion process, sided by a sound background for the interpretation of results and calibration of the extrusion simulation.